

2019

A GIS-Based Modeling Approach To High-Resolution Anthropogenic Heat Flux And Building Energy Demand In Los Angeles

Yuanfan Zheng
Indiana State University

Follow this and additional works at: <https://scholars.indianastate.edu/etds>

Recommended Citation

Zheng, Yuanfan, "A GIS-Based Modeling Approach To High-Resolution Anthropogenic Heat Flux And Building Energy Demand In Los Angeles" (2019). *All-Inclusive List of Electronic Theses and Dissertations*. 1822.

<https://scholars.indianastate.edu/etds/1822>

This Dissertation is brought to you for free and open access by Sycamore Scholars. It has been accepted for inclusion in All-Inclusive List of Electronic Theses and Dissertations by an authorized administrator of Sycamore Scholars. For more information, please contact dana.swinford@indstate.edu.

A GIS-BASED MODELING APPROACH TO HIGH-RESOLUTION ANTHROPOGENIC
HEAT FLUX AND BUILDING ENERGY DEMAND IN LOS ANGELES

A dissertation

Presented to

The College of Graduate and Professional Studies

Department of Earth and Environmental Systems

Indiana State University

Terre Haute, Indiana

In Partial Fulfillment

of the Requirements for the Doctoral Degree

in Spatial and Earth Sciences

by

Yuanfan Zheng

August 2019

© Yuanfan Zheng 2019

Keywords: Geographic Information Systems, Anthropogenic Heat Flux, Building Energy Demand, High-Resolution Modeling, Climate Change

ProQuest Number:22583446

All rights reserved

INFORMATION TO ALL USERS

The quality of this reproduction is dependent upon the quality of the copy submitted.

In the unlikely event that the author did not send a complete manuscript and there are missing pages, these will be noted. Also, if material had to be removed, a note will indicate the deletion.



ProQuest 22583446

Published by ProQuest LLC (2019). Copyright of the Dissertation is held by the Author.

All rights reserved.

This work is protected against unauthorized copying under Title 17, United States Code
Microform Edition © ProQuest LLC.

ProQuest LLC.
789 East Eisenhower Parkway
P.O. Box 1346
Ann Arbor, MI 48106 – 1346

CURRICULUM VITAE

EDUCATION

- 2019 Ph.D., Department of Earth and Environmental Systems, Indiana State University, Terre Haute, Indiana
- 2011 M.A., Department of Geosciences and Environment, California State University, Los Angeles, California.
- 2008 B.S., Department of Geography, Fujian Normal University, Fuzhou, China.

PROFESSIONAL EXPERIENCE

- 08/2018 – 05/2019 Graduate Assistant, Department of Earth and Environmental Systems, Indiana State University.
- 08/2017 – 12/2017 Graduate Assistant, Department of Earth and Environmental Systems, Indiana State University.
- 07/2011 – 09/2011 Graduate Assistant, Department of Geosciences and Environment, California State University, Los Angeles.

PUBLICATIONS

- Zheng, Y., & Weng, Q., (2019). Modeling the effect of climate change on building energy demand in Los Angeles County by using a GIS-based high spatial- and temporal-resolution approach. *Energy*, 176, 641-655. doi:10.1016/j.energy.2019.04.052
- Zheng, Y., & Weng, Q., (2018). High spatial- and temporal- resolution anthropogenic heat discharge estimation in Los Angeles County, California. *Journal of Environmental Management*, 206, 1274–1286. doi:10.1016/j.jenvman.2017.07.047
- Zheng, Y., Weng, Q., and Zheng, Y. X. (2017). A hybrid approach for three-dimensional building reconstruction in Indianapolis from LiDAR data, *Remote Sensing*, 9(4), 310. doi:10.3390/rs9040310
- Zheng, Y. and Weng, Q. (2015). Model-driven reconstruction of 3D buildings using LiDAR data, *IEEE Geoscience and Remote Sensing Letters*, 12(7), 1541–1545.

COMMITTEE MEMBERS

Committee Chair: Qihao Weng, Ph.D.

Professor, Department of Earth and Environmental Systems

Indiana State University

Committee Member: Stephen Aldrich, Ph.D.

Associate Professor, Department of Earth and Environmental Systems

Indiana State University

Committee Member: Gregory Bierly, Ph.D.

Professor, Department of Earth and Environmental Systems

Indiana State University

Committee Member: Jeffrey Kinne, Ph.D.

Associate Professor, Department of Mathematics and Computer Science

Indiana State University

Committee Member: James Speer, Ph.D.

Professor, Department of Earth and Environmental Systems

Indiana State University

ABSTRACT

Anthropogenic heat flux (Q_f) originates from energy consumption in buildings, industrial plants, vehicle exhaust, and human metabolism. Q_f is an important component of the urban Surface Energy Balance (SEB) system and a key to understanding many urban environmental issues. Climate change affects building energy consumption in many ways, and building energy consumption is the largest contributor to Q_f in many cities. One of these contributions comprises changes in heating and cooling demands in buildings. The increase in annual energy use in cities results in more carbon emissions and constitutes a great challenge to urban sustainability because traditional fossil fuels remain major resources for the production of electricity for heating and cooling in buildings. The primary objectives of this dissertation are to 1) develop a high spatial and temporal Q_f profile that can be readily incorporated into the urban energy balance models and be used to analyze Q_f across multiple spatial and temporal scales; 2) develop a useful database that can allow a city government to foresee the different regional sensitivities to climate change in the city from building energy demand increases at different spatial and temporal scales; and 3) test the potential mitigation effects of green roofs and solar photovoltaic (PV) systems on buildings that are more vulnerable to climate change. Los Angeles County, California, USA, was chosen as the study area, because it was the most populous county in the USA and contained various microclimate conditions.

To achieve the objectives of this study, a hybrid Q_f modeling approach was developed that combined census inventory data and Geographic Information System (GIS) methods to

create a 365-day hourly Q_f profile at 120-m spatial resolution for Los Angeles County. In a subsequent step, a GIS-based approach was used to combine climate change modeling, building energy simulation, and fine-scale (individual building) inventory data of building characteristics to quantify the effect of climate change on building energy demand at the sub-city scale. In the final step, the potential mitigation effects of PV-green roofs for building energy demand were assessed based on selected buildings that were predicted to have increased energy needs in the context of climate change.

The results showed different magnitudes and diurnal patterns in Q_f between workdays, with one peak in the morning and the other in the evening rush hours (dual-peak shape) and weekends/holidays. Additionally, Q_f varied seasonally and among different land use types. Building energy consumption was identified as the dominant contributor to Q_f in the downtown area of Los Angeles, which was found to have the largest mean Q_f among all neighborhoods throughout the entire year. Most building types showed increased energy demands under both scenarios of climate change. Larger changes were observed at finer time scales. The energy demand for buildings increased from April to October, whereas it decreased from November to March. Areas with dense tall commercial buildings would see the largest increase in energy demand. All buildings with green roofs showed positive energy savings with regard to total energy and electricity. In addition, the energy saving ability of green roofs was affected by seasonal effect, building types and technologies, and irrigation saturation, which is the threshold of soil moisture that allows for irrigation. All three objectives of this dissertation were achieved, and the methodology allows city governments to foresee the sensitivity of building energy demands at different spatiotemporal scales and tailor needed strategies.

ACKNOWLEDGMENTS

First, I would like to acknowledge my advisor Dr. Qihao Weng for his guidance and encouragement at every stage of my Ph.D. study. Under his instruction and assistance, I have not only developed solid research skills but also achieved a milestone in my academic career: published four peer-reviewed journal articles.

I would like to acknowledge my committee members, Dr. Stephen Aldrich, Dr. Gregory Bierly, Dr. James Speer, and Dr. Jeffrey Kinne, for their valuable suggestions and support throughout my preliminary exam, proposal preparation, and dissertation completion. I would like to acknowledge my lab mate, Dr. Yanhua Xie, for his assistance in the early stage of my academic writing and encouragement.

I would also like to acknowledge Elsevier for allowing me to retain the right to include two of my publications in this dissertation for non-commercial purposes. According to Elsevier, permission is not required. I have cited both of these publications in the text and listed in the references.

Last but not least, I wish to acknowledge all of my family members, because this dissertation would not have been completed without their support and encouragement. I want to thank my wife, Chengxian Cai, for her understanding and encouragement; my parents for their support, both mentally and financially; and my parents-in-law for taking care of my son.

TABLE OF CONTENTS

COMMITTEE MEMBERS	ii
ABSTRACT	iii
ACKNOWLEDGMENTS	v
LIST OF TABLES	ix
LIST OF FIGURES	xi
LIST OF ABBREVIATIONS/ACRONYMS	xv
INTRODUCTION	1
1.1 Research Background	1
1.2 Problem Statement	3
1.3 Research Objectives	9
1.4 Research Questions	10
1.5 Structure of the Dissertation	11
LITERATURE REVIEW	13
2.1 Introduction	13
2.2 Anthropogenic Heat Discharge Estimation in Urban Areas	13
2.3 Estimating the Effect of Climate Change on Building Energy Demand in Urban Areas	17
2.4 Studies on the Roles of Green Roofs in Building Energy Consumption Reduction in Urban Areas	20

2.5 Summary	24
STUDY AREA AND DATA	25
3.1 Study Area	25
3.2 Datasets	26
METHODOLOGY	30
4.1 Introduction.....	30
4.2 Anthropogenic Heat Discharge Estimation	30
4.3 Modeling the Effects of Climate Change on Building Energy Demand	45
4.4 Green Roof and Solar Photovoltaic Setting.....	50
4.5 Summary.....	54
HIGH SPATIAL AND TEMPORAL RESOLUTION ANTHROPOGENIC HEAT DISCHARGE ESTIMATION IN LOS ANGELES COUNTY.....	55
5.1 Introduction.....	55
5.2 Temporal Variations of the Anthropogenic Heat Flux	55
5.3 Anthropogenic Heat Fluxes on Extremely Hot Summer Days.....	56
5.4 Anthropogenic Heat Fluxes in the Urban Core Area.....	60
5.5 Discussion and Conclusions	62
MODELING THE EFFECT OF CLIMATE CHANGE ON BUILDING ENERGY DEMAND IN LOS ANGELES COUNTY USING A GIS-BASED HIGH SPATIAL AND TEMPORAL RESOLUTION APPROACH.....	65
6.1 Introduction.....	65
6.2 Impact of Climate Change on the Building Energy Demand at Different Temporal Scales	66

6.3 Spatial Variations of Energy Demand Change at the Neighborhood Scale.....	77
6.4 Discussion and Conclusions	81
MODELING THE PERFORMANCE OF GREEN ROOF SYSTEMS AND PHOTOVOLTAIC PANELS FOR BUILDING ENERGY SAVINGS.....	84
7.1 Introduction.....	84
7.2 Evaluation of Green Roofs and Photovoltaic Panels on building Energy Savings at Different Temporal Scales	84
7.3 Evaluation of the Green Roof Model Sensitivity.....	97
7.4 Discussion and Conclusions	98
CONCLUSIONS AND FUTURE DIRECTIONS.....	101
8.1 Introduction.....	101
8.2 Summary of Major Findings.....	101
8.3 Limitations and Future Directions	107
REFERENCES	110
APPENDIX A: FULL ARTICLE OF PUBLICATION (ZHENG & WENG, 2018).....	123
APPENDIX B: FULL ARTICLE OF PUBLICATION (ZHENG & WENG, 2019).....	137

LIST OF TABLES

Table 3.1 Greenhouse gas (GHG) emissions in Los Angeles County by sector (Energy Atlas, 2017; Zheng & Weng, 2019)	27
Table 3.2 Datasets used in this study and data sources (Zheng & Weng, 2018)	29
Table 4.1 Schedule of working population during the working day (Zheng & Weng, 2018)	34
Table 4.2 Energy released per person as a function of hour of day (W) (Zheng & Weng, 2018)	35
Table 6.1 Relative change (%) and absolute difference (MJ/m ²) in the average annual building energy demand between 2050 and present (1991–2005) in Los Angeles County under the RCP8.5 emission scenario (Zheng & Weng, 2019)	68
Table 6.2 Relative change (%) and absolute difference (MJ/m ²) in the average annual building energy demand between 2050 and present (1991–2005) in Los Angeles County under the RCP6.0 emission scenario (Zheng & Weng, 2019)	69
Table 6.3 The percentage of residential and commercial building floor areas in the 7 weather zones in Los Angeles County (Zheng & Weng, 2019)	77
Table 7.1 Selected buildings for performance evaluation of PV-green roof mitigation effects on potential building energy savings.	87
Table 7.2 Simulation of annual electricity produced by photovoltaic panels in 2050 for the tested buildings under the RCP8.5 emission scenario	88
Table 7.3 Relative change (%) in annual total energy demand between 2050 and present (1991–2005) in all tested buildings under RCP8.5 emission scenario	93

Table 7.4 Relative change (%) in annual electricity energy demand between 2050 and present (1991–2005) in all tested buildings under the RCP8.5 emission scenario.	93
Table 7.5 Key parameters for the social-economic benefit analysis of installing green roofs (Bianchini & Hewage, 2012).	94
Table 7.6 Return on investment (%) after 20 years and payback periods (years) for installing green roofs and photovoltaic systems on all tested buildings.	94
Table 7.7 Characteristics of different settings of green roofs simulated under the RCP8.5 emission scenario.	98

LIST OF FIGURES

Figure 3.1. The location of the study area, Los Angeles County, California, USA.	26
Figure 4.1. Flowchart of time-dependent hourly Q_f estimation.....	32
Figure 4.2. TMY3 climate zones in Los Angeles County (Zheng & Weng, 2019).....	46
Figure 4.3. Current monthly temperatures ($^{\circ}$ C) in seven TMY3 locations in Los Angeles County (Zheng & Weng, 2019).	46
Figure 4.4. The calibrated annual building energy consumption intensity in megajoules (MJ) per square meter (m^2) for 18 types of buildings in Los Angeles County. The simulation was based on historical TMY3 data (1991–2005) (Zheng & Weng, 2019).....	51
Figure 4.5. The method used to analyze the potential mitigation effect of green and PV-green roofs on building energy demand caused by climate change.	52
Figure 5.1. Diurnal variation of Q_f , Q_b , Q_v , and Q_m (w/m^2) in Los Angeles, USA., based on the average values from all (a) spring workdays, (b) spring nonworkdays, (c) summer workdays, (d) summer nonworkdays, (e) fall workdays, (f) fall nonworkdays, (g) winter workdays, and (h) winter nonworkdays; comparison of the diurnal variation of Q_f in different seasons on (i) workdays and (j) nonworkdays in Los Angeles, USA (Zheng & Weng, 2018).	57
Figure 5.2. (a) Comparison between Q_f (w/m^2) on an extremely hot summer workday (August 25, 2005) and the average of all summer workdays; (b) time series of the ratios between the anthropogenic heat fluxes, building emissions, and traffic emissions on	

the extremely hot summer workday and those of average summer workdays (Zheng & Weng, 2018).....	59
Figure 5.3. Spatial distribution of Q_f (w/m^2) in (a) Los Angeles County and (b) downtown Los Angeles (Zheng & Weng, 2018).....	61
Figure 5.4. Comparison of diurnal variations of Q_f (w/m^2) in downtown Los Angeles for different seasons on (a) workdays and (b) nonworkdays (Zheng & Weng, 2018).....	62
Figure 5.5. Percentage breakdown (%) of the individual components contributing to Q_f from (a) 9 am to 5 pm on workdays and (b) 5 am to 9 am on nonworkdays in downtown Los Angeles (Zheng & Weng, 2018).....	62
Figure 6.1. Differences in the total annual energy consumption intensity (a), space cooling (b), and space heating (c) (MJ/m^2) for commercial buildings between the 2050 and 1991–2005 under the RCP8.5 emission scenario (Zheng & Weng, 2019).....	70
Figure 6.2. Absolute difference in average monthly (a) total, (b) cooling, and (c) heating building energy intensity (MJ/m^2) between 2050 and 1991–2005 under the RCP8.5 emission scenario across building types; change in monthly energy intensity (MJ/m^2) under the RCP8.5 emission scenarios across different TMY3 weather zones in Los Angeles County: (d) monthly total energy intensity change; (e) monthly cooling energy intensity change; and (f) monthly heating energy intensity change (Zheng & Weng, 2019).....	73
Figure 6.3. Energy consumption intensity differences (MJ/m^2) by month for commercial buildings constructed at different times between the year 2050 and 1991–2005 under the RCP8.5 emission scenario: (a) total energy consumption; (b) space cooling; and (c) space heating (Zheng & Weng, 2019).....	74

Figure 6.4. Diurnal change in absolute difference in the average building energy intensity (MJ/m²) between 2050 and 1991–2005 under the RCP8.5 emission scenario across building types in Los Angeles in August: (a) total energy and (b) cooling energy; change in energy intensity (KJ/m²) under the RCP8.5 emission scenario across different TMY3 weather zones in Los Angeles in August: (c) diurnal total energy intensity change and (d) diurnal cooling energy intensity change (Zheng & Weng, 2019).76

Figure 6.5. The spatial variation of total energy consumption changes in 2050 due to climate change in Los Angeles: (a) annual relative change (%) under the RCP8.5 scenario; (b) annual relative change (%) under the RCP6.0 scenario; (c) annual energy intensity absolute difference (MJ/m²) under RCP8.5 scenario; (d) annual energy intensity absolute difference (MJ/m²) under the RCP6.0 scenario. Note: this sixth version of neighborhood boundaries were defined by the Los Angeles Times in June 2010, which represents the boundaries of communities and social organizations within each city (Zheng & Weng, 2019).79

Figure 6.6. The spatial variation of cooling energy consumption changes by 2050 caused by climate change in Los Angeles County at the neighborhood scale: (a) annual relative change (%) under the RCP8.5 scenario; (b) annual relative change (%) under the RCP6.0 scenario; (c) annual energy intensity absolute difference (MJ/m²) under the RCP8.5 scenario; (d) annual energy intensity absolute difference (MJ/m²) under the RCP6.0 scenario; the spatial variation of the absolute difference in cooling energy consumption per building in 2050 caused by climate change in Los Angeles County

at the neighborhood scale (MJ/m ²): (e) under the RCP8.5 scenario; (f) average floor area per building (m ²) (Zheng & Weng, 2019).....	80
Figure 7.1. The location of the two study sites for evaluation of green roofs and photovoltaic panels on building Energy Savings: Glendale and Koreatown, Los Angeles County, California, USA.	86
Figure 7.2. Annual energy savings (MJ/m ²) for green roofs on the tested buildings compared to traditional roofs under the RCP8.5 emission scenario in 2050: (a) Glendale; (b) Koreatown.....	89
Figure 7.3. Percentage breakdown (%) of the individual components contributing to the simulated annual electricity savings from green roofs compared with traditional roofs under the RCP8.5 emission scenario in 2050: (a) Glendale; (b) Koreatown.....	90
Figure 7.4. Percentage (%) of annual electricity savings from the integration of green roofs and photovoltaic systems compared with traditional roofs under the RCP8.5 emission scenario in 2050: (a) Glendale; (b) Koreatown.....	91
Figure 7.5. Percentage (%) of monthly electricity savings from green roofs compared with traditional roofs under the RCP8.5 emission scenario in 2050: (a) Glendale; (b) Koreatown.....	96
Figure 7.6. Differences (%) in monthly electricity savings for various green roof settings applied to the selected full-service restaurant constructed before 1980 under the RCP8.5 emission scenario in 2050 in Glendale, Los Angeles County, USA.	99

LIST OF ABBREVIATIONS/ACRONYMS

AADT	Annual Average Daily Traffic
ACH	Air Changes Per Hour
AD	Absolute Difference
AR4	Fourth Assessment Report
AR5	Fifth Assessment Synthesis Report
ASHRAE	The American Society of Heating, Refrigerating and Air-Conditioning Engineers
ASTER	Advanced Spaceborne Thermal Emission and Reflection Radiometer
BIM	Building Information Modeling
Bsk	Cold Semiarid
CBECS	Commercial Buildings Energy Consumption Survey
CCWorldWeatherGen	Climate Change World Weather File Generator
COP	Coefficient of Performance
Csa	Hot Summer Mediterranean
Csb	Warm Summer Mediterranean
CTPP	Census Transportation Planning Product
DOE	Department of Energy
EIA	Energy Information Administration
EUI	Energy Use Intensity

GCAM	Global Change Assessment Model
GJ	Gigajoule
GHG	Greenhouse Gas
GIS	Geography Information Systems
HVAC	Heating, Ventilation, and Cooling
IECC	International Energy Conservation Code
IPCC	Intergovernmental Panel on Climate Change
KJ	Kilojoule
LAI	Leaf Area Index
LST	Land Surface Temperature
MJ	Megajoule
NDVI	Normalized Difference Vegetation Index
NSRDB	National Solar Radiation Data Base
OMIS	Operative Modular Imaging Spectrometer
PeMS	Performance Measurement System
PV	Photovoltaic
Q_b	Building Energy Consumption
Q_f	Anthropogenic Heat Flux
Q_m	Human Metabolism
Q_v	Traffic Emission
RC	Relative Change
RCPs	Representative Concentration Pathways
RCP2.6	Mitigation Scenario in Representative Concentration Pathways

RCP4.5	Low-medium Emission Scenario in Representative Concentration Pathways
RCP6.0	High-medium Emission Scenario in Representative Concentration Pathways
RCP8.5	High Emission Scenario in Representative Concentration Pathways
RECS	Residential Energy Consumption Survey
SEB	Surface Energy Balance
TMY	Typical Meteorological Year
TMY3	The Third Typical Meteorological Year Collection
UBL	Urban Boundary Layer
UCL	Urban Canopy Layer
UHI	Urban Heat Island
VMT	Vehicle Miles Traveled
W	Watt

CHAPTER 1

INTRODUCTION

1.1 Research Background

Although urban areas cover only approximately 2% of the total global land area, 55% (4.2 billion) of the world's population lives in urban areas as of 2018. This proportion is expected to increase to 68% by 2050, which could add another 2.5 billion people to urban areas (United Nations Department of Economic and Social Affairs, 2018). North America is the most urbanized region worldwide, with 82% of its population living in urban areas as of 2018 (United Nations Department of Economic and Social Affairs, 2018). The unprecedented rate of urbanization could bring many unforeseen environmental problems. Increased energy demand is one of the most important issues to be considered. Urbanized areas account for 67–76% of global final energy consumption and 71–76% of fossil fuel-related greenhouse gas (GHG) emissions (Gunalp et al., 2017; Seto et al., 2014). Because the world's urban population will continue to increase, energy demand in cities is predicted to increase over the next 20 years and likely beyond (International Energy Agency, 2009; Quah & Roth, 2012). Continued urbanization will impact urban climate, as the increasing anthropogenic heat flux (Q_f) associated with growing energy consumption in cities can directly affect the urban boundary layer (UBL) and urban canopy layer (UCL) over different spatial and temporal scales (Oke, 1976; Oke, 2006). The UCL lies below the mean roof level and consists of many microclimates as a result of the

heterogeneous nature of the urban environment, while the UBL is the overlying layer of UCL, which has characteristics that are modified by the integration of the UCL effects into a regional or mesoscale climate (Roth, Oke, & Emery, 1989). Q_f can originate from energy consumption in buildings, releases from industrial plants and vehicle exhaust, and human metabolism effects within cities. Q_f is an important component of the urban Surface Energy Balance (SEB) system, which is a key to understanding urban environmental issues and can be quantified by the following equation (Oke, 1987):

$$R_n + Q_f = H + LE + G \quad (1)$$

where R_n is net radiation, Q_f is anthropogenic heat flux, H is sensible heat, LE is latent heat, and G is ground heat. The sum of the net radiation and anthropogenic heat denotes the total available energy in urban environments, whereas the sum of sensible heat, latent heat, and ground heat is the dissipation of available energy through turbulent transport, evaporation, condensation, and advection (Nie, Sun, & Ni, 2014).

For dense cities with high-energy demands, Q_f can potentially be an important or even a dominant component of the SEB (Hamilton et al., 2009; Hu, Yang, Zhou, & Deng, 2012; Nie et al., 2014). In previous studies, a comparison between Q_f and solar radiation indicated that Q_f can be equal to, or even greater than, the incident solar radiation during winter (Hamilton et al., 2009; Nie et al., 2014). Moreover, Q_f was demonstrated to be a major contributor to urban heat island (UHI) formation (Fan & Sailor, 2005; Hu et al., 2012; Ohashi et al., 2003; Wong et al., 2015). The notion of an UHI effect can be characterized by a large stretch of nonevaporating

impervious materials covering urban areas such as concrete, brick, and asphalt, with a consequent rise in sensible heat flux at the expense of latent heat flux (Oke, 1987).

Building energy consumption is the largest contributor to Q_f (Hamilton et al., 2009; Nie et al., 2014; Quah & Roth, 2012; Sailor & Lu, 2004; Zhou, Weng, Gurney, Shuai, & Hu, 2012) in many cities. Building energy consumption accounted for 41% of U.S. primary energy consumption in 2010, and approximately 50% of building energy consumption was for space heating and cooling (United States Department of Energy, 2012; Huang & Gurney, 2016). Climate change will affect the energy system in a number of ways, one of which is through changes in the demands for heating and cooling in buildings (Wang & Chen, 2014; Xu, Huang, Miller, Schlegel, & Shen, 2012; Zhou, Eom, & Clarke, 2013). Tropical, subtropical, and some mid-latitude cities can expect different levels of increase in annual building energy use because the increase in cooling energy consumption cannot be offset by the decrease in heating energy consumption that might result from climate warming. The increase in annual building energy usage in these cities will result in higher carbon emissions, as traditional fossil fuels are still the major electricity production resources that are used for heating and cooling in buildings. Since buildings account for major parts of a city's energy consumption, it is vital to more seriously consider building sector energy in support of urban sustainability (Mastrucci, Baume, Stazi, & Leopold, 2014; Shi, Fonseca, & Schlueter, 2017), especially in the context of global warming.

1.2 Problem Statement

Because Q_f is significant for understanding the urban SEB, urban energy transfer, and its effect on urban climate, numerous studies have been conducted to estimate Q_f in mid-latitude cities (Chapman, Watson, & McAlpine, 2016; Ferreira, de Oliveira, & Soares, 2010; Grimmond, 1992; Hamilton et al., 2009; Ichinose, Shimodozono, & Hanaki, 1999; Lee, Song, Baik, & Park,

2009; Nie et al., 2014; Papachristos, 2015; Sailor & Lu, 2004; Smith, Lindley, & Levermore, 2009; Zhou et al., 2012), subtropical cities (Chow et al., 2014; Park, Schade, Werner, Sailor, & Kim, 2016; Wong et al., 2015), tropical cities (Quah & Roth, 2012; Zhang, Weng, Lin, & Zhang, 2015), and at the global scale (Allen, Lindberg, & Grimmond, 2011; Flanner, 2009; Makar et al., 2006). The winter Q_f profile is generally greater in magnitude than the corresponding summer profile in mid-latitude cities (Lee et al., 2009; Sailor & Lu, 2004). However, in subtropical or tropical cities, Q_f in warmer months is equal to or larger than Q_f in cooler months (Ichinose et al., 1999; Quah & Roth, 2012; Wong et al., 2015). In addition to the climate effect, the population density also contributes to differences in Q_f among cities (Ichinose et al., 1999; Wong et al., 2015). The magnitude of Q_f varies greatly not only between cities but also within cities, and is subject to per capita energy use, building density, and meteorological conditions (Chapman et al., 2016; Chow et al., 2014; Hamilton et al., 2009; Heiple & Sailor, 2008; Ichinose et al., 1999; Quah & Roth, 2012; Smith et al., 2009).

The majority of previous studies used one of three approaches to estimate Q_f : (1) the energy budget residual approach, (2) the inventory approach, and (3) the Geographic Information Systems (GIS) modeling approach. The energy balance residual approach estimates Q_f through Equation (1) by measuring net radiation, sensible heat, latent heat, and ground heat using remote sensing meteorological data (Hu et al., 2012; Kato & Yamaguchi, 2005; Kato, Yamaguchi, Liu, & Sun, 2008; Wong et al., 2015; Xu, Wooster, & Grimmond, 2008; Yang, Chen, & Cui, 2014; Zhou et al., 2012), and long-term eddy covariance from a flux tower (Chow et al., 2014; Park et al., 2016). The inventory approach, which is also called top-down approach, estimates anthropogenic heat based on population density and energy consumption statistical data from buildings and vehicles (Grimmond, 1992; Ichinose et al., 1999; Kłysik, 1996; Pigeon, Legain,

Durand, & Masson, 2007; Sailor, Georgescu, Milne, & Hart, 2015; Sailor & Lu, 2004; Smith et al., 2009). The GIS modeling approach (Hamilton et al., 2009; Heiple & Sailor, 2008; Quah & Roth, 2012; Sailor, Brooks, Hart, & Heiple, 2007; Zhou et al., 2012) is also called the bottom-up approach. Unlike the inventory approach, the GIS approach uses energy consumption modeled at fine scales (e.g., individual buildings) to aggregate the information up to broader scales of interest (Quah & Roth, 2012).

These three approaches have their respective advantages and disadvantages. The limitation of the inventory approach is that the estimation accuracy relies on data availability and quality. Moreover, it would be difficult to quantify Q_f at fine scales due to spatial (usually county or statewide) and temporal (usually annual or monthly) resolution limitations on the data. The energy balance residual approach is more straightforward, but each component in the model can introduce uncertainties and propagate errors towards the final estimated result (Zhou et al., 2012). The approach can also be limited by the spatial and temporal resolutions of remote sensing satellite images and meteorological data, as it is difficult to account for hourly variations in Q_f emissions. The GIS-based spatial analysis approach is the only approach that can measure Q_f at any temporal (e.g., annual, monthly, weekly, daily, and diurnal) or spatial resolution. In other words, the GIS-based approach is more reliable than the other two approaches as it can directly measure Q_f from each of the contributing sources at fine spatial (individual building level) and temporal (daily and diurnal) scales. However, this approach is time consuming and requires large volumes of data. A common drawback in the existing studies is the absence of validation for the estimated Q_f at fine scales.

The difficulties in estimating Q_f mainly originate from the uncertainties in building energy consumption, which is a major contributor to Q_f because buildings in urban areas were

constructed during different periods and with different technologies, functions, schedules, and vacancy statuses. However, in developing urban sustainability strategies, policy makers need to consider more sustainable means of building energy supply and consumption. These means may include efforts to transfer building energy sources from traditional fossil fuels to renewable energy sources (Chemisana & Lamnatou, 2014; Feng, Zheng, Wang, Yu, & Su, 2015; Waibel, Evins, & Carmeliet, 2017), increasing the efficiency of energy transport (Sathaye et al., 2012; Sathaye et al., 2013), and advancing the energy-saving abilities of new and existing buildings (Dimond & Webb, 2017; Herrera-Gomez, Quevedo-Nolasco, & Pérez-Urrestarazu, 2017; Tang & Qu, 2016; Taylor, de Menezes, & McSharry, 2006). Decision making for urban building energy savings must not only consider current regional environmental and social-economic factors in specific cities but also project future changes, including climate change, which may impact or exacerbate the current urban environmental issues caused by greenhouse gases emitted by buildings. Previous researchers have used different approaches to study the impact of climate change on building energy demand (Andrić et al., 2016; Huang & Gurney, 2016; Sailor, 2001; Shen, 2017; Wang & Chen, 2014; Xu et al., 2012). This impact can be affected by many environmental and social-economic factors, such as current local climate conditions, city function, economic status, population density, and building thermal characteristics. The approaches that have been used in existing studies can be grouped into two categories: top-down and bottom-up strategies. The top-down strategy focuses on the broader spatial (global, national, and state levels) and temporal scales (annual), which compare the impacts of climate change on heating and cooling energy across different states and countries. On the other hand, the bottom-up strategy focuses on fine spatial (district, neighborhood, and individual building) and temporal (hourly) scales (Andrić et al., 2016; Berger et al., 2014; Cellura, Guarino, Longo, & Tumminia,

2018; Dirks et al., 2015; Huang & Gurney, 2016; Li et al., 2018; Shen, 2017; Wan, Li, Pan, & Lam, 2012; Wang & Chen, 2014). This strategy typically simulates future energy demands for individual buildings based on detailed building or building prototype information and the projected future climate. Then, the simulated energy demands are compared with current energy demands to quantify the differences.

The other important direction in urban sustainability research is to apply mitigation strategies such as urban greening and increasing renewable energy sources to ease environmental problems, especially the UHI caused by urbanization. Urban greening is one of the most effective strategies that can reduce UHIs by intercepting solar energy, providing shade to the surface and increasing latent heat exchange for the evapotranspiration process (Wang & Akbari, 2016). Research on urban greening strategies mainly include tree planting (Mohajerani, Bakaric, & Jeffrey-Bailey, 2017; Wang, Akbari, & Chen, 2016; Wang & Akbari, 2016), façade greening (Li & Ratti, 2018; Moren & Korjenic, 2017), and roof greening (Morakinyo, Dahanayake, Ng, & Chow, 2017; Sailor, 2008; Shafique, Kim, & Rafiq, 2018; Susca, Gaffin, & Dell'osso, 2011). In high-density urban commercial areas, street trees provide limited contributions to UHI mitigation because their canopies cannot provide shade for buildings taller than the trees themselves. Moreover, there are ground surface area limitations for ground level tree planting (Morakinyo et al., 2017). Therefore, green roofs and rooftop solar photovoltaic (PV) systems research (Dimond & Webb, 2017; Lukač & Žalik, 2013; Schuffert, 2013; Zheng & Weng, 2014) have become popular. A green roof is a roof with suitable growing media and vegetation. Since green roofs and PV systems are both commonly accepted as sustainable roofing systems, a few studies (Chemisana & Lamnatou, 2014; Lamnatou & Chemisana, 2014, 2015; Moren & Korjenic, 2017; Scherba, Sailor, Rosenstiel, & Wamser, 2011; Schindler et al., 2018) have assessed the benefits

of PV-green roofs, which integrate green roofs with PV systems. However, the majority of these studies focus on life cycle analyses (Lamnatou & Chemisana, 2014) and the effect of green roofing on PV performance (Chemisana & Lamnatou, 2014; Lamnatou & Chemisana, 2015; Moren & Korjenic, 2017; Schindler et al., 2018). Scherba et al. (2011) is the only study that has attempted to assess the benefits of the PV-green roofs in urban sustainability by comparing these systems with other roofing technologies, such as dark roofs, cool roofs, green roofs, and PV roofs in terms of sensible heat reduction. Unfortunately, studies that focus on the mitigation effects of PV-green roofs on building energy demand caused by climate change do not yet exist.

To develop a sustainable environment for a specific city under the context of climate change, policy makers must understand the characteristics of Q_f as well as its major contributors, as these factors may exacerbate the UHI effect under a warmer climate in the future. Since Q_f has large spatial and temporal variations, there is a need for high spatial and temporal resolution simulations. However, such simulations of Q_f are subject to data availability from multiple sources and the robustness of time-dependent simulation models (Sailor, 2011) and are difficult to conduct using a single approach. Therefore, a hybrid approach that estimates each component of Q_f with high spatial and temporal resolution in large urban areas is in high demand.

Attention should be given to building energy consumption, as this factor is the major component of Q_f and is also sensitive to climate change. Existing studies have either combined climate change modeling with broad-scale (annual and state level) inventory data of buildings and social-economic activities or used representative building prototypes to assess the effects of climate change in different climate zones. However, cities, especially megacities, are mixed with different types of buildings, which may be constructed during different periods and with different technologies, functions, and schedules. Therefore, for municipal governments, the sustainable

development goals are different even among neighborhoods. In developing “green and sustainable” communities, municipalities would need disaggregated data, which cover an entire city with high spatial and temporal resolutions to understand the current urban energy flows and potential changes in future energy demands at local scales. Only in this way can appropriate measures be chosen that are targeted to specific locations. Clearly, the approaches used in the existing studies cannot aid in achieving those sustainable development goals. In other words, an essential city government approach that assesses the impact of climate change on building energy demand at fine scales (sub-city level) is lacking. Moreover, in many cases, the mitigation potential of building energy consumption increases induced by climate change has been briefly discussed in existing publications (Cellura et al., 2018; Herrera-Gomez et al., 2017; Li et al., 2018; Sathaye et al., 2012; Shafique et al., 2018). Little research has been conducted to test the performance of mitigation options, such as sustainable roofs (green roofs, PV roofs, or PV-greens), based on the results of previous studies, which can be valuable in guiding policy makers.

1.3 Research Objectives

The GIS modeling technique has a strong ability to capture, manipulate, analyze, and manage large amounts of inventoried data with geographic attributes at high spatial and temporal resolutions. However, GIS modeling has not been applied fully in urban building energy use and sustainable urban energy management studies. The objective of this dissertation is to fill gaps in the current literature by proposing a novel hybrid Q_f modeling approach, which combines inventory and GIS modeling methods to create a 365-day, hourly Q_f profile at the sub-city scale. In the following section, a GIS-based approach that combines climate change modeling, building energy simulations, and fine-scale (individual building level) inventory data of building characteristics is detailed to quantify the effects of climate change on building energy demand.

Finally, the potential mitigation effects of PV-green roofs on increased building energy demand were assessed for selected buildings, as these buildings were found to have greater energy increases than others in the context of climate change. More specifically, the objectives of this dissertation are:

- 1) To develop a high spatial and temporal resolution Q_f profile that can be readily incorporated into urban energy balance and analyze Q_f across multiple spatial and temporal scales;
- 2) To develop an analytical method and useful database that can allow the city government to foresee the sensitivity of different city regions to climate change regarding building energy demand at different spatial and temporal scales; and
- 3) To test the potential mitigation effects of green roofs and PV-green roofs on the buildings that are more vulnerable to climate change in terms of energy demand increase. Through this research, the development of a useful approach for the city government to work towards a sustainable city is expected by tailoring adaption and mitigation strategies for buildings in different districts.

1.4 Research Questions

In this dissertation, an attempt was made to answer the following research questions:

- 1) What are the typical diurnal Q_f profiles for all four seasons during workdays and weekends across different land use types, and what are the major contributors to Q_f ?
- 2) What changes in annual building energy demand are predicted to occur by 2050, and do these trends remain the same when examined at finer temporal scales?
- 3) Which city areas are more vulnerable to climate change and what are the driving forces?

- 4) To what extent do green roofs or PV-green roofs mitigate the building energy demand increase caused by climate change? What building types can receive the most benefit from energy savings?

To answer the four research questions, five hypotheses are put forth:

- 1) Building energy demand is the major contributor to Q_f , and building energy demand can make the typical diurnal Q_f profiles across all four seasons appear to have different shapes due to changes in cooling and heating demands;
- 2) The majority of building types show an obvious annual increase in energy demand by 2050, and the variation in energy increases across different building types will be even larger at finer temporal scales (i.e., monthly and diurnal);
- 3) Areas with more commercial buildings are more vulnerable to climate change because commercial buildings have higher energy consumption intensities than residential buildings;
- 4) The installation of PV-green roofs can reduce at least 20% of net building energy demand increase caused by climate change for all chosen types of test buildings, and the reduction extent will vary by building type; and
- 5) Building types that are predicted to have the highest energy demand increase caused by climate change receive the most benefits in terms of energy savings.

1.5 Structure of the Dissertation

This dissertation comprises eight chapters. In Chapter one, an introduction of the research background, problem statement, research objectives, and research questions are presented. In Chapter two, previous efforts related to the proposed study are reviewed, including Q_f modeling, simulations of climate change impacts on building energy demand, and relevant studies on green

roofs and PV-green roofs. A brief description of the study area and dataset used are provided in Chapter three. In Chapter four, the methodology of the study is described, including research design, data acquisition, and data processing. The results of the Q_f profile estimation at high spatial and temporal resolutions are presented in Chapter five. In Chapter six, the results of modeling climate change effects on building energy demand are described. The results of Chapter 5 and Chapter 6 have been published (Zheng & Weng, 2018; Zheng & Weng, 2019) and are available in Appendix A and B. The potential mitigation effects of green roofs and PV-green roofs on buildings that are more vulnerable to climate change in terms of energy demand increase are analyzed in Chapter seven. This work will be submitted to *Energy and Buildings* for publication. Finally, in Chapter eight, the major findings of this dissertation and future work are discussed.

CHAPTER 2

LITERATURE REVIEW

2.1 Introduction

In this chapter, the existing publications related to the proposed study are reviewed. More specifically, the literature covering the following topics was discussed: 1) the methods used to estimate Q_f ; 2) energy demand changes for different building types in different climate zones caused by climate change, and the methods applied to model this effect; and 3) studies evaluating the role of green roofs and PV-green roofs to reduce building surface temperature, sensible heat, and building energy consumption.

2.2 Anthropogenic Heat Discharge Estimation in Urban Areas

Based on the SEB theory, UHI is mainly caused by the combination of energy consumption, vegetation decreases, and impervious surface area increases (Kato & Yamaguchi, 2005; Zhou et al., 2012). Quantifying Q_f and its spatial pattern is important for improving the understanding of human impacts on the urban environment, which is a key issue in global climate change (Zhou et al., 2012). In this section, three major categories of approaches used in previous studies are discussed to estimate Q_f : (1) the energy budget residual approach, (2) the inventory approach, and (3) the GIS modeling approach.

2.2.1 Anthropogenic Heat Flux Estimation Using the Energy Budget Residual Approach

The energy budget residual approach was designed based on the energy balance equation developed by Oke (1987), which estimates Q_f as the residual term of sensible heat flux, latent heat flux, ground heat flux, and net radiation. The majority of studies (Hu et al., 2012; Kato & Yamaguchi, 2005; Kato et al., 2008; Wong et al., 2015; Xu et al., 2008; Yang et al., 2014; Zhou et al., 2012) have used a combination of remote sensing and meteorological data. Kato and Yamaguchi (2005) were the first to separate Q_f from natural heat radiation in sensible heat flux, based on the energy balance model using Advanced Spaceborne Thermal Emission and Reflection Radiometer (ASTER) imagery and ground meteorological data. Xu et al. (2008) used the Operative Modular Imaging Spectrometer (OMIS) along with a survey map and meteorological data to model urban sensible heat in Shanghai, China, at multiple spatial scales. The researchers considered Q_f to be the increased sensible and latent heat value forms. Hu et al. (2012) were the first to apply a continuous layer of meteorological data along with remote sensing data (two ASTER images) in the estimation of Q_f and its seasonal and spatial variations in Beijing, China. Wong et al. (2015) developed a novel algorithm to model Q_f for mixed pixels, which decomposed image pixels of HJ-1B satellite imagery into fractions of impervious surfaces and vegetation. Some other studies (Chow et al., 2014; Park et al., 2016) used data from long-term eddy covariance flux towers, which are the stations built near an urban center that utilize micrometeorological techniques to measure the fluxes over the surface, to estimate daily local Q_f .

Although the energy balance residual approach is simpler and more convenient, this approach contains notable limitations and drawbacks. First, the model can introduce uncertainties and propagate errors towards the final estimated result (Zhou et al., 2012) due to algorithm complexity, inconsistencies in spatial and temporal resolutions between remote

sensing and meteorological data, and difficulty in obtaining surface morphometric input data. The accumulation of errors in the measurements of sensible heat, latent heat, and ground heat can result in under- or over-estimation of Q_f (Park et al., 2016). Moreover, this approach can be limited by the spatial and temporal resolutions of remote sensing satellite images and meteorological data, as it is difficult to account for hourly variations in Q_f emissions. Although studies that use data from long-term eddy covariance flux towers have obtained hourly estimations of Q_f , the locations of long-term eddy covariance flux towers can be a disadvantage, as the towers are not available in most parts of a studied city.

2.2.2 Anthropogenic Heat Flux Estimation Using the Inventory Approach

The inventory approach, which is also called the top-down approach, estimates anthropogenic heat based on population density and energy consumption statistics data from buildings and vehicles (Grimmond, 1992; Ichinose et al., 1999; Kłysik, 1996; Pigeon et al., 2007; Sailor et al., 2015; Sailor & Lu, 2004; Smith et al., 2009). The inventory approach requires data at broad aggregate scales (e.g., annual) and downscales these data into finer scales of interest (e.g., hourly) (Quah & Roth, 2012). Since energy consumption data are available at broad scales, this approach has been applied to estimate Q_f in cities throughout the world, for example, in Vancouver, Canada (Grimmond, 1992), Lodz, Poland (Kłysik, 1996), Tokyo, Japan (Ichinose et al., 1999), Toulouse, France (Pigeon et al., 2007), and Manchester, United Kingdom (Smith et al., 2009). The limitation of an inventory approach is that estimation accuracy relies on data availability and quality. As mentioned in the Introduction, due to the limitations in the spatial (usually county or statewide) and temporal (usually annual or monthly) resolution of inventory data, it is difficult to quantify Q_f at fine spatial (within-city level) and temporal (daily or hourly) scales.

2.2.3 Anthropogenic Heat Flux Estimation Using the GIS Modeling Approach

In contrast to the inventory approach, the GIS modeling approach (Hamilton et al., 2009; Heiple & Sailor, 2008; Quah & Roth, 2012; Sailor et al., 2007; Zhou et al., 2012) uses energy consumption modeled at fine spatial scales (e.g., individual buildings) to aggregate the information to broader scales of interest (Quah & Roth, 2012). Earlier studies (Kikegawa, Genchi, Kondo, & Hanaki, 2006; Kikegawa, Genchi, Yoshikado, & Kondo, 2003; Masson, 2000; Ohashi et al., 2007) simply estimated Q_f by integrating building energy simulation results with an urban canopy meteorological model. Recent studies (Hamilton et al., 2009; Heiple & Sailor, 2008; Sailor et al., 2007; Zhou et al., 2012) have integrated more detailed building energy simulations for prototypical buildings with GIS database containing attributes such as building types, ages, and sizes. Other studies (Chapman et al., 2016; Ferreira et al., 2010; Lee et al., 2009; Quah & Roth, 2012) have added traffic emissions and human metabolism to Q_f estimations.

The GIS approach is considered more reliable than the other two approaches, since this approach measures Q_f directly from each of the contributing sources, such as building energy consumption, traffic emission, industrial emission, and human metabolism. The GIS approach has the advantage of measuring Q_f at any temporal (annual, monthly, weekly, daily, and diurnal) or spatial resolution because any unrelated information can be related, such as hourly meteorological data and individual building information by using location as the key index variable. In the existing studies, a common drawback of this approach is the absence of validation data. For example, Zhou et al. (2012) simulated building energy consumption at the individual building level in the city of Indianapolis but used commercial and residential building energy consumption survey data for the entire Census Division to validate their simulation

results. Using validation data at broader scales, such as national, central census division, or at the state level provides limited aid in improving the accuracy of within-city simulations.

2.2.4 Anthropogenic Heat Flux Estimation Using the Hybrid Approach

Because the above three approaches have their respective advantages and disadvantages, the integration of multiple approaches is needed. Although the majority of previous studies were restricted to a single approach, a few studies in recent years combined multiple approaches to estimate Q_f (Chow et al., 2014; Nie et al., 2014; Park et al., 2016; Zhou et al., 2012). Zhou et al. (2012) examined the similarities of Q_f spatial patterns estimated by the energy balance residual approach and the GIS modeling approach. However, the GIS modeling approach only included building energy consumption modeling and ignored emissions from traffic, human metabolism, and industrial plants. These studies (Chow et al., 2014; Nie et al., 2014; Park et al., 2016) were also restricted to small study areas at the local spatial scale. The data required by the energy balanced residual approach (Chow et al., 2014; Park et al., 2016) were measured by a long-term eddy covariance flux tower built near the study area, which is not available in every city or every part of the city. The inventory approach adopted by Nie et al. (2014) was based on an on-campus survey, which may be infeasible at broader spatial scales due to the unavailability of such data. In addition, the differences between workdays and weekends were ignored due to lack of high temporal Q_f simulation. Therefore, despite combined approaches, the greatest challenge in the estimation of Q_f that remains unsolved is the availability and quality of data from multiple sources and the robustness of time-dependent simulation models.

2.3 Estimating the Effect of Climate Change on Building Energy Demand in Urban Areas

Building energy consumption is a major component of Q_f and UHI. Previous studies have applied different approaches to study the impact of climate change on building energy demand.

Approaches used in the existing studies can be grouped into two categories: top-down and bottom-up strategies.

2.3.1 Top-down Strategy of Building Energy Demand Modeling

The top-down strategy focuses on broad spatial (global, national, and state levels) and temporal scales (annual), which compare the impact of climate change on heating and cooling energy across different states and countries. There are two types of widely used approaches in the top-down strategy: observation based regression/prediction (Sailor, 2001; Sathaye et al., 2012; Sathaye et al., 2013; Xu et al., 2012) and global/regional energy modeling (McFarland et al., 2015; Scott et al., 2015; Zhou et al., 2014; Zhou & Gurney, 2010; Zhu, Pan, Huang, & Xu, 2016). The observation-based approach uses the historical relationship of energy consumption and climate data to predict future energy consumption under a changing climate. Although this approach makes predictions based on the reference data, the output resolution is determined by the historical input data resolution, and the estimation accuracy depends on the quality of the selected regression model (Huang & Gurney, 2016). Moreover, this approach ignores the effect of changing building technologies, which may play an important role in energy consumption. The global/regional energy modeling approach uses a numerical model to estimate national/state-level building energy consumption by combining building technologies, policy, economy, population growth, and climate. The impact of global warming on building energy consumption is based on simulations of different Intergovernmental Panel on Climate Change (IPCC) scenarios. For example, Zhou et al. (2014) presented a detailed building energy model with U.S. state-level representation, nested in an integrated assessment framework of the Global Change Assessment Model (GCAM). This study revealed the spatial heterogeneity of the global warming

impact on heating and cooling energy and fuel uses in the building sector across all 50 states of the United States.

2.3.2 Bottom-up Strategy of Building Energy Demand Modeling

The bottom-up strategy focuses on fine spatial (district, neighborhood, and individual building) and temporal (hourly) scales (Andrić et al., 2016; Berger et al., 2014; Cellura et al., 2018; Dirks et al., 2015; Ghedamsi et al., 2016; Huang & Gurney, 2016; Li et al., 2018; Shen, 2017; Wan et al., 2012; Wang & Chen, 2014). This strategy typically simulates future energy demands for individual buildings based on detailed information of the building or building prototype and the projected future climate. Then, the simulated energy demands are compared with the current energy demands to quantify the differences. Berger et al. (2014) calculated and compared heating and cooling demands from nine selected office buildings under current and future conditions in Vienna, Australia. This study discovered distinct differences in the energy performance of buildings from different periods of construction that adopted various building technologies. Andrić et al. (2016) compared the energy simulation results from a district of buildings in Lisbon, Portugal, from 2010 and 2050 and discovered that heat demand density could decrease by 22.3–52.4% by 2050. Huang and Gurney (2016) used the building prototypes developed by the U.S. Department of Energy (DOE), which included 18 types and three age groups, and weather data from different climate zones to assess the variations in climate change impact on different spatial and temporal scales. Their results suggested that the impact variation within climate zones can be larger than the variation between climate zones and that the potential bias may be substantial when estimating climate-zone scale changes with a small number of representative buildings. Shen (2017) downscaled the future climate data into hourly scales using

a “morphing” method to predict the future energy use of residential buildings in the United States.

Although the bottom-up strategy can quantify the impact of climate change on building energy demands at the scale of individual building, a common drawback in this approach is that only a few buildings were assessed. The conclusions drawn cannot represent the entire building stocks in the study area.

2.4 Studies on the Roles of Green Roofs in Building Energy Consumption Reduction in Urban Areas

Since ground trees can provide only limited cooling in high-density cities, especially for buildings taller than tree canopies, green roofs have become popular as a potential alternative means for re-establishing the connection between nature and a city (Alcazar, Olivieri, & Neila, 2016), enhancement of the aesthetic appearance of buildings (Catalano, Marcenò, Laudicina, & Guarino, 2016) and improvement of environmental quality (Morakinyo et al., 2017). Modern green roofs generally consist of a number of layers, including vegetation, growth substrate, filter fabric, drainage elements, root barriers, insulation, and water proofing membranes, which are dependent upon location and city requirements (Hashemi, Mahmud, & Ashraf, 2015; Lamera, Becciu, Rulli, & Rosso, 2014; Morakinyo et al., 2017; Vijayaraghavan, 2016). These layers can enhance the insulation capacity of a conventional roof by controlling heat transfer into buildings (Tam, Wang, & Le, 2016). Because solar radiation is often the main heat source in buildings, roof vegetation can absorb solar heat and evaporate water through evapotranspiration, which creates a cooling effect in the surrounding environment. Green roofs can be classified into intensive and extensive based on the thickness of the substrate layer and the vegetation species planted. Extensive green roofs have thinner substrate layers (up to 15 cm) and limited types of

grasses planted on top (Heusinger, Sailor, & Weber, 2018). The intensive green roofs, which are also called roof gardens, have thicker substrate layers and are planted with taller vegetation, such as shrubs and small trees (Heusinger et al., 2018).

Existing studies have examined the performance of green roofs in building indoor temperature reduction and energy consumption savings by considering various factors, including climate (Morakinyo et al., 2017; Susca et al., 2011; Sailor, Elley, & Gibson, 2012; Semaan & Pearce, 2016; Yang et al., 2018), green roof types (Morakinyo et al., 2017; Silva, Gomes, & Silva, 2016), spatial coverage (Morakinyo et al., 2017), maintenance status (Heusinger et al., 2018; Yang et al., 2018), building density (Morakinyo et al., 2017), and building height (Herrera-Gomez et al., 2017). The majority of existing studies simulated the performance of green roofs using an energy balance model of vegetated rooftops integrated in EnergyPlus software, which was developed by Sailor (2008). This energy balance model was initially designed and has been updated based on validated data collected from monitored green roofs in Florida and Oregon.

Morakinyo et al. (2017) presented a parametric study on the effects of four green roof types (full-extensive, semi-extensive, full-intensive, and semi-intensive) on outdoor/indoor temperature and cooling demand under four different climates (hot-dry, hot-humid, warm-humid, and temperate) and three urban densities. Their results suggested that during the daytime, the cooling effect of green roofs was more apparent in the full-intensive type under all climate conditions. However, the extensive green roof types were demonstrated to have better UHI mitigation potential due to less solar heat absorption during the daytime. Moreover, the cooling effect was also found to follow the order of hot-dry (Cairo), hot-humid (Hong Kong), warm-humid (Tokyo), and temperate (Paris) from strongest to weakest, which can be explained by the interplay between solar intensity, air temperature, and relative humidity. Morakinyo et al. (2017)

also suggested that spatial coverage and building density had less effect than climate conditions and green roof types in cooling performance. Herrera-Gomez et al. (2017) conducted a case study in Seville, Spain, to discuss green roofs as a supplement to existing urban green spaces to buffer the negative effect of increased maximum temperatures due to climate change. They verified the inverse relationship between Land Surface Temperature (LST) and the abundance of vegetation, expressed by the Normalized Difference Vegetation Index (NDVI), and predicted that at least 207 ha of green roof surface (11.3% of the existing roofs) should be added. The researchers also suggested that green roofs can be even more efficient when the height of the building is less than 10 meters, and that the installation of green roofs on taller buildings could have its own benefits, such as providing a cooling effect above the street canopy. Heusinger et al. (2018) discovered that maintenance, such as irrigation, played a vital role in the performance of green roofs. Their results suggested that green roofs reduced urban excess heat by 15–75% when using different irrigation methods in comparison to traditional roofs. However, green roofs only reduced the urban excess heat by 3% when irrigation was not performed. Moren and Korjenic (2017) suggested that plants in the wall-mounted PV-green systems can grow behind PV systems mounted on the façade and promote the performance of the PV systems by reducing their operating temperatures. They further stated that a PV-green system could achieve better performance if it was installed on the south side of a building.

Many existing studies (Sailor et al., 2012; Silva et al., 2016; Susca et al., 2011; Yang et al., 2018) compared green roofs with cool roofs in terms of their cooling abilities; cool roofs are roofs made of a highly reflective type of paint to reflect more sunlight and absorb less heat (United States Department of Energy, 2018). Yang et al. (2018) examined the UHI mitigation potential of green roofs in a tropical climate (Singapore). Their results showed that during peak

hours (9 am to 5 pm), cool roofs reduced heat gain by approximately 0.14 kWh/m² (8%) and green roofs mitigated considerably less at approximately 0.008 kWh/m² (0.4%). For the whole of a summer design day, cool and green roofs can reduce heat gain by 15.53% (37%) and 13.14 (31%) kWh/m², respectively. However, Susca et al. (2011) suggested the opposite results, as they concluded that green roofs saved more building energy than cool roofs at all four testing sites in New York City. Despite the performance in temperature cooling and energy saving, green roofs can provide multiple ecosystem benefits to air quality, biodiversity, retention performance, and microclimate in contrast to single benefit of cool roofs (Heusinger et al., 2018).

In recent years, a few studies (Chemisana & Lamnatou, 2014; Lamnatou & Chemisana, 2014, 2015; Moren & Korjenic, 2017; Scherba et al., 2011; Schindler et al., 2018) have suggested the integration of green roofs with a solar PV system. Scherba et al. (2011) modeled the impact of PV-green roofs on sensible heat reduction in cities located in six climate zones. Their results indicated that the replacement of a traditional black membrane roof with a PV-green roof would reduce the total sensible flux by 50%. Chemisana and Lamnatou (2014) stated that vegetation provided a cooling effect to the PV systems, which can lead to an increase in output, and this cooling effect varies by plant species. Lamnatou and Chemisana (2014) suggested that PV systems can also bring benefits to roof vegetation by protecting the vegetation from exposure to too much sunlight during the summer. Schindler et al. (2018) indicated that the presence of vegetation did not provide any benefit to PV electricity production. However, they stated that the lack of irrigation for vegetation could be the reason because little evapotranspiration occurred.

Although many studies have estimated the cooling effect of green roofs, few studies have evaluated their performance under the context of climate change, especially when integrated with

PV systems. Scherba et al. (2011) are the only researchers thus far who have attempted to assess the benefits of PV-green roofs in sensible heat reduction by comparing it with other roofing technologies. However, they did not quantify the potential mitigation effect of green roofs on building energy demand caused by climate change.

2.5 Summary

Previous attempts related to the research topics in this study were reviewed in this chapter. The greatest remaining challenges in the estimation of Q_f are data availability and quality from multiple sources, and the robustness of time-dependent simulation models. Therefore, a hybrid approach that estimates each component of Q_f with high spatial and temporal resolutions in large urban areas is urgently needed. In developing green and sustainable communities, municipal governments need disaggregated data, which covers the entire city in high spatial and temporal resolutions, to understand current urban energy flows and the potential change in future energy demands at local scales as a result of climate change. Clearly, the approaches discussed in the existing literature cannot aid in achieving these goals. In other words, an approach essential to municipal governments that assesses the impact of climate change on building energy demand at fine scales (sub-city level) is lacking. In addition, the potential mitigation effects of green roofs and PV-green roofs on building energy demand in the context of climate change have not been fully evaluated. The intent of this dissertation is to fill these research gaps by developing an integrated approach of GIS, modeling, and climate change simulation, which has great potential for applications in urban use planning and sustainable urban energy management.

CHAPTER 3

STUDY AREA AND DATA

3.1 Study Area

The study area, Los Angeles County, is located in California, USA (Figure 3.1). The county has a population of 9,818,605 according to the 2010 U.S. Census (United States Census Bureau, 2017), making this county the most populous in the nation. Los Angeles County occupies three climate zones according to the Koppen climate classification. The coastal area has a “warm summer Mediterranean” (Csb) climate with dry and warm summers and moist winters. The inland area, on the other hand, has a “hot summer Mediterranean” (Csa) climate with hotter summers than the coastal area. The northern part of Los Angeles County has a “cold semiarid” (Bsk) climate, which has warm to hot summers and cold winters. The microclimate, which is caused by the topography, makes the county unique, because there are large temperature variations among nearby areas. For example, during the summer, the average temperature along the Santa Monica coast is less than 27 °C (80.6 °F), but inland areas are greater than 32 °C (89.6 °F).

The 2010 inventory data provided by the Energy Atlas show that the building sector emitted the largest amount of greenhouse gases, which accounted for 39.2% of the annual total greenhouse gas emissions (Table 3.1). Therefore, managing building energy consumption under

the climate change context is important for developing a sustainable urban environment in Los Angeles County.

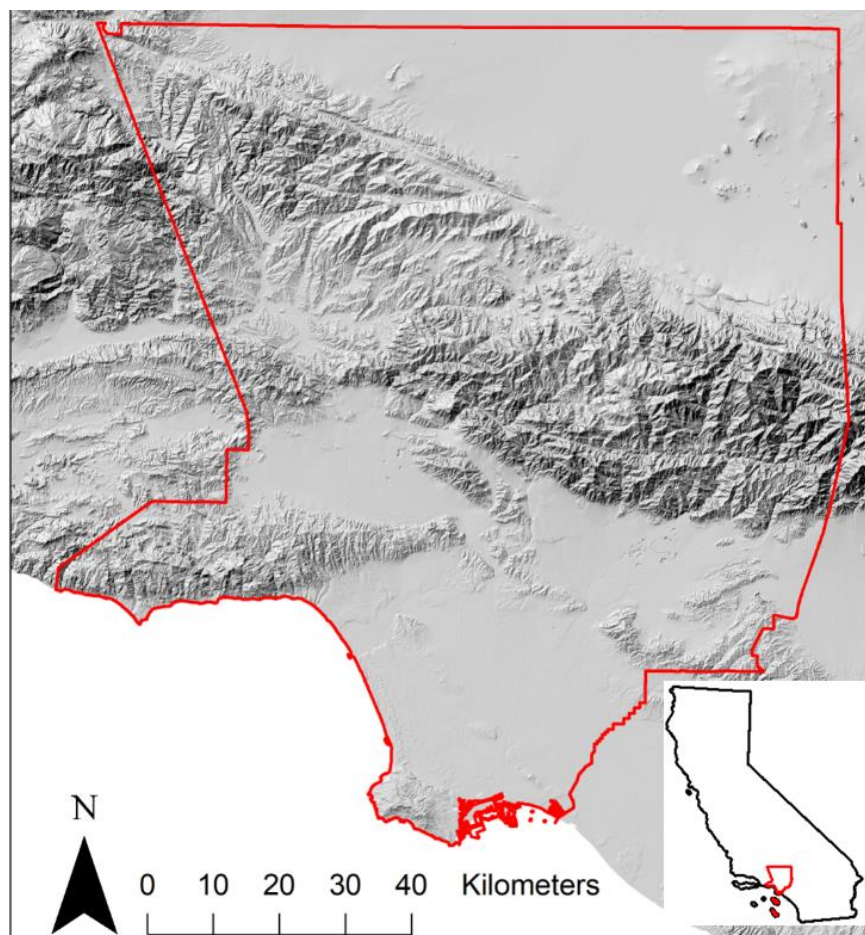


Figure 3.1. The location of the study area, Los Angeles County, California, USA.

3.2 Datasets

The major datasets used in this study area are listed in Table 3.2. To simulate 365-day hourly building energy consumption, datasets included Los Angeles countywide building outlines, building prototypes, Los Angeles County parcel shapefiles, and typical meteorological year (TMY) records. Building outlines provided information on building height, building area, type, and year of construction. The outlines were captured from stereo imagery as part of the LAR-IAC2 Project (2008 acquisition) and updated as part of the LAR-IAC4 (2014) imagery

Table 3.1

Greenhouse gas (GHG) emissions in Los Angeles County by sector (Energy Atlas, 2017; Zheng & Weng, 2019).

Sector	Emissions (MT CO₂e)	Percent of Inventory
Building Energy	38,900,762	39.2%
On-Road Transportation	33,226,317	33.5%
Stationary Sources	19,516,169	19.7%
Solid Waste	4,327,123	4.4%
Water Conveyance	1,117,283	1.1%
Ports	1,059,131	1.1%
Off-Road Transportation	515,044	0.5%
Wastewater Treatment	443,832	0.4%
Agriculture	26,105	0.0%
Los Angeles World Airport	2,760	0.0%
Total	99,134,526	

acquisition. On the other hand, the Los Angeles County parcel data contain information on land use types, which were collected from the Los Angeles County Enterprise GIS website. This sixth version of neighborhood boundaries was defined by the Los Angeles Times (<http://boundaries.latimes.com/set/la-county-neighborhoods-v6/>) in June 2010, which expanded beyond the city to cover all of Los Angeles County and represents the boundary of communities and social organizations within each city; these data were downloaded from the Los Angeles County Enterprise GIS website. Building prototypes and typical meteorological year records were obtained from the U.S. DOE and National Solar Radiation Data Base (NSRDB), respectively. The TMY data was a collation of hourly weather data, which was selected from a database containing data from multiple years, for a specific location in a one-year period. The data included seasonal and diurnal variations and represented the typical climatic conditions for a location. Census Transportation Planning Product (CTPP) shapefiles were used for hourly human metabolism estimation. Annual average daily traffic (AADT) data and county road shapefiles

were acquired to estimate hourly traffic emissions. The annual county energy consumption data were downloaded from the Energy Atlas website, which recorded historical energy consumption data from different sectors (commercial, residential, and industrial) by year and were used for validation and calibration. Finally, open-source solar potential data for all houses in the United States were published by Google on their Project Sunroof website (<https://www.google.com/get/sunroof#p=0>). This data explorer estimates the technical potential of solar power for a single house or region chosen by the user, which was used to analyze the performance of PV-green roofs in the study area.

Diverse spatial scales were found in the data obtained from different sources (Table 3.2). For example, AADT data were collected at a broader scale than the road shapefiles, which can bring challenges to the traffic emission modeling because the heterogeneity at the fine scale (road shapefiles) cannot be reflected at the broad scale (AADT). This dissertation applied different solutions to bridge the gap between broad- and fine-scale datasets in different parts to avoid biases in the modeling results. A downscaling method was used to adjust the AADT data, which were initially at the 1:25,000 scale, and to assign the estimated traffic volumes to all road segments at the 1:12,000 scale. TMY data was not downscaled in the building energy demand simulation because no literature has suggested that temperature, which is the most important factor that affecting building energy consumption (Huang & Gurney, 2016; Sailor & Lu, 2004), varies at the individual building (1:5,000) or neighborhood (1:24,000) scale. Therefore, the same meteorological data were used for different buildings, if they were located within the same TMY weather zone. The specific workflows for scale integration in the building energy consumption simulation and traffic emission modeling are presented in detail in Sections 4.2.2 and 4.2.3, respectively.

Table 3.2

Datasets used in this study and data sources (Zheng & Weng, 2018).

Data	Source	Scale
Census Transportation Planning Product (CTPP) shapefiles	U.S. Census website	Approx. 1:12,000
Los Angeles countywide building outline dataset	Los Angeles County Data Portal	Approx. 1:5,000
Building prototypes	U.S. Department of Energy (DOE)	No Spatial Scale
Los Angeles County parcel shapefiles	Los Angeles County Enterprise GIS	Approx. 1:5,000
Los Angeles County neighborhood shapefiles	Los Angeles County Enterprise GIS	Approx. 1:24,000
Typical meteorological year (TMY3) weather data	National Solar Radiation Database	1:250,000
Annual average daily traffic (AADT) data	California Department of Transportation website	1:25,000
Los Angeles County road shapefiles	U.S. Census website	1:12,000
Annual county energy consumption statistics	Energy Atlas	No Spatial Scale
Solar potential data	Google Project Sunroof website	Approx. 1:12,000

CHAPTER 4

METHODOLOGY

4.1 Introduction

In this chapter, the research methodology developed to fulfill the three objectives in this dissertation are described. This chapter includes three major parts: 1) the inventory and GIS approach are combined to create a 365-day hourly Q_f profile at a 120-m spatial resolution for Los Angeles County; 2) a GIS approach is developed to combine climate change modeling, building energy simulation, and fine-scale (individual buildings) inventory data of building characteristics to quantify the effects of climate change on building energy demand at the sub-city scale; and 3) the potential mitigation effects of PV-green roofs in building energy demand are evaluated for selected buildings, which have shown more energy increases than other buildings under a climate change context. The following sections detail the specific methods used for each part. The methodology described in Section 4.2 and 4.3 have been published (Zheng & Weng, 2018; Zheng & Weng, 2019).

4.2 Anthropogenic Heat Discharge Estimation

The Q_f sources can be divided into three major categories of wasted heat (Sailor & Lu, 2004):

$$Q_f = Q_b + Q_v + Q_m \quad (2)$$

where Q_b , Q_v , and Q_m represent heat fluxes emitted by buildings, transportation, and human metabolism, respectively. Figure 4.1 shows a flowchart for the proposed methods. Q_m was determined by the inventory approach at the 1:12,000 scale, while Q_b and Q_v were simulated by using a combined GIS modeling and inventory approach at the 1:5,000 and 1:12,000 scales, respectively. This dissertation calculated the Q_f as the sum of Q_b , Q_v , and Q_m . A gridded algorithm (Heiple & Sailor, 2008; Smith et al. 2009; Zhou et al., 2012) was adopted to quantify the Q_f and each of its components. A 120-m resolution grid was created in the shapefile format, and the spatial extent was matched with Landsat imagery. Therefore, the original modeling results of Q_b , Q_v , and Q_m were overlaid with the grid layer before they were summed.

4.2.1 Human Metabolism Simulation

Human metabolism (Q_m) is the heat released by human bodies during daily activities, which varies with population density, activity phase, and time of day. This study offered a diurnal time-dependent population density-based method to simulate human metabolism in Los Angeles County. The CTPP shapefiles created by the U.S. Census Bureau, which contained information on the total population, number of workers in a work place, time of arrival at a work place, school enrollment population, and employment status, were used to simulate hourly population density. For working days, population density can be estimated by using the following equation:

$$PD = (WP1 + WP2 + UE + S) / A \quad (3)$$

where WP1 is the working population of a workplace; WP2 is the population of people working at home; UE is the unemployment population; S is the student population; and A is the census

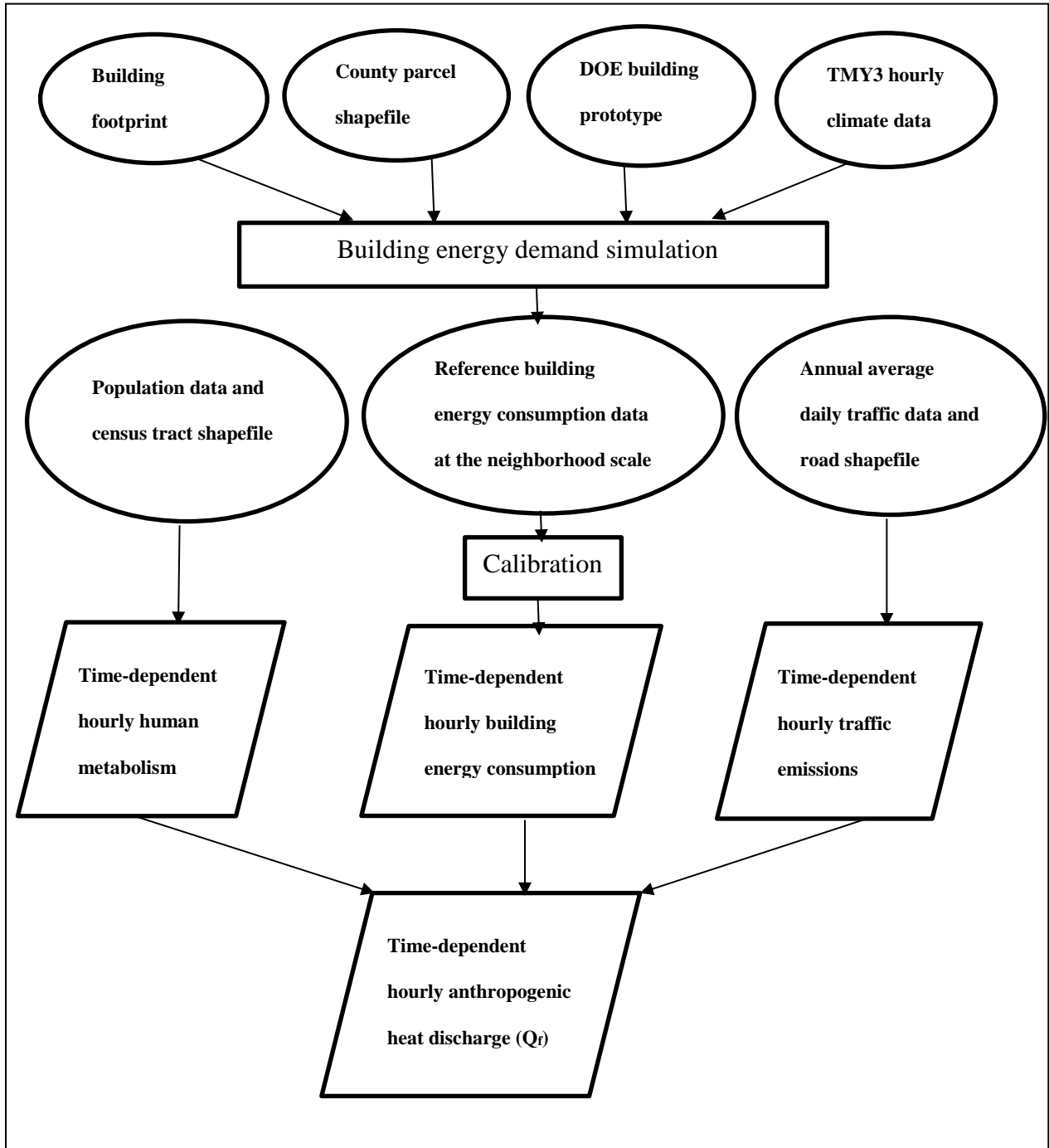


Figure 4.1. Flowchart of time-dependent hourly Q_f estimation.

tract area. In the subsequent step, a diurnal human metabolism simulation model was created from the time-dependent population distribution within each hour, which was based on data of 1)

working/student population arriving at workplace/school and 2) working/student population leaving home at each time interval. Table 4.1 presents the time schedule of where the typical working population would be during the day. The schedule was designed based on several assumptions: 1) the average daily working hours was 8 hours; 2) a 1-hour lunch break was incorporated; and 3) the average time needed for each daily commute was 1 hour. Therefore, the time between people leaving their home to work and arriving back home from work was set to 10 hours. The commuter flow for each census tract was estimated based on the following two cases:

Case 1: If the population at a work place was (working hours) > residential population, more workers and students from other census tracts were coming into this census tract than going out. Thus, the time-dependent population can be calculated as follows:

$$5 \text{ am} - 11 \text{ am: } Pop(t) = PP2 + \sum_{t=5}^n (PP1 - PP2) \times AR(t)/AR(total) \quad (4)$$

$$12 \text{ pm} - 2 \text{ pm: } Pop(t) = PP1 \quad (5)$$

$$3 \text{ pm} - 8 \text{ pm: } Pop(t) = PP1 - \sum_{t=15}^n (PP1 - PP2) \times AR(t-10)/AR(total) \quad (6)$$

$$9 \text{ pm} - 4 \text{ am: } Pop(t) = PP2 \quad (7)$$

where PP1 is the population at working day during working hours; PP2 is the total population (residential) in each census tract; AR(t) is the population of workers and students arriving at work places during time interval “t”, and AR(total) is the total population of workers and students arriving at work places during an entire day.

Case 2: If the population at working day during working hours was < residential population, workers and students from places other than this census tract were less than workers

and students going to other census tracts during working hours. Then, the time-dependent population at each census tract can be calculated as follows:

$$5 \text{ am} - 11 \text{ am: } Pop(t) = PP2 - \sum_{t=5}^n (PP2 - PP1) \times L(t)/L(total) \quad (8)$$

$$12 \text{ pm} - 2 \text{ pm: } Pop(t) = PP1 \quad (9)$$

$$3 \text{ pm} - 8 \text{ pm: } Pop(t) = PP1 + \sum_{t=15}^n (PP2 - PP1) \times L(t-10)/L(total) \quad (10)$$

$$9 \text{ pm} - 4 \text{ am: } Pop(t) = PP2 \quad (11)$$

where $L(t)$ is the population of workers and students leaving home during time interval “ t ”, and $L(total)$ is the total population of workers and students leaving home.

Table 4.1

Schedule of working population during the working day (Zheng & Weng, 2018).

Arrival time at work place/time leaving home	Return time to home from work
5:00 – 5:59 am	3:00 – 3:59 pm
6:00 – 6:59 am	4:00 – 4:59 pm
7:00 – 7:59 am	5:00 – 5:59 pm
8:00 – 8:59 am	6:00 – 6:59 pm
9:00 – 9:59 am	7:00 – 7:59 pm
10:00 – 10:59 am	8:00 – 8:59 pm
11:00 – 11:59 am	9:00 – 9:59 am

In the final step, human metabolism was calculated as follows:

$$Q_m = PD \times Mt \quad (12)$$

where PD is the population density per square meter and Mt is the amount of energy released per person as a function of day in watts (W). In this study, 175 W was set for Mt to represent the daytime metabolic rates in the urban area, according to Sailor and Lu (2004). Table 4.2 lists the energy released per person as a function of hour of day (W). Since the initial Q_m layer was at the

same scale as the census tract (1:12,000), it was overlaid with the 120-m grid for Q_f modeling at the final step. Since the area of one census tract in Los Angeles County was larger than a 120-m grid, the spatial relation between these two was used to determine the Q_m value for each grid. If a grid was completely within a census tract, the Q_m value of that census tract was assigned to this grid. If a grid intersected with two or more census tracts, the average value of Q_m from all intersected tracts was assigned to this grid.

Table 4.2

Energy released per person as a function of hour of day (W) (Zheng & Weng, 2018).

Time Period	Time-dependent energy release per hour
12:00 am – 4:59 am	75 W
5:00 am – 7:59 am	125 W
8:00 am – 7:59 pm	175 W
8:00 pm – 11:59 pm	125 W

4.2.2 Building Energy Consumption Simulation

Q_b was simulated as the energy consumption sum from industrial plants and commercial and residential buildings. Although there is a time lag between the energy consumption and heat emission into the atmosphere, detailed information on the ventilation systems and fabric of buildings for the time delay estimation is not generally available (Smith et al., 2009). Moreover, it is difficult to determine the percentage of consumed energy that was rejected as wasted heat because this percentage was dependent on varying insulation levels and heat exchange rates in different buildings (Sailor & Lu, 2004). Therefore, it was assumed in this study that all energy consumed within the buildings was fully and instantaneously emitted into the environment as wasted heat.

Building energy consumption includes space heating, cooling, lighting, ventilation, and equipment use. The amount of energy consumption for individual buildings can vary, which

depends on the physical parameters, prototype, operation schedule, occupant behaviors, and regional climate conditions. For example, space heating and cooling accounted for approximately 50% of building energy consumption (United States Department of Energy, 2012), but this percentage can be much higher during extreme weather conditions. Therefore, there is a need for high-resolution simulations of building energy consumption, especially for large areas such as Los Angeles County, which has microclimates and heterogeneous land cover. In this case, the bottom-up GIS modeling approach is more suitable than the top-down inventory approach, which is based on simulations of individual buildings by considering their attributes.

EnergyPlus, a well-known building energy simulation tool developed by the U.S. DOE was used to simulate 365-day building energy consumption at hourly intervals in this study. This software has been extensively tested and validated for the American Society of Heating, Refrigerating and Air-Conditioning Engineers (ASHRAE) standards and widely used by engineers and scientists to model building energy consumption (Huang & Gurney, 2016). Local climate datasets and building prototypes (Table 3.2) were the two required input data sources. The simulation models allowed for the customization of occupancy behaviors by providing settings for attributes such as daylight schedule, balanced-point temperature, heating, ventilation, and cooling (HVAC) operation hours, and the amount of equipment, which directly determined the energy demand of buildings. The output included hourly site energy consumption by end-use and fuel type for a building prototype under a given weather condition.

4.2.2.1 Local Climate Datasets and Building Prototypes

The hourly weather data files (Table 3.2) used in EnergyPlus were retrieved from the third (and latest) TMY3 collection. Each TMY3 file included hourly weather data (temperature, solar radiation, precipitation, relative humidity, and so on) in one-year durations for a specific

location, which is developed based on either 1991–2005 weather data or 1976–2005 weather data if the latter existed (Huang & Gurney, 2016). Because Los Angeles County covers a large area, the climate can be different due to the urban island effect and the influences from different topographies and land uses. Hourly TMY3 data from seven weather locations distributed throughout the entire county were used to simulate hourly building energy consumption.

Sixteen commercial building prototypes developed by the U.S. DOE (<https://www.energy.gov/eere/buildings/commercial-reference-buildings>) were used for the simulations. The DOE created these building prototypes based on Commercial Buildings Energy Consumption Survey (CBECS) data collected by the U.S. Energy Information Administration (EIA), which provided information on building characteristics, including thermal properties, operation schedules, and three different age categories (pre-1980, post-1980, and post-2004). The age categories reflected differences in the building insulation, envelope, HVAC systems, lighting, and equipment technologies for each building type, which led to different energy-saving abilities under the same outdoor environmental conditions. Buildings with newer technology had more energy-efficient equipment, better insulation to mitigate the impact of nonoptimal outside temperatures, smaller energy intensity of lighting, and more energy-efficient HVAC systems (Deru et al., 2011; Huang & Gurney, 2016).

Two prototypes of residential buildings, i.e., multifamily low-rise apartment buildings and single-family detached houses, were developed by the DOE in 2009 based on building codes specified in the International Energy Conservation Code (IECC) and Residential Energy Consumption Survey (RECS). Each prototype was modified to represent three types of heating systems (electric resistance, gas furnace, and heat pump), resulting in six residential sub-

prototype residential houses (Huang & Gurney, 2016). An inventory approach was used to disaggregate the industrial energy consumption data from broad scale to fine scale.

4.2.2.2 Schedules of Building and Occupant Behavior

In this study, separate profiles were designed for workdays and weekends/holidays to obtain an accurate 365-day building energy-use simulation, which was usually ignored in previous studies. The differences in operation hours and occupancy statuses between workdays and weekends/holidays can result in a difference in energy use to a certain extent. The DOE-generated building prototypes contained specific operation hours for each type of building on workdays, weekends, and public holidays in the Los Angeles area based on the CBECS survey. Office buildings, school buildings, and outpatient service buildings were set as closed during the weekend and public holidays, while buildings such as fast-food restaurants, hospitals, and hotels were set as open seven days a week, 24 hours a day.

Residential buildings did not have routine operational hours like commercial buildings, and the energy consumption statuses of residential buildings are completely dependent on occupancy behaviors. Therefore, during the workdays, a population distribution-based modeling method was used. The hourly profiles of the population that works at home, the unemployed population, and time leaving home and returning to home used to calculate human metabolism were applied to determine whether a residential house was occupied. The occupancy number in a residential house in each census district can be calculated by dividing the time-dependent population by the number of residential houses. If the population number is lower than the number of houses, it can be assumed that some houses were vacant during that particular time period, and then, the energy consumption for vacant houses was set to zero. For occupied houses, lighting load was determined from the time of sunset and the time of the sunrise, which assumed

that lights turned on in the evening during sunset and turned off during sleep time, and this time was set to 12 pm; lights were considered to be turned on again before sunrise in the morning. On weekends and public holidays, all residential buildings were set as occupied at all times.

For commercial and residential buildings, heating and cooling energy consumption was simulated depending on the comparison between indoor temperature and the balanced-point temperature at which no cooling or heating was required. If the indoor temperature was higher than the setup temperature, it can be assumed that the cooling system was working to maintain the setup temperature; if the indoor temperature was lower than the comfort temperature, the heating system was assumed to be turned on. The balanced-point temperature was usually assumed to be 18.3 °C (65 °F) in previous studies (Wang & Chen, 2014). This dissertation assigned 20 °C (68 °F) as the temperature that was set up by the occupants on thermostats, which was close to the balanced-point temperature.

Energy use in the industrial sector did not show a large difference from commercial and residential buildings due to the relative insensitivity to variations in weather and a much more uniform diurnal and seasonal distribution (Sailor, 2011). It is fairly common that energy consumption in the industrial sector was assumed to be uniformly distributed among all 8,760 hours of the year (Sailor, 2011; Sailor & Lu, 2004).

4.2.2.3 Initial Annual Building Energy Consumption Simulation and Calibration

The 365-day building energy consumption simulation was categorized into eight different “seasonal and day type” profiles: (1) spring workdays; (2) spring weekends/holidays; (3) summer workdays; (4) summer weekends/holidays; (5) fall workdays; (6) fall weekends/holidays; (7) winter workdays; and (8) winter weekends/holidays. The annual building energy consumption from commercial and residential sectors was calculated based on the aggregation of energy

consumed during each particular hour, day, and season. First, the hourly building energy use intensity (EUI), defined as the hourly energy use per square meter, was simulated using EnergyPlus. For commercial buildings, there were 2,688 different EUI values, which resulted from the combination of eight “seasonal and day type” profiles, seven weather zones, 16 building prototypes, and three age groups. Residential buildings exhibited 366 different values of EUIs, which resulted from the combination of eight “seasonal and day type” profiles, seven weather zones, and six prototypes.

The energy consumption for an individual building (BE) i within a particular hour j can be calculated by the following equation:

$$BE_{hour(i,j)} = EUI_{i,j} \times A_{building(i)} \times FN_{building(i)} \quad (13)$$

where $A_{building(i)}$ is the footprint area of building i , and $FN_{building(i)}$ is the floor number, which was estimated based on building height. The daily energy consumption of building i for day j was calculated as follows:

$$BE_{day(i,j)} = \sum_{j=1}^{24} BE_{hour(i,j)} \quad (14)$$

The building energy consumption within a season k was calculated as follows:

$$BE_{season(k)} = \sum_{j=1}^{t1} BE_{workday(i,j,k)} + \sum_{j=1}^{t2} BE_{non-workday(i,j,k)} \quad (15)$$

where $BE_{workday(i,j,k)}$ and $BE_{nonworkday(i,j,k)}$ are the EUI at a particular hour i within day j during season k on workdays and nonworkdays (weekends and holidays), respectively; and t_1 and t_2 are the number of workdays and nonworkdays within season k , respectively. The annual building energy consumption for sector l was calculated as follows:

$$BE_{annual(l)} = \sum_{k=1}^4 BE_{season(k)} \quad (16)$$

Although the GIS modeling approach can simulate building energy consumption at much finer spatial (individual building level) and temporal scales (hourly) than the inventory approach, discrepancies remained between the simulation results and the actual energy consumption (Herrando et al., 2016), which can be caused by uncertainties between the simulation and the truth. Therefore, annual energy consumption data from the California Energy Commission (CEC, 2016) (<http://ecdms.energy.ca.gov/elecbycounty.aspx>) and the Energy Atlas (<http://www.energyatlas.ucla.edu/>) were used as references to calibrate the simulation model. The Energy Atlas is a database of building energy consumption created by the California Center for Sustainable Communities (CCSC) at the University of California, Los Angeles (UCLA). The building energy consumption data were created from a separate and confidential geospatial relational database that contained approximately five billion unique records (<http://www.energyatlas.ucla.edu/>). These records related the private account-level monthly energy consumption data to building characteristics and census information (<http://www.energyatlas.ucla.edu/>). This data source provided detailed historical annual energy consumption data from all building energy sectors, including commercial, residential and

industrial sectors at a fine scale (city neighborhood level). Compared to previous studies, which used county, state, or census division-level energy consumption data to calibrate the simulation, the use of neighborhood-level reference data allowed us to address the regional variation in energy consumption patterns in each building sector.

The annual energy consumptions of commercial buildings and residential buildings in each neighborhood were calculated and compared to reference energy consumption data. In the next step, the EUI of each type of commercial and residential building was calibrated using the ratio between the simulated results and reference energy consumption data. Energy consumption data for the industrial sector in some neighborhoods were masked out because many industrial consumers did not share their data with the public. Therefore, the countywide consumption percentage was used to obtain the total volume of industrial energy consumption in those neighborhoods and applied the metrics of median consumption per square meter and total floor areas of industrial plants in each neighborhood to create the EUI curve of industrial plants in each neighborhood.

4.2.2.4 Final Building Energy Consumption Simulation

After EUI calibration for each type of building, the gridded algorithm was adopted to quantify the building energy consumption in Los Angeles County for 8,760 individual hours throughout the year. The 120-m grid layer was overlaid with building footprint layers, and each grid cell contained 0, 1, or multiple fractions of buildings. Building energy consumption in a grid cell can be estimated using the following equation:

$$Q_b = \frac{\sum_{j=1}^n EUI(j) \times A(j) \times FN(j)}{A2} \quad (17)$$

where $EUI(j)$, $A(j)$, and $FN(j)$ are the hourly energy intensity index, floor areas, and floor numbers of building prototype j , respectively. The algorithm summarized hourly energy consumption from all the building prototypes in the given grid cell and divided this value by the grid area A_2 , which equals 14,400 square meters.

4.2.3 Traffic Emission Simulation

Hourly traffic emissions within a particular day were simulated based on normalized AADT data, which were adjusted by a seasonal scaling factor, weekday scaling factor, and diurnal scaling factor. The 2010 AADT data, which were calculated by dividing 365 from the total traffic volume of a road for one calendar year, were collected as point shapefiles from the California Traffic Census Program in 808 traffic count stations. The data were distributed throughout major roads in the study area. The 120-m grid, AADT traffic counts, and road shapefiles were overlain together. The hourly traffic count values from the AADT were directly assigned to the major road segments if the data were located within the same grid cell as AADT points. For grid cells not containing the AADT points, the average values of traffic volume for all the points in the same neighborhood were assigned. The traffic volume of the minor roads was calculated by dividing the traffic volume of the major roads by 10 (Smith et al., 2009).

Similar to the building energy simulations, profiles for eight different types of days were created. The temporal traffic variations for each day type were calculated by applying the seasonal scaling factors and diurnal variation factors for the hourly traffic volume calculated by AADT traffic counts. The seasonal scaling factors and the diurnal variation factors were calculated using the hourly vehicle miles traveled (VMT) metric, which was available in the Caltrans Performance Measurement System (PeMS) Database established by the California Department of Transportation. The PeMS database contains historical hourly VMT data for each

individual day from 1993 to present. VMT data from 2010 were used to construct the diurnal vehicle volume profiles for 8 different types of days. The hourly vehicle volume factor was simulated by averaging all the VMT values from the same time during days that were in the same category.

The traffic emissions in each grid cell were calculated using the formula similar to Smith et al. (2009), which is as follows:

$$Q_v = \sum(N_{mxi}(t) \times L_{xi}) \times EF_m/A_i \quad (18)$$

where Q_v represents the vehicle emissions in watts per square meter (W/m^2), N_{mxi} is the normalized traffic count number for vehicle type m on road x in grid cell i , t is the hour of day, L_{xi} is the length of all roads x within the grid cell i , EF_m is the fuel consumption emission factor (J/m), which can be calculated, and A_i is the area of each grid cell ($120 \times 120 = 14,400 \text{ m}^2$). The fuel consumption emission factor (W/m) was calculated using the equation of Sailor and Lu (2004):

$$EF_m = NHC \times \rho_{fuel}/FE(J/m) \quad (19)$$

where NHC is the mean net heat of vehicle gasoline and diesel combustion in kilojoules (KJ) per gram, which is 45.85 KJ/g for petrol and 46 KJ/g for diesel (Smith et al., 2009); ρ_{fuel} is the mean density of gasoline (0.75 kg/l) and diesel (0.832 kg/l) (U.S. Energy Information Administration, 2014; Chow et al., 2014); FE is the mean fuel efficiency of all vehicles (7.5 km/l in 2010) (United States Department of Transportation, 2011; Chow et al., 2014). Based on annual data

from gasoline and diesel sales collected by the California State Board of Equalization (<http://www.boe.ca.gov/sptaxprog/spftrpts.htm>), the ratio between the number of gasoline vehicles and diesel vehicles in Los Angeles County was set to 5.25:1, and the mean fuel consumption emission factor (EF) was estimated to be 4.668 KJ/m.

4.3 Modeling the Effects of Climate Change on Building Energy Demand

4.3.1 Future Weather Data Construction

Los Angeles County consisted of seven weather zones in the TMY3 dataset (Figure 4.2), including Burbank-Glendale, Los Angeles International Airport, Long Beach, Van Nuys, Lancaster, Palmdale, and Point Mugu. Each weather zone contained different hourly weather data collected from 1991–2005. Figure 4.3 shows the current average monthly temperature (°C) in seven TMY3 locations in Los Angeles County. The Long Beach, Los Angeles International Airport, and Point Mugu weather zones had relatively smaller ranges of monthly temperatures because these areas are located in coastal areas and all have Csb climates. The Lancaster and Palmdale weather zones had the highest temperatures during the summer months but the lowest temperatures during the winter months due to their “cold semiarid” climates. The Burbank-Glendale and Van Nuys weather zones, with the Csa climate, had similar temperatures during the wintertime as the coastal areas but higher temperatures during the summer months.

The future hourly weather data were projected using HadCM3. Among all future weather data construction models, HadCM3 has a smaller grid spacing, which means that the simulation resolution is higher than other models and results in higher precision (Shen, 2017). This model contains the atmospheric model HadAM3, with a horizontal resolution of 2.5 degrees latitude by 3.75 degrees longitude, which covers all Los Angeles County. This model provides monthly changes in dry-bulb temperature, diurnal temperature variation, relative humidity, wind speed,

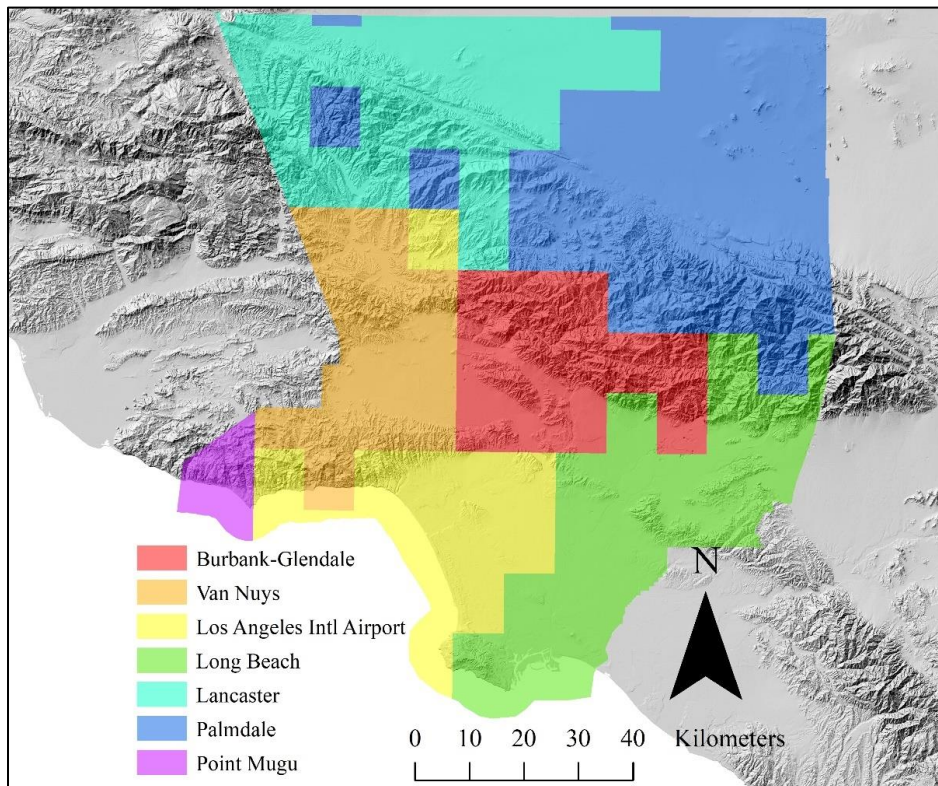


Figure 4.2. TMY3 climate zones in Los Angeles County (Zheng & Weng, 2019).

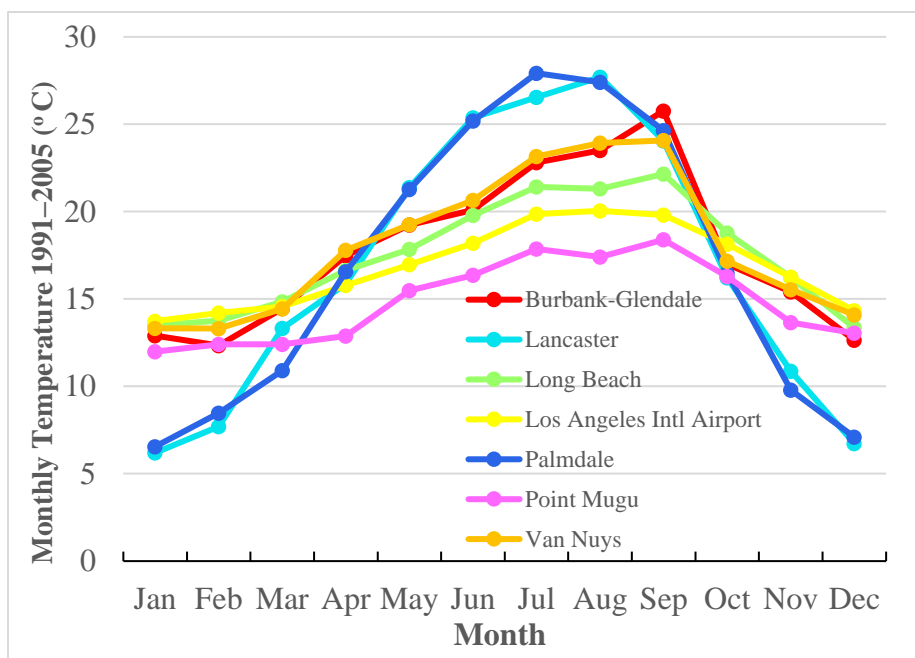


Figure 4.3. Current monthly temperatures (°C) in seven TMY3 locations in Los Angeles County (Zheng & Weng, 2019).

and solar radiation, which have a major impact on building heating and cooling loads.

There are various carbon dioxide emission scenarios projected by the IPCC, which is associated with the likely global development projections to the year 2100, including technologies, climate and energy policies, and social-economic developments. The most recent IPCC Fifth Assessment Synthesis Report (AR5) <https://www.ipcc.ch/report/ar5/syr/>, which was released in 2014, used Representative Concentration Pathways (RCPs) to make projections based on these factors (Intergovernmental Panel on Climate Change [IPCC], 2014) to describe four different 21st century pathways of GHG emissions and atmospheric concentrations, air pollutant emissions, and land use. The RCPs include a stringent mitigation scenario (RCP2.6), two intermediate scenarios (RCP4.5 and RCP6.0) and one scenario with very high GHG emissions (RCP8.5).

In this study, RCP8.5 (high emission) and RCP6.0 (medium emission) were chosen for simulations. The RCP6.0 scenario fits the current energy policies and emphasizes regional differences, which is suitable for county/city level examinations. On the other hand, the RCP8.5 scenario represents the worst case and can be used for hazard assessment purposes. The low emission scenario (RCP2.6) was not chosen because it assumes that the global annual GHG emissions peak occurs between 2010 and 2020, and a decline thereafter likely keeps global warming below 2 °C, which is overly optimistic according to the current trend, and unlikely to occur in the near future. To create hourly data for 2050, the Climate Change World Weather File Generator (CCWorldWeatherGen) tool was used; this tool was developed by the Sustainable Energy Research Group (University of Southampton). CCWorldWeatherGen uses hourly historical weather data (TMY2 and TMY3) as primary input and applies the HadCM3 model to construct future hourly data. This tool uses the IPCC Fourth Assessment Report (AR4) model

summary data of the HadCM3 A2 scenario, which is close to the intermediate scenario (RCP6.0) in AR5. CCWorldWeatherGen has been widely adopted by a large number of researchers (Andrić et al., 2016; Rey-Hernández et al., 2018; Rubio-Bellido, Pérez-Fargallo, & Pulido-Arcas, 2016; Shen, 2017; Wang & Chen, 2014; Wong, Jusuf, Syafii, Li, & Tan, 2012; Yi & Peng, 2014) in recent years. Because the HadCM3 model only provides monthly weather variation data, which is insufficient for hourly energy simulation, the CCWorldWeatherGen tool applies a morphing method to downscale monthly weather data to hourly weather data. The algorithm to calculate future hourly weather data uses the following equation:

$$\mathbf{X} = \mathbf{X}_o + \Delta x_m + a_m(\mathbf{X}_o - (\mathbf{X}_o)_m) \quad (20)$$

where \mathbf{X}_o is the hourly weather data from the existing historical data (TMY2 or TMY3), Δx_m is the predicted monthly average change obtained from HadCM3, a_m is the stretching factor calculated based on the changes in monthly average value of a specific variable from future weather files relative to the existing reference weather file, and $(x)_m$ is the monthly average of current weather data. Because the CCWorldWeatherGen tool can only simulate future weather data under the IPCC A2 carbon emission scenario, a pattern-scaling method developed by the Finnish Environment Institute (Ruosteenoja, Carter, Jylha, & Tuomenvirta, 2003) was adopted to calculate future weather data under the A1F1 carbon emission scenario, which is close to the very high GHG emissions (RCP8.5) observed in AR5. This pattern-scaling method can provide the magnitude for future temperature changes under different IPCC scenarios based on a series of factors, which also varies with locations in the world.

4.3.2 Building Prototypes

The same commercial and residential building prototypes as the ones used in the Q_f simulation were used for the simulation. The DOE created these building prototypes based on CBECS data from the U.S. EIA and provided information on building characteristics in three age categories: pre-1980, post-1980, and post-2004. The age categories reflected differences in building insulation, envelope, HVAC systems, lighting, and equipment technologies for each building type, which led to different energy consumption abilities under the same outdoor environmental conditions. Buildings with newer technologies had more energy-efficient equipment, better insulation to mitigate the impact of nonoptimal outside temperatures, lower lighting energy intensities, and more energy-efficient HVAC systems (Huang & Gurney, 2016). Two prototypes of residential buildings, i.e., multifamily low-rise apartment buildings and single-family detached houses, were developed by the DOE in 2009 based on building codes specified in the IECC and RECS. This study assumed the building stock structure in Los Angeles County remained unchanged throughout the simulation period.

4.3.3 Calibration of Reference Data

The calibration method used in the Q_f estimation was adopted in this research to calibrate the simulated current building energy consumption. Compared to the existing study that calibrated building energy consumption at a coarse scale, such as the census division (Huang & Gurney, 2016), the neighborhood-level reference data in this study can address the regional variation in energy consumption patterns in both the commercial and residential sectors, which was essential for the purpose of a local-scale study. Moreover, these data can overcome the spatial resolution limitation, which was caused by the resolution of weather data (TMY3 data). Figure 4.4 presents the calibrated annual building energy consumption intensity for 16 types of

commercial buildings in Los Angeles County, which was the simulation result based on the historical TMY3 data (1991–2005). The two types of restaurants (full-service and fast-food) consumed the largest amount of energy per square meter per year. The ratio between the before and after-calibrated building energy consumption results was computed to calibrate the simulated future building energy consumption under the two emission scenarios (RCP8.5 and RCP6.0).

4.4 Green Roof and Solar Photovoltaic Setting

To evaluate the performance of green and PV-green roof mitigation effects on the potential building energy use increase caused by climate change, EnergyPlus software was used in this dissertation to simulate hourly building energy consumption in Los Angeles County with the proper green roof and photovoltaic modules. This strategy has been widely used in previous research (Gargari, Bibbiani, Fantozzi, & Campiotti, 2016; Heusinger et al., 2018; Morakinyo et al., 2017; Sailor et al., 2007; Sailor et al., 2012; Scherba et al., 2011; Silva et al., 2016; Tang & Qu, 2016; Yang et al., 2018) to estimate green roof cooling effects for reduction in indoor temperature and sensible heat fluxes, which can potentially lead to building energy reduction in the summer months. However, studies that evaluate the mitigation potential of green roofs on building energy increases caused by climate change are rare. The purpose of this part of the dissertation is to fill this gap in the current literature and provide a means of evaluating the potential contribution of green roofs based on the results of studies that modeled climate change effects on building energy demand.

Figure 4.5 presents the methodology used in this study. The vulnerable buildings that are susceptible to the largest increases in energy demand under the context of climate change were identified based on the results from previous sections of this dissertation. Because solar potential varies at the individual building level, this section was focus on a small study area, which

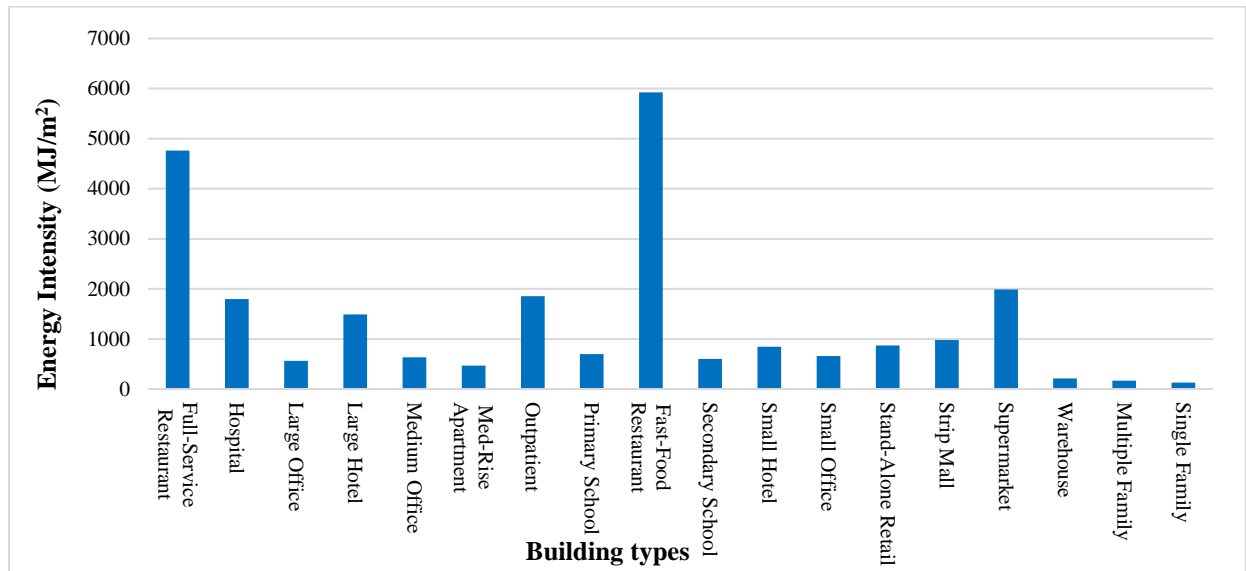


Figure 4.4. The calibrated annual building energy consumption intensity in megajoules (MJ) per square meter (m²) for 18 types of buildings in Los Angeles County. The simulation was based on historical TMY3 data (1991–2005) (Zheng & Weng, 2019).

contains less than 30 buildings in total, rather than all buildings in Los Angeles County. Multiple study sites containing a high percentage of vulnerable buildings were selected. The solar potential for each building roof was rated using the open-source roof solar potential data from the Google Project Sunroof database (<https://www.google.com/get/sunroof#p=0>). According to Google Project Sunroof, roofs in Los Angeles County should have at least 1,405 hours of usable sunlight per year to be ranked as high solar potential roofs. Hours of usable sunlight per year were estimated based on the daily analysis of weather patterns. In this dissertation, building roofs with high solar potential were added to both green roofs and PV systems during the simulation. However, only green roofs were added to buildings with low solar potential. The simulation results of building energy consumption with green roofs or PV-green roofs under the projected climate in 2050 were compared with the scenario of buildings with traditional roofs.

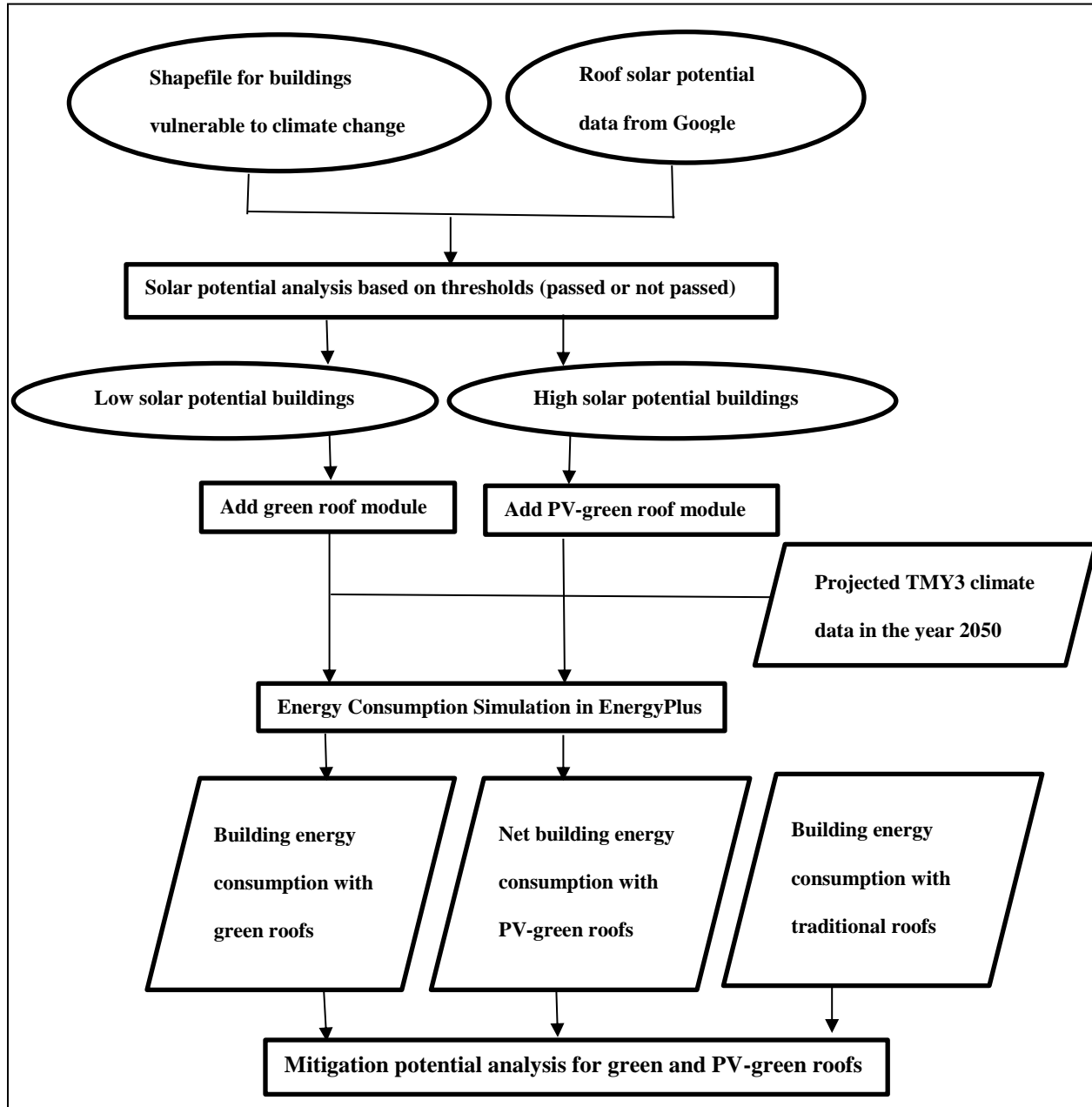


Figure 4.5. The method used to analyze the potential mitigation effect of green and PV-green roofs on building energy demand caused by climate change.

4.4.1 EnergyPlus Green Roof Module Setting

In this study, the EnergyPlus green roof module was used to model green roof fluxes. This module functions as an integral component of the simulation software, performing an energy balance on a vegetated rooftop within each time step (Sailor et al., 2012). The input of various green roof-related parameters, such as the Leaf Area Index (LAI), plant height, leaf emissivity, soil layer thickness, soil thermal properties, and stomatal resistance, are allowed. The module also accounts for longwave and shortwave radiative exchanges within the plant canopy, plant canopy effects on convective heat transfer, evapotranspiration from soil and plants, and heat conduction and storage in the soil layer (Scherba et al., 2011). Moreover, the module allows the user to define different irrigation types and to set up specific schedules.

According to Heusinger et al. (2018), extensive green roofs have much lower static requirements and are less expensive, so green roofs are generally favored over intensive roof types. Therefore, in this dissertation, an extensive green roof type was chosen instead of the intensive green roof type. Additionally, other studies combined the extensive green roofs with the solar PV system instead of intensive green roofs for PV-green roofs. The setting of parameters in extensive green roofs used in this dissertation was follow the settings in Sailor (2008), which was based on validated data in two monitored buildings installed with green roofs at Portland State University, Oregon. The key green roof parameters include plant height (0.2 m), LAI (2), soil depth (20 cm), dry soil conductivity (0.4 w/m-k), dry soil specific heat (1,000 J/kg-k), and dry soil density (500 kg/m³). For roof irrigation systems, a “smart schedule” was chosen that follows the precipitation schedule and did not allow irrigation when soil is already moist (30% saturation). This schedule was also activate an early morning irrigation system if the soil volumetric moisture content falls below 0.15 m³/m³.

4.4.2 EnergyPlus Solar Photovoltaic Module Setting

EnergyPlus offers different module performance algorithms for predicting the electricity produced by solar electric PV panels. The three different options are (1) Simple, (2) Equivalent One-Diode, and (3) Sandia; and the algorithm choice will determine the mathematical models used to simulate energy production. The simple algorithm allows the user to input an arbitrary efficiency that requires prior knowledge about different PV panel types. The other two models use empirical relationships to predict PV operating performance based on many environmental variables. In this dissertation, the Sandia PV performance algorithm, which is based on extensive measurements and data collection performed at Sandia National Laboratory to predict electricity generated by PV systems, was chosen for simulation. The Sandia model can accurately predict daytime PV cell temperatures and aggregate multiple PV modules by defining the number of cells in series and parallel. These parameters were set differently for each single building based on recommendations such as the area available for solar panels and the recommended solar installation size provided by the Google Project Sunroof website.

4.5 Summary

In this chapter, the methodology of this dissertation has been discussed in detail. The results of this dissertation will aid municipal governments to tailor adaption and mitigation strategies in different regions within megacities such as Los Angeles, which have a high degree of diversity in building composition and population density. The mitigation potential assessment of PV-green roofs is a good reference for reducing building net energy consumption by increasing the supply of renewable energy while decreasing energy use.

CHAPTER 5

HIGH SPATIAL AND TEMPORAL RESOLUTION ANTHROPOGENIC HEAT DISCHARGE ESTIMATION IN LOS ANGELES COUNTY

5.1 Introduction

In this chapter, the results obtained from the estimation of the Q_f profile at high spatial and temporal resolutions in Los Angeles County are explained. The methods were presented in detail in Section 4.2. This chapter has been divided into five sections. Section 5.2 outlines the results of the temporal variation of Q_f . Section 5.3 presents the results of Q_f on extremely hot summer days. Section 5.4 illustrates Q_f in the urban core area. Section 5.5 discusses the significance of the proposed work and presents a comparison with previously published work based on the results and the applicability of the methodology. Results of this study were published in *Journal of Environmental Management* (Zheng & Weng, 2018, Appendix A).

5.2 Temporal Variations of the Anthropogenic Heat Flux

The diurnal variation of the mean hourly Q_f and its components on spring workdays, spring nonworkdays, summer workdays, summer nonworkdays, fall workdays, fall nonworkdays, winter workdays, and winter nonworkdays in Los Angeles County are presented in Figure 5.1. In general, Q_b and Q_v contributed similar proportions to Q_f but at different time, and Q_m contributed the least to Q_f regardless of it being a workday or nonworkday. In all profiles, the workday diurnal profiles of Q_f exhibited two peaks, i.e., morning and evening peaks,

while the nonworkday diurnal profiles of Q_f exhibited parabola shapes with only the peak in the evening hours. These shapes are related to traffic emissions peaking not only during the evening rush but also during the morning rush on workdays. The peak values on workdays were higher than on nonworkdays because many buildings were not in operation on nonworkdays. The lowest values of Q_f were found at 4 am on workdays and 5 am on nonworkdays.

Figure 5.1 also compares the diurnal variation of Q_f in different seasons for (i) workdays and (j) nonworkdays. The diurnal variations of Q_f exhibited similar shapes but small differences in magnitude. The Q_f profiles in the summer exhibited higher values at noon (7.76 w/m^2) and in the evening on workdays and nonworkdays than that of the other seasons (Figure 5.1g). The reason is that building energy consumption was highest at noon and in the evening hours in summer (Figures 5.1c and d) due to extra energy being consumed for cooling. Moreover, the Q_f values on winter mornings on workdays and nonworkdays were higher than in the other seasons because of the higher building energy consumption (Figures 5.1h and i) for heating to offset the large difference between the indoor and outdoor temperatures on winter mornings. This reason also explains why winter was the only season with the highest workday Q_f value occurring in the morning peak instead of the evening peak.

5.3 Anthropogenic Heat Fluxes on Extremely Hot Summer Days

Q_f appeared to have the highest values on summer workdays in Los Angeles County, with its maximum value reaching 7.76 w/m^2 (Figure 5.1g). Because traffic emissions and human metabolisms did not exhibit obvious seasonal variations, the most significant driver of the increased energy use in summer came from the building sector, which required increased energy consumption for cooling. This study performed compared Q_f on an extremely hot summer workday with the averaged summer workday value to examine if there was an obvious increase

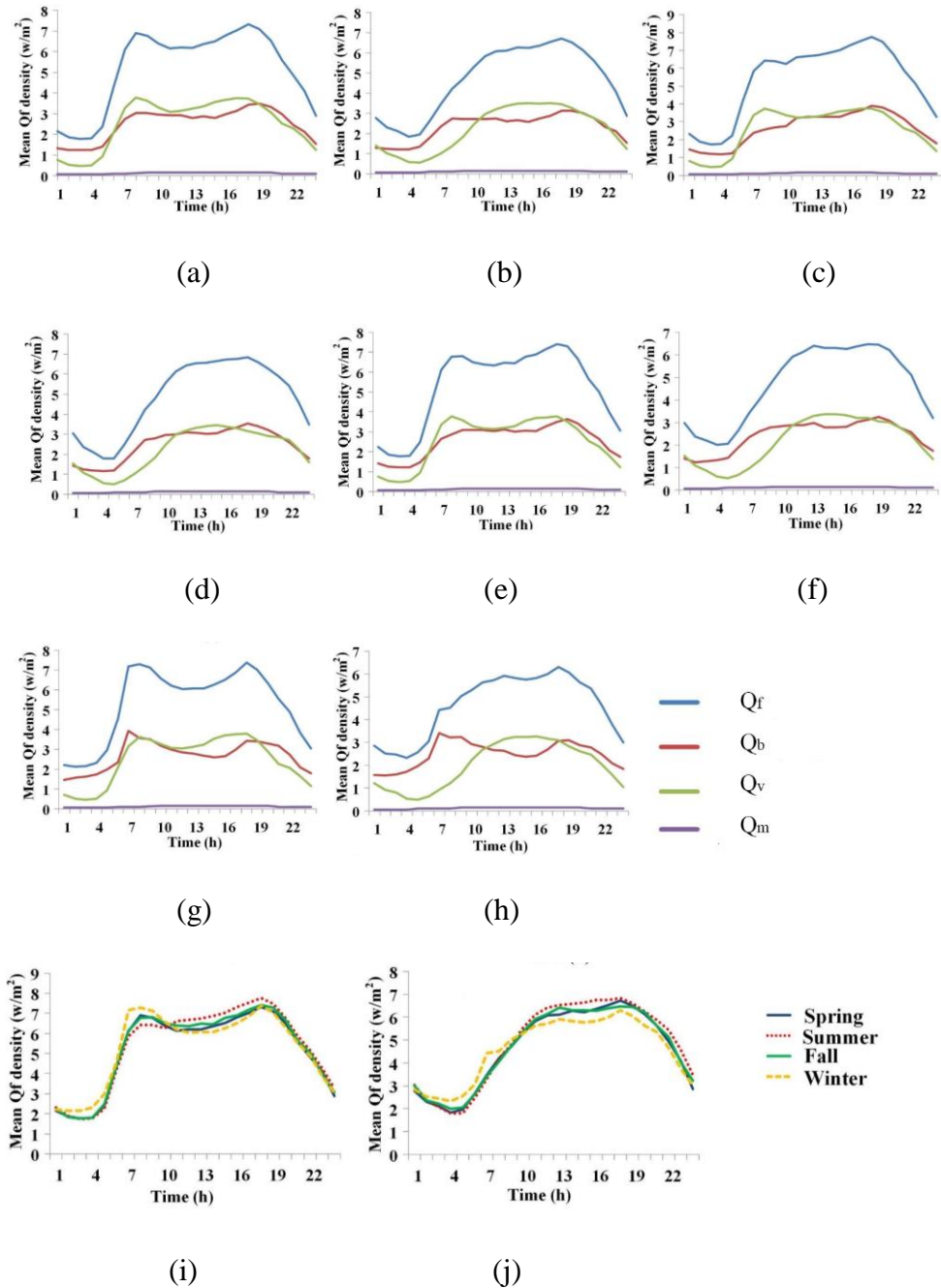


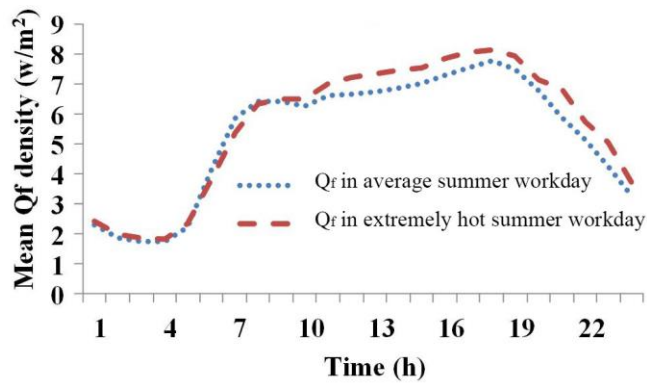
Figure 5.1. Diurnal variation of Q_f , Q_b , Q_v , and Q_m (w/m²) in Los Angeles, USA., based on the average values from all (a) spring workdays, (b) spring nonworkdays, (c) summer workdays, (d) summer nonworkdays, (e) fall workdays, (f) fall nonworkdays, (g) winter workdays, and (h) winter nonworkdays; comparison of the diurnal variation of Q_f in different seasons on (i) workdays and (j) nonworkdays in Los Angeles, USA (Zheng & Weng, 2018).

in building energy demand on extremely hot days and to what extent the energy use increased.

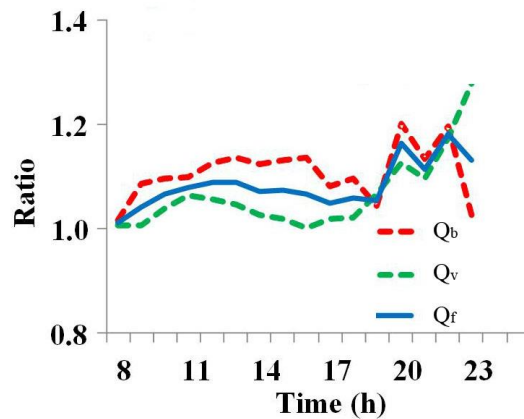
August 25, 2015, was selected as the extremely hot summer workday for comparison in this study because the high temperature reached 37 °C (98.6 °F) at 1 pm. The temperature remained above 30 °C (86 °F) for 10 hours (from 10 am to 7 pm). Figure 5.2a presents a comparison between Q_f on the selected extremely hot summer workday (August 25, 2015) and the average of all summer workdays. On the extremely hot summer workday, Q_f was substantially higher than the average of all summer workdays from 8 am to 11 pm, with its maximum value reaching 8.14 w/m².

Figure 5.2b shows the time series of the ratio between the anthropogenic heat fluxes (blue solid), building emissions (red dash), and traffic emissions (green dash) on the extremely hot summer workday and for the average of all summer workdays. When the heat fluxes on the extremely hot summer workday exceeded those of the average of all summer workdays, the ratio was larger than 1. Higher ratios indicated enhanced heat fluxes were produced on the extremely hot summer day. The major contributor of the higher anthropogenic heat fluxes on the extremely hot summer day varied with time. According to Figure 5.2b, building emissions were the major contributor for most of the day (from 9 am to 6 pm and from 8 pm to 9 pm), as the ratio was significantly higher than that of the traffic emissions and anthropogenic heat fluxes during these periods. The building ratio increased gradually from 8 am to 11 am because the temperature difference between the extremely hot summer day and the average of all summer workdays increased. This ratio remained high from 12 pm to 4 pm because the temperature difference reached its maximum during the daytime, and the air condition systems consumed more energy to offset the larger indoor/outdoor temperature difference on the extremely hot summer day. During the daytime (8 am to 6 pm), traffic emission contributed less to the higher Q_f on the

extremely hot summer day, as indicated by the traffic ratio being generally lower than the building ratio. However, at night, the traffic ratio increased dramatically while the building ratio remained high, which resulted in a larger Q_f increment on the extremely hot summer workday. The reason that there was a significantly larger traffic volume on the selected day must be further studied. Possible factors included traffic congestion or nighttime activities.



(a)



(b)

Figure 5.2. (a) Comparison between Q_f (w/m^2) on an extremely hot summer workday (August 25, 2005) and the average of all summer workdays; (b) time series of the ratios between the anthropogenic heat fluxes, building emissions, and traffic emissions on the extremely hot summer workday and those of average summer workdays (Zheng & Weng, 2018).

5.4 Anthropogenic Heat Fluxes in the Urban Core Area

Although the daily maximum Q_f estimated in Los Angeles County on the extremely hot summer workday did not exceed the average of all summer workdays by 10 w/m^2 , there was a large within-county variation in Q_f for different regions. Figure 5.3 presents the spatial distribution of Q_f estimated at 5 pm on the summer workdays in Los Angeles County, when Q_f exhibited its highest value (Figure 5.2). The spatial distribution of Q_f was uneven, with high values (larger than 100 w/m^2) being located in some clusters, such as the downtown area, Korean Town, Beverly Hills, Hollywood, West Los Angeles, Long Beach, and Santa Monica, which are characterized as commercial and industrial zones. Moreover, high Q_f values can be found along the major freeways due to heavy traffic emissions during the evening rush hours. Moderate Q_f values (20 to 100 w/m^2) were detected in residential zones with high housing and population density, while low Q_f values (less than 20 w/m^2) were located in cities with small populations (Palmdale and Lancaster), low-density residential zones, and minor roads. The downtown area was found to have the highest mean Q_f throughout the year because there are more densely distributed tall commercial buildings in this area. Figure 5.3b shows the spatial distribution of Q_f in the downtown area at 5 pm during summer workdays. The spatial variation of Q_f is characterized by low values in the southeast part of the downtown area, with values increasing dramatically towards the northwest. This spatial distribution reflected the fact that most of the tall commercial buildings are located in northwest part of the downtown area. Less tall commercial buildings, historical office buildings, apartment complexes, and warehouses are located in the southeast part of the downtown area, contributing to a lower Q_f value. Some areas with high Q_f values in this region are representative of freeways.

Figure 5.4 shows a comparison of the diurnal variation of Q_f in downtown Los Angeles for different seasons on (a) workdays and (b) nonworkdays. It can be concluded that Q_f in the downtown was much higher on workdays than that on nonworkdays, and its maximum value reached 100 w/m^2 (4 pm on summer workdays). From 9 am to 5 pm, Q_f on summer workdays was higher than on other workdays (Figure 5.4a), while from 5 am to 9 am, Q_f on winter weekends was highest (Figure 5.4b). Building energy consumption was the most important factor that contributed to Q_f (Figure 5.5).

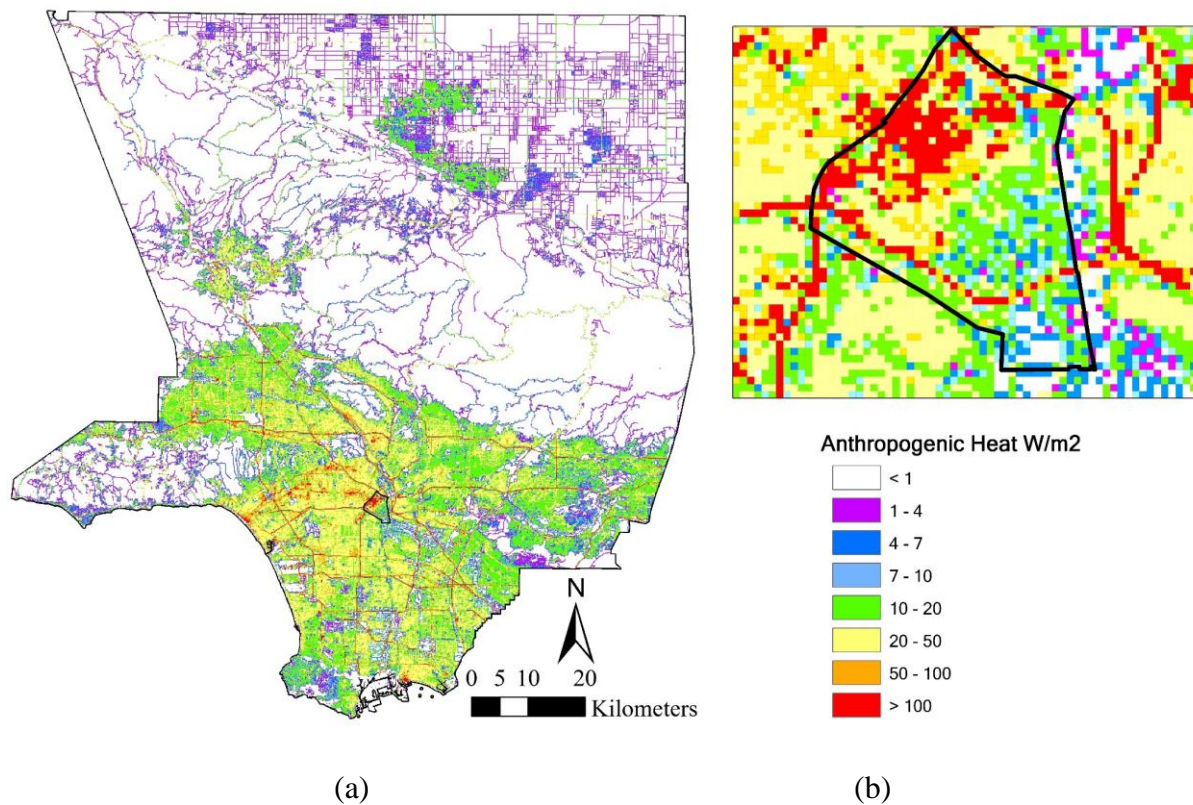


Figure 5.3. Spatial distribution of Q_f (w/m^2) in (a) Los Angeles County and (b) downtown Los Angeles (Zheng & Weng, 2018).

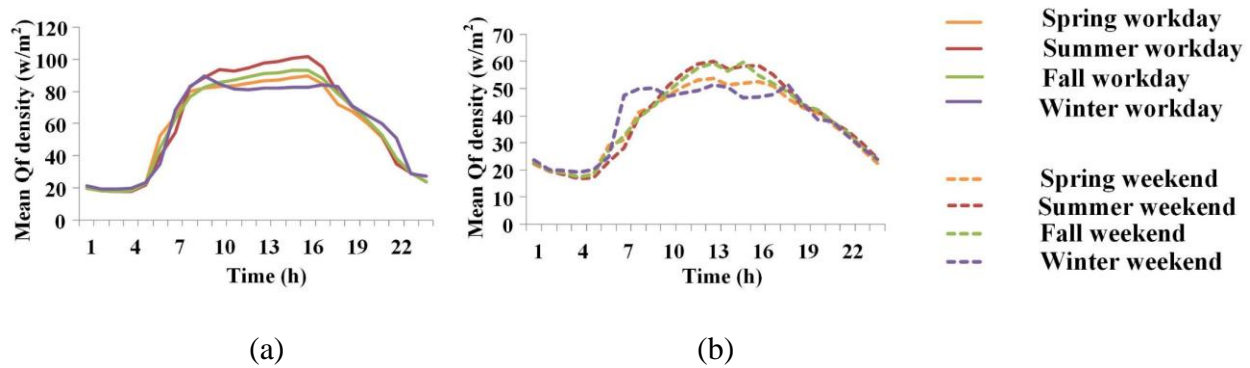


Figure 5.4. Comparison of diurnal variations of Q_f (w/m^2) in downtown Los Angeles for different seasons on (a) workdays and (b) nonworkdays (Zheng & Weng, 2018).

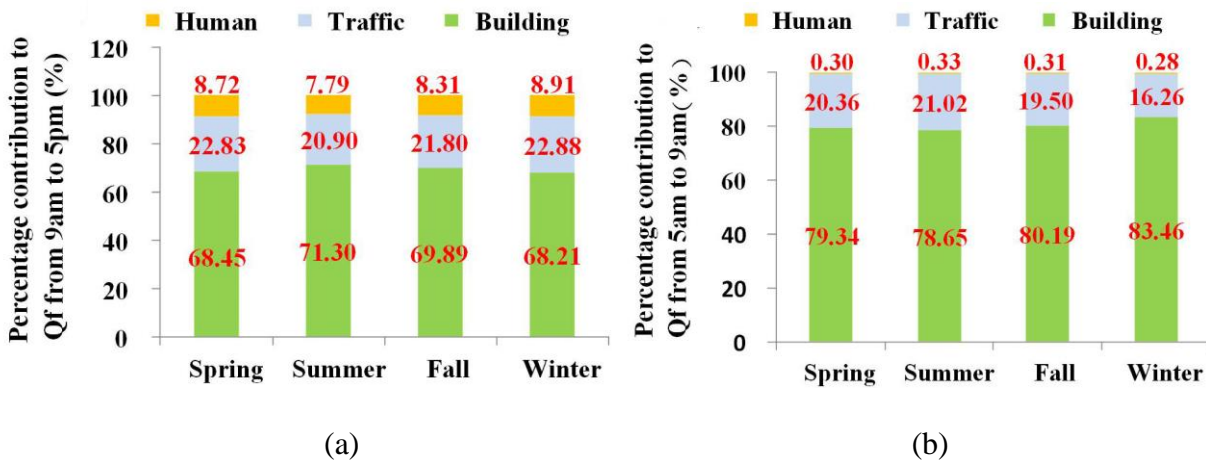


Figure 5.5. Percentage breakdown (%) of the individual components contributing to Q_f from (a) 9 am to 5 pm on workdays and (b) 5 am to 9 am on nonworkdays in downtown Los Angeles (Zheng & Weng, 2018).

5.5 Discussion and Conclusions

This section discusses the significance of the aforementioned results. Compared to prior studies, the advantage of the approach used in this study is the design of separate profiles for workdays and weekends. In this way, higher values of Q_f on winter mornings and summer

evenings on workdays can be identified. These contrasts would be less significant if workday and weekend Q_f profiles were not separated from each other.

In addition, a large within-county difference in Q_f was uncovered for different regions and land use types in the studied area, which agrees with the results of many previous studies (Chapman et al., 2016; Chow et al., 2014; Hamilton et al., 2009; Ichinose et al., 1999; Quah & Roth, 2012; Smith et al., 2009). The intensity of Q_f can be affected by the spatial extent that was used for measurement. Downtown Los Angeles was found to have the largest mean Q_f throughout the year, among all neighborhoods. The maximum Q_f value in the downtown Los Angeles can exceed 100 w/m^2 (Figure 5.4a) on workdays, which was significantly higher than that throughout the county (7.76 w/m^2) (Figure 5.1g). Building energy consumption was identified as the dominant contributor to the overall Q_f in the downtown area. When compared with previous studies (Ichinose et al., 1999; Nie et al., 2014; Quah & Roth, 2012; Wong et al., 2015) which estimated Q_f in cities or regions with higher population densities (Tokyo, Hong Kong, Singapore), traffic emissions were found to account for a higher percentage of Q_f in Los Angeles County, while human metabolism contributed less.

This study proposed an approach to estimate Q_f at high spatial and temporal resolution for a large metropolitan area with diverse geographic settings. However, the data availability was still a major limitation in this study and resulted in uncertainties. The discrepancies between the building simulation results and the actual building energy consumption can be caused by many factors. First, the simulation model used in EnergyPlus cannot account for all factors that determine actual building energy consumption, such as the occupancy status and behaviors. Moreover, the building prototypes were developed based on the most common building technologies/characteristics in the survey data for Los Angeles County, which may not represent

all buildings in reality. Therefore, for validation purposes, this dissertation used the actual building energy consumption data at the neighborhood scale to validate the building energy consumption simulation results. The simulated energy consumption from all buildings within each neighborhood and each sector were aggregated to compare with the corresponding sector in each neighborhood in the referenced data. For all neighborhoods, the ratio between the simulated results and the reference data ranged from 0.85 (West Los Angeles) to 1.92 (Avalon), with a mean value of 1.38. This validation result suggests that the building energy simulation model tended to overestimate the actual building energy consumption. After calibration, potential bias and uncertainty in the simulated results can be corrected at the neighborhood scale, while the differences among individual sectors and buildings within a neighborhood over a given time period remain. This result is essential for city governments to work towards a sustainable city by tailoring adaption and mitigation strategies at the regional level.

The proposed approach has a higher degree of applicability for Q_f estimation in large areas than approaches proposed in previous studies, as all the data used were available to the public. Compared with other recent studies (Chow et al., 2014; Nie et al., 2014; Park et al., 2016), which relied on data that were only available for local regions, this research was not restricted to small study areas because all data were available for all of Los Angeles County. Therefore, this approach can be readily applied to similar studies in different study areas with different climates. Q_f in the mid-latitude cities should have its peak value during winter mornings when the offset between the indoor and outdoor temperature reaches its maximum value, especially on workdays, because more buildings would be in operation than on weekends.

CHAPTER 6

MODELING THE EFFECT OF CLIMATE CHANGE ON BUILDING ENERGY DEMAND IN LOS ANGELES COUNTY USING A GIS-BASED HIGH SPATIAL AND TEMPORAL RESOLUTION APPROACH

6.1 Introduction

The effect of climate change on the building energy demand in Los Angeles County is discussed in this chapter, which comprises four sections. The methods were presented in detail in Section 4.3. In Section 6.2, the impact of climate change on the building energy demand at different temporal scales (annual, monthly, and hourly) is presented. The spatial variations of the energy demand change at the neighborhood scale are described in Section 6.3. Major findings, implications, and the strengths and limitations of the approach applied in this study compared previously published works are discussed in Section 6.4. Results of this study were published in *Energy* (Zheng & Weng, 2019, Appendix B).

The impact of climate change on buildings can be influenced by multiple factors. Each factor was analyzed for seven TMY weather zones, three building technologies, eighteen building prototypes, and two IPCC carbon dioxide emission scenarios. This chapter analyzes the climate impact at three different temporal scales (annual, monthly, and hourly) and assesses changes in the spatial patterns of the building energy demand across the Los Angeles County using the relative change (RC) and absolute difference (AD). The RC can be calculated by the

following formula:

$$RC = (E_f - E_p) / E_p * 100\% \quad (21)$$

The RC reflects the energy consumption difference between the calibrated current energy consumption (E_p) and projected future energy consumption (E_f). The AD represents the difference in energy consumption intensity, which can be calculated as follows:

$$AD = (E_f - E_p) / FA \quad (22)$$

where FA is the building floor area, which is the product of the number of floors in a particular building and the area of each floor.

6.2 Impact of Climate Change on the Building Energy Demand at Different Temporal Scales

6.2.1 Variation at the Annual Scale

The variation across building types, ages, and weather zones at the annual scale was first analyzed. Tables 6.1 and 6.2 show the annual average building energy demand, as measured by the RC and AD, between 2050 and the present (1991–2005) in Los Angeles County for commercial and residential buildings. The majority of building types showed an apparent increase in energy demand under both emission scenarios, and the energy demand increase was higher under the high-emission scenario. A large variation in energy consumption change across different types of buildings was identified. For example, the ADs ranged from -28.7 MJ/m^2 (warehouse) to 68.2 MJ/m^2 (Outpatient), and the RCs ranged from -11.8% (warehouse) to 7.9%

(medium office) under the RCP8.5 scenario. Due to the higher energy consumption intensity under the current climate, the majority of commercial buildings showed higher ADs than two types of residential houses.

Because of global warming, the cooling energy intensity for all types of buildings should increase under both emission scenarios, while the energy intensity for heating in all types of buildings should decrease. The change in the cooling and heating energy demand in the future showed even greater changes than the total energy demand change. The RC for cooling energy increase ranged from 5.9 MJ/m² (warehouse) to 166.8 MJ/m² (full-service restaurant) under the RCP8.5 scenario. However, the dramatic changes in the cooling and heating energy demand can easily be ignored due to the smaller changes in the total energy demand, if no further analysis was performed. For example, under the RCP8.5 scenario, the full-service restaurant category showed much larger AD than the hospital category with regard to both the cooling and heating energy intensity, although the increase in cooling would nearly be offset by the decrease in heating, resulting in a smaller total energy AD than that of the hospital category. The two types of restaurants showed the largest ADs in cooling and heating energy intensity among all types of buildings, which might be attributed to their large exposure to the outdoor environment and air intake in addition to the need for regulating waste heat from cooking. Moreover, restaurants should experience a larger heating energy demand decline under a warmer climate because the internal heat gain through high-intensity cooking can compensate for the need for space heating energy in winter months. Therefore, restaurants should expect to be more sensitive to climate change.

Table 6.1

Relative change (%) and absolute difference (MJ/m²) in the average annual building energy demand between 2050 and present (1991–2005) in Los Angeles County under the RCP8.5 emission scenario (Zheng & Weng, 2019).

Building Type	Total AD	Total RC	Cooling AD	Heating AD
Commercial				
Full-Service Restaurant	1.3	0.1%	166.8	-169.2
Hospital	14	1.0%	44.6	-38
Large Hotel	51.5	3.5%	74.1	-30.6
Large Office	24.4	4.8%	29.5	-12.8
Mid-Rise Apartment	30.45	4.5%	49.8	-25.15
Medium Office	46.9	7.9%	55	-12.3
Outpatient	68.2	4.0%	102.9	-36.3
Primary School	31.5	4.8%	51.5	-24.6
Fast-Food Restaurant	18.3	0.3%	151	-142.9
Secondary School	36.7	6.2%	68	-38.9
Small Hotel	40.7	5.2%	45.8	-9.2
Small Office	31	4.9%	43.3	-13.8
Stand-Alone Retail	6.8	1.0%	54.6	-47.5
Strip Mall	4.1	0.4%	57.7	-53.2
Supermarket	-18.1	-0.9%	34.7	-114.1
Warehouse	-28.7	-11.8%	5.9	-34.1
Residential: Multiple Family	7.2	4.1%	10.9	-5.9
Residential: Single Family	2.8	2.3%	10.4	-9.5

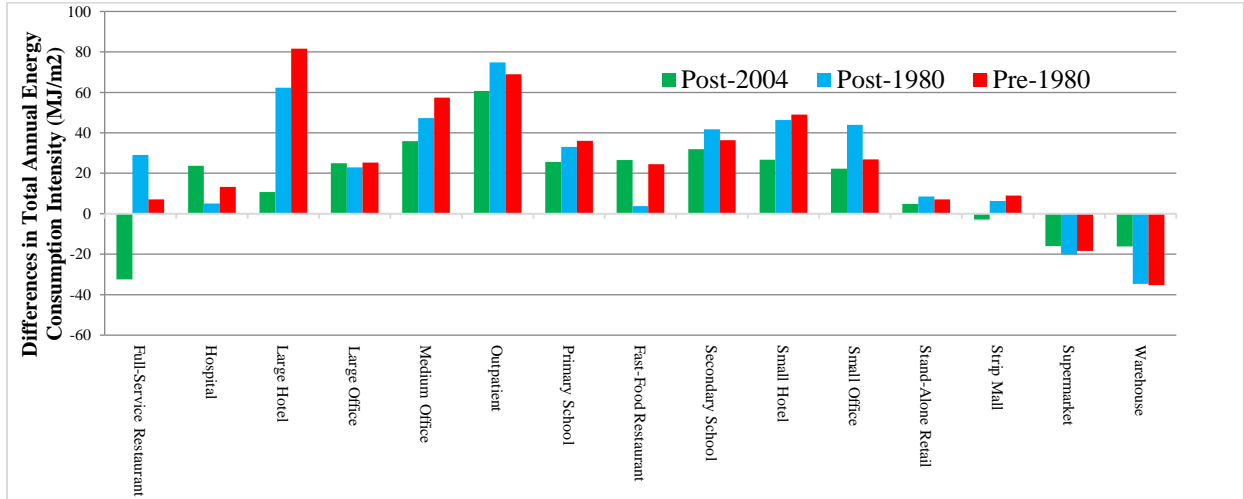
The effect of building technologies on the energy performance was further analyzed. Figure 6.1 presents the differences in total annual energy consumption intensity (a), cooling (b), and heating (c) for commercial buildings between the year 2050 and 1991–2005 under the RCP8.5 emission scenario, presented for three periods of time: after 2004 (post-2004), 1980 to 2004 (post-1980), and before 1980 (pre-1980). Although no substantial differences can be observed between the pre-1980 and post-1980 buildings regarding the energy consumption caused by global warming, the post-2004 buildings exhibited the smallest increase in the annual total energy demand for the majority of the studied building types. As shown in Figure 6.1b, the

post-2004 buildings had the smallest increase in space cooling energy demand for all types of buildings. It can be concluded that the newly constructed buildings in Los Angeles County should be less sensitive to higher outdoor temperatures in the future. They have the ability to maintain a comfortable indoor environment more efficiently due to their better insulation and advanced energy-saving technologies (Deru et al., 2011), such as the installation of air-conditioning systems with a higher coefficient of performance (COP) to decrease the energy demand, especially electricity demand on hot summer days.

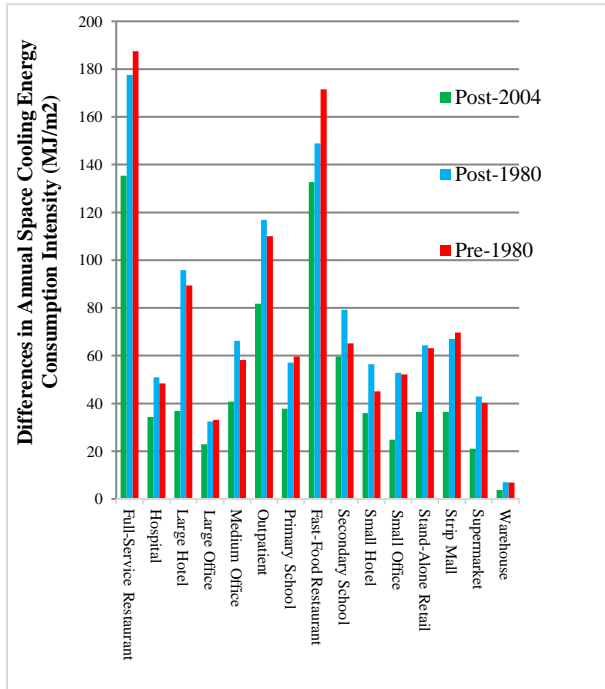
Table 6.2

Relative change (%) and absolute difference (MJ/m²) in the average annual building energy demand between 2050 and present (1991–2005) in Los Angeles County under the RCP6.0 emission scenario (Zheng & Weng, 2019).

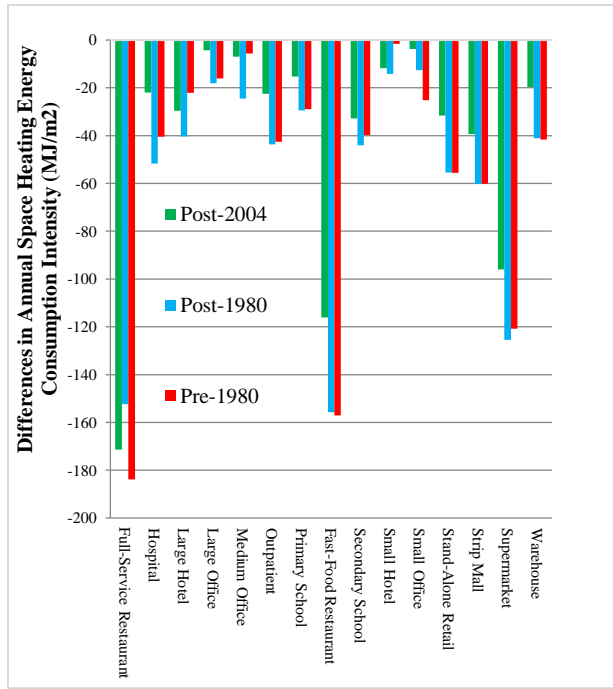
Building Type	Total AD	Total RC	Cooling AD	Heating AD
Commercial				
Full-Service Restaurant	-20.4	-0.4%	119.7	-137.4
Hospital	8.6	0.5%	31.2	-29.3
Large Hotel	34.4	2.2%	53.4	-24.9
Large Office	16.7	3.1%	21.6	-10.5
Mid-Rise Apartment	20.75	3.0%	36.05	-19.3
Medium Office	32.9	5.5%	40.9	-9.3
Outpatient	53.1	3.1%	75.8	-25.3
Primary School	20.4	3.1%	37.5	-20
Fast-Food Restaurant	-6.9	0.0%	107.6	-116.4
Secondary School	21.7	3.7%	48.8	-31.6
Small Hotel	28.5	3.5%	33	-7.4
Small Office	20.7	3.4%	31.4	-11.2
Stand-Alone Retail	-0.1	0.1%	40.7	-38.5
Strip Mall	-2.5	-0.2%	42.8	-43.1
Supermarket	-24.1	-1.1%	25	-90.3
Warehouse	-23.9	-9.8%	4.2	-27.4
Residential: Multiple Family	4.8	2.7%	8.3	-4.9
Residential: Single Family	1.3	1.1%	7.8	-7.7



(a)



(b)



(c)

Figure 6.1. Differences in the total annual energy consumption intensity (a), space cooling (b), and space heating (c) (MJ/m²) for commercial buildings between the 2050 and 1991–2005 under the RCP8.5 emission scenario (Zheng & Weng, 2019).

6.2.2 Variation at the Monthly Scale

Because the impact of global warming on the building energy demand may have larger variations at finer geographical scales, this study further analyzed the impact at monthly scales. The RCP8.5 scenario was assessed at finer time scales to examine the vulnerability of buildings under extreme hot weather. Although the majority of buildings had positive annual AD values, all of them had both positive and negative monthly AD values throughout the year. Moreover, all buildings showed increased cooling energy demand and decreased heating energy demand in all months (Figures 6.2b and c). The largest positive AD in total energy for all buildings occurred in August (Figure 6.2a), when the increase in cooling reached its peak and there was little heating demand. From April to October, the total energy demand increased because the increased cooling energy exceeded the decreased heating energy, and from November to March, the total energy demand declined because the increased heating demand could not be offset by the decreased cooling demand. Residential buildings showed smaller ADs than commercial buildings, regardless of the month and energy type. The total energy AD varied from -1.09 MJ/m^2 (January) to 2.02 MJ/m^2 (August) for multiple-family apartments, which showed a slightly larger variation than single-family houses. Commercial buildings showed not only larger monthly ADs but also a greater variation among the different building types. In January, the AD in the total energy ranged from -25.8 MJ/m^2 (full-service restaurant) to 2.9 MJ/m^2 (outpatient buildings), and the increased heating energy use was the major driver. In August, as the cooling energy demand reached its peak, the AD in total energy ranged from 1.8 MJ/m^2 (warehouse) to 30.9 MJ/m^2 (full-service restaurant).

Figure 6.2d shows the AD in the monthly energy intensity under the RCP8.5 emission scenarios across the different TMY3 weather zones. The Burbank-Glendale weather zone

presented the largest increase in the total energy intensity from April to October. Because the Burbank-Glendale weather zone exhibited the largest cooling energy increase (Figure 6.2e), which was caused by its basin topography, there would likely be a larger temperature increase than in the other weather zones. The Lancaster and Palmdale weather zones exhibited the largest negative ADs in the context of the total energy demand from October to March because they had the largest decrease in heating energy demand. This finding could be the result of the cold, semiarid steppe climate of these areas, which have colder and windier winters than the other zones. These weather zones were not found to have a large positive AD for cooling. Because the average temperature in summer under the current climate is already much higher than the comfort temperature (18.3 °C) (Figure 4.3), they already have a high cooling demand. Figure 6.3 presents the total (a), space cooling (b), and space heating (c) monthly energy consumption intensity differences (MJ/m²) between the year 2050 and 1991–2005 under the RCP8.5 emission scenario for commercial buildings constructed at different times. The post-2004 buildings exhibited the smallest increase in the cooling energy demand and decrease in the heating energy for all months, which contributed to the smallest change in the total energy demand throughout the year.

6.2.3 Variation at the Hourly Scale

It was discovered that the largest total energy increase occurred in the summer months, especially in August. This section presents a more detailed analysis of the hourly ADs across different weather zones in August. Diurnal time series were created to explain the hourly energy consumption changes. For each specific time period, the average value of the energy consumption during the same hour over 31 days in August was used. Because there is usually little heating energy demand in August, the analysis was only based on total and cooling energy

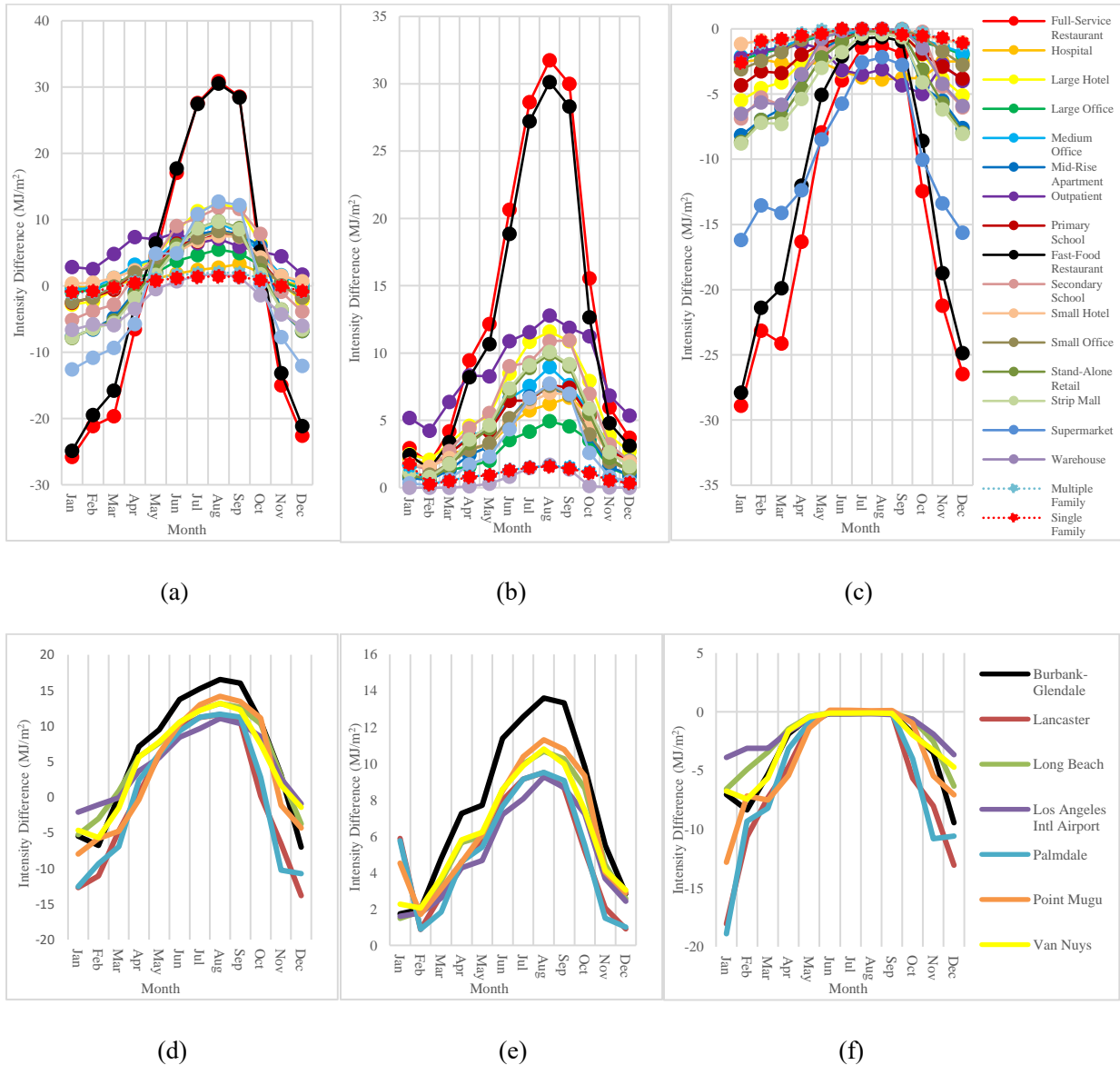
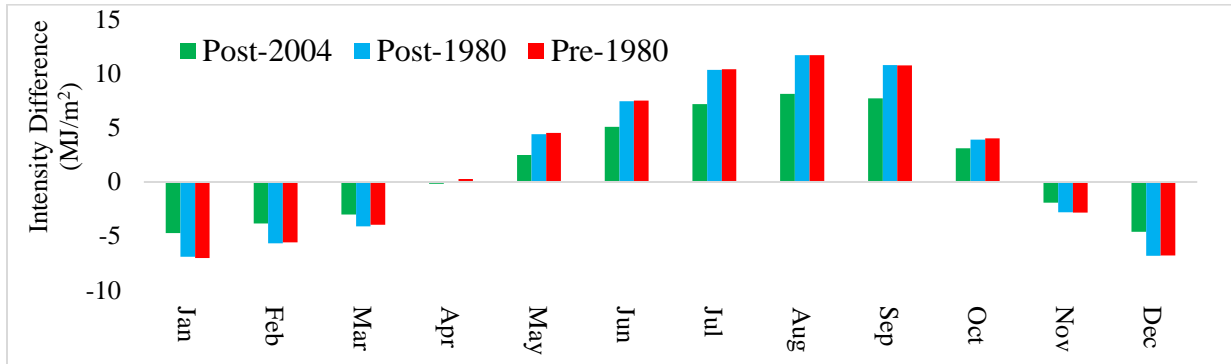
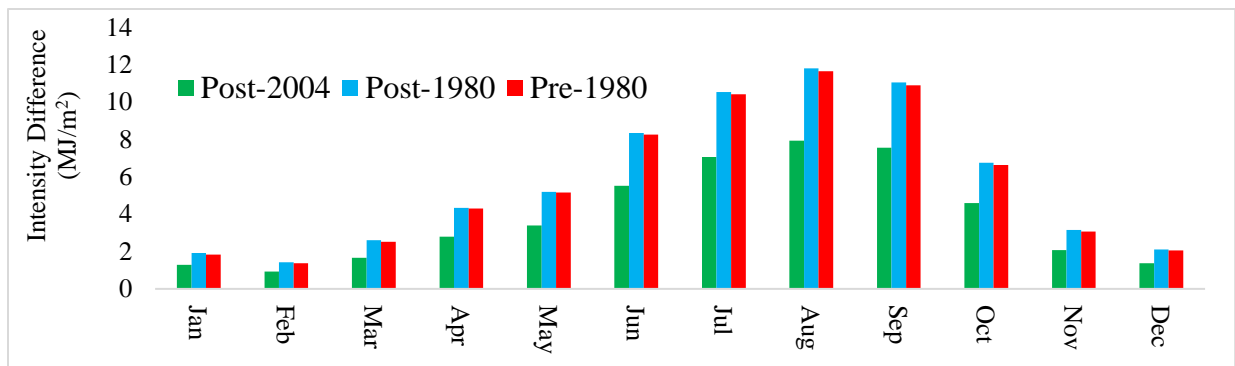


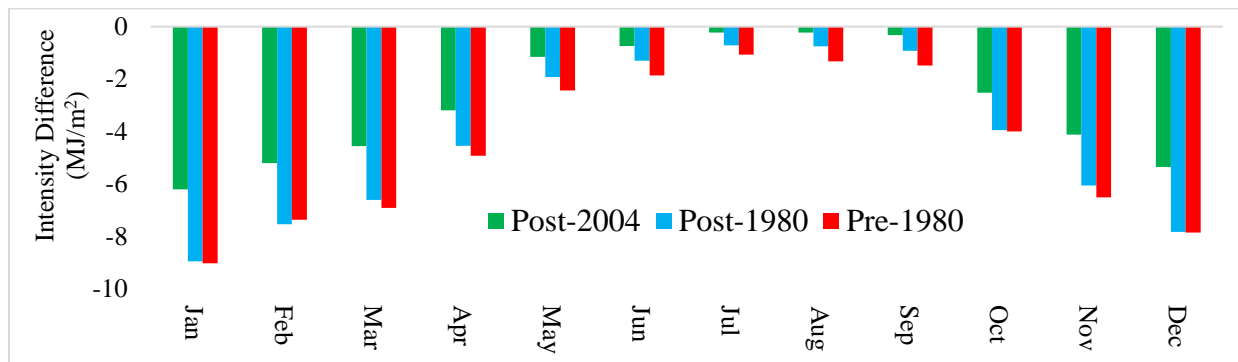
Figure 6.2. Absolute difference in average monthly (a) total, (b) cooling, and (c) heating building energy intensity (MJ/m²) between 2050 and 1991–2005 under the RCP8.5 emission scenario across building types; change in monthly energy intensity (MJ/m²) under the RCP8.5 emission scenarios across different TMY3 weather zones in Los Angeles County: (d) monthly total energy intensity change; (e) monthly cooling energy intensity change; and (f) monthly heating energy intensity change (Zheng & Weng, 2019).



(a)



(b)



(c)

Figure 6.3. Energy consumption intensity differences (MJ/m^2) by month for commercial buildings constructed at different times between the year 2050 and 1991–2005 under the RCP8.5 emission scenario: (a) total energy consumption; (b) space cooling; and (c) space heating (Zheng & Weng, 2019).

demands. Figures 6.4a and b show the average hourly building total and cooling energy intensity AD between 2050 and 1991-2005 under the RCP8.5 emission scenario across building types. Although all buildings exhibited increased total and cooling energy demand throughout the day, all commercial buildings showed a larger positive AD and greater variation. Restaurants showed a considerably larger positive AD in total energy than the other building types, with a maximum AD of 67.5 KJ/m^2 (fast-food restaurants at 12 pm). All commercial buildings showed a larger positive AD in the daytime than at night, although the time of the peak AD was different for some building categories. The majority of commercial buildings showed the largest positive AD from 9 am to 5 pm, whereas hotels and residential buildings showed positive ADs in the early morning hours and at night. Restaurants observed two AD peaks during the daytime, corresponding to lunch and dinner.

The variation in the diurnal cooling energy demand was much smoother than that of the total energy (Figure 6.4c and d) because the total energy demand was affected by additional factors in addition to the diurnal temperature variation. The diurnal variation in the total and cooling energy ADs at the Los Angeles International Airport was much closer to that of commercial buildings. This was surprising because the Los Angeles International Airport weather zone possessed the highest percentage of commercial building floor area (30.82%) (Table 6.3). The diurnal variation patterns of the total and cooling energy ADs in the Lancaster weather zone appeared similar to that of residential buildings because this area had the highest percentage of residential building floor area (91.10%).

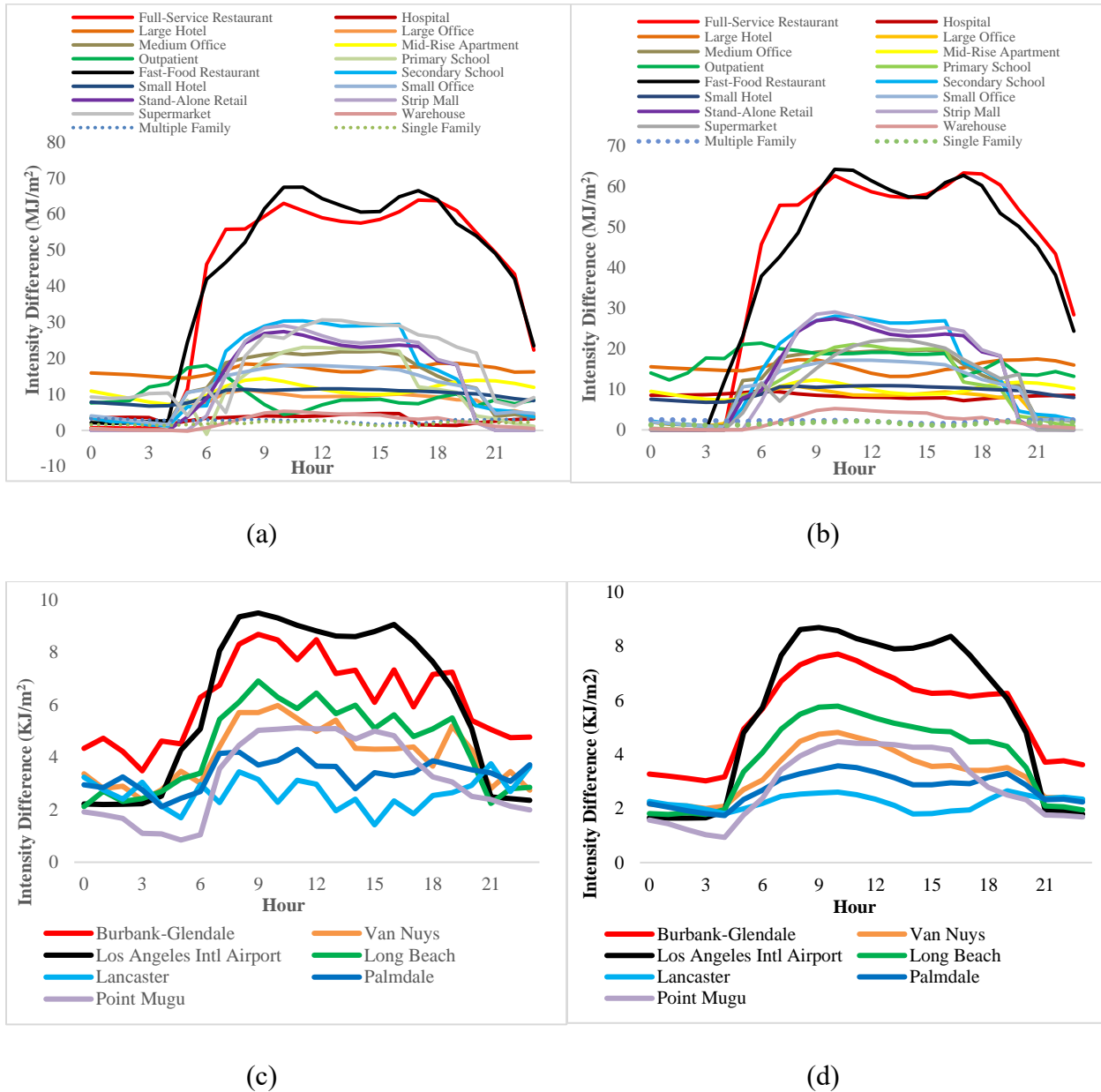


Figure 6.4. Diurnal change in absolute difference in the average building energy intensity (MJ/m^2) between 2050 and 1991–2005 under the RCP8.5 emission scenario across building types in Los Angeles in August: (a) total energy and (b) cooling energy; change in energy intensity (KJ/m^2) under the RCP8.5 emission scenario across different TMY3 weather zones in Los Angeles in August: (c) diurnal total energy intensity change and (d) diurnal cooling energy intensity change (Zheng & Weng, 2019).

Table 6.3

The percentage (%) of residential and commercial building floor areas in the 7 weather zones in Los Angeles County (Zheng & Weng, 2019).

	Percentage of Residential Building	Percentage of Commercial Building
Burbank-Glendale	81.66%	18.34%
Van Nuys	85.51%	14.49%
Los Angeles Intl Airport	69.18%	30.82%
Long Beach	80.27%	19.73%
Lancaster	91.10%	8.90%
Palmdale	84.52%	15.48%
Point Mugu	86.89%	13.11%

6.3 Spatial Variations of Energy Demand Change at the Neighborhood Scale

This section presents the spatial variation of changes in energy demand by 2050 due to climate change at the neighborhood scale. Figure 6.5 presents the spatial variation of total energy consumption changes (both RC and AD) in 2050 under the RCP8.5 and RCP6.0 scenarios. Large within-county RC and AD variations can be seen under both scenarios. In general, the RC and AD in the annual total energy variation followed the same pattern, represented by a larger increase in the south part of the county and a smaller increase or even decrease in the north part. This finding is because the current climate is warmer in the south, resulting in a low current heating energy demand. Thus, there is a limitation to the heating energy consumption decrease because the minimum heating energy demand cannot be less than zero, whereas there is no limitation to the increase in the cooling energy demand. Because the climate would be warmer in 2050, the slight decrease in the heating energy demand in the south cannot be offset by the larger cooling energy demand, leading to a larger increase in the total energy demand than in the north. The increased energy demand was found to be more substantial under the RCP8.5 scenario than under the RCP6.0 scenario. The number of neighborhoods with an annual total energy demand

increasing by more than 4.5% was 188 under the RCP8.5 scenario and only 33 under the RCP6.0 scenario. A similar difference can be observed when using the AD as the metric. The number of neighborhoods with an increase in the total energy demand exceeding 17 MJ/m^2 was 145 under the RCP8.5 scenario and only 45 under the RCP6.0 scenario.

The increase in the cooling energy demand should be more severe than that of the total energy demand (Figures 6.6a through d). The RC in the cooling energy demand ranged from 27% to 122% under the RCP8.5 scenario and 25% to 95% under the RCP6.0 scenario, much larger than -1.8% to 7.9% and -1.8% to 6.7% for the total energy demand RCs, respectively. Neighborhoods with a RC in the cooling energy demand of more than 100% were mostly located in the Los Angeles International Airport weather zone because it had the highest percentage of commercial buildings (Table 6.3). Commercial buildings were found to have a higher energy demand increase than residential buildings, as discussed in the previous section. The dramatic positive RC for commercial buildings could cause a huge challenge for the cooling energy supply, while frequent power outages could happen in the future if no changes are made to the current electronic system configuration. The AD in the cooling energy demand under the RCP8.5 scenario did not follow the same trend as the AD in the total energy demand. The “hotspots” (larger than 30 MJ/m^2) in the cooling energy demand in response to climate change were found in the Burbank-Glendale weather zone. The probable cause is a greater number of warmer months in this zone than in other locations because it is located in a valley. Moreover, building size and density played an important role in the energy demand AD. Neighborhoods with the largest increase in energy consumption intensity were located in the major commercial zones with high density of tall buildings. As shown in Figures 6.6e and f, the downtown area had the highest increase of per building energy demand because it had the largest average building floor

area (more than 3,000 m²) among all neighborhoods in the Los Angeles County.

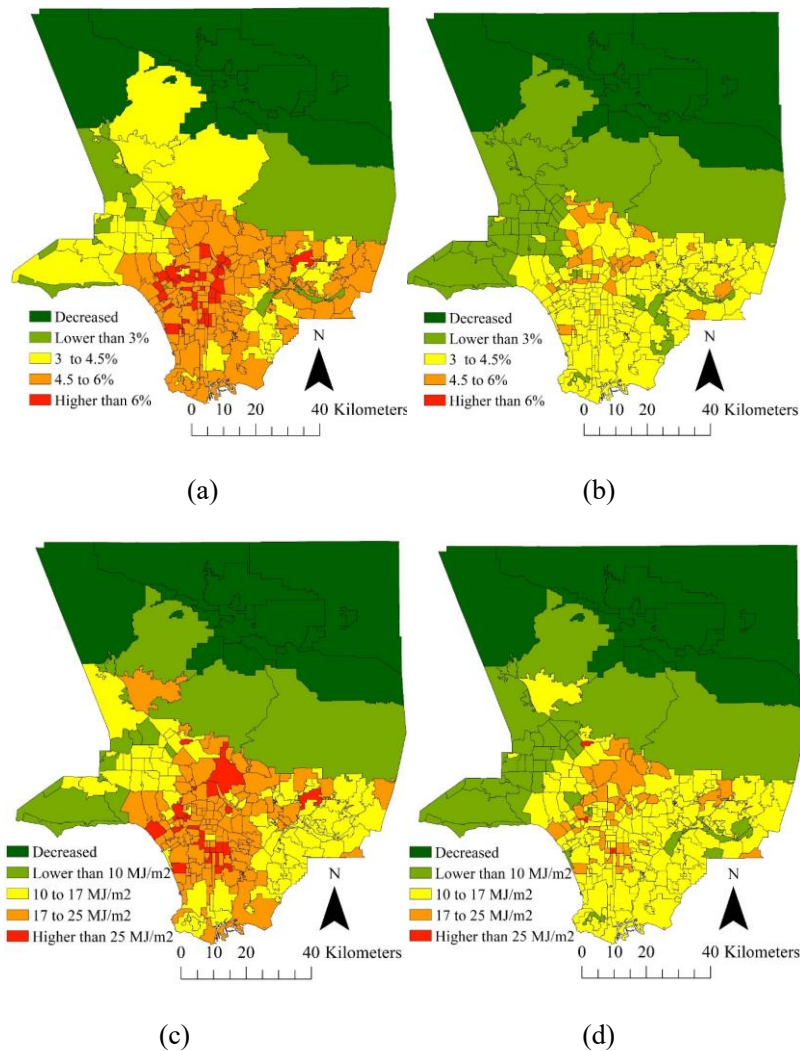


Figure 6.5. The spatial variation of total energy consumption changes in 2050 due to climate change in Los Angeles: (a) annual relative change (%) under the RCP8.5 scenario; (b) annual relative change (%) under the RCP6.0 scenario; (c) annual energy intensity absolute difference (MJ/m²) under RCP8.5 scenario; (d) annual energy intensity absolute difference (MJ/m²) under the RCP6.0 scenario. Note: this sixth version of neighborhood boundaries were defined by the Los Angeles Times in June 2010, which represents the boundaries of communities and social organizations within each city (Zheng & Weng, 2019).

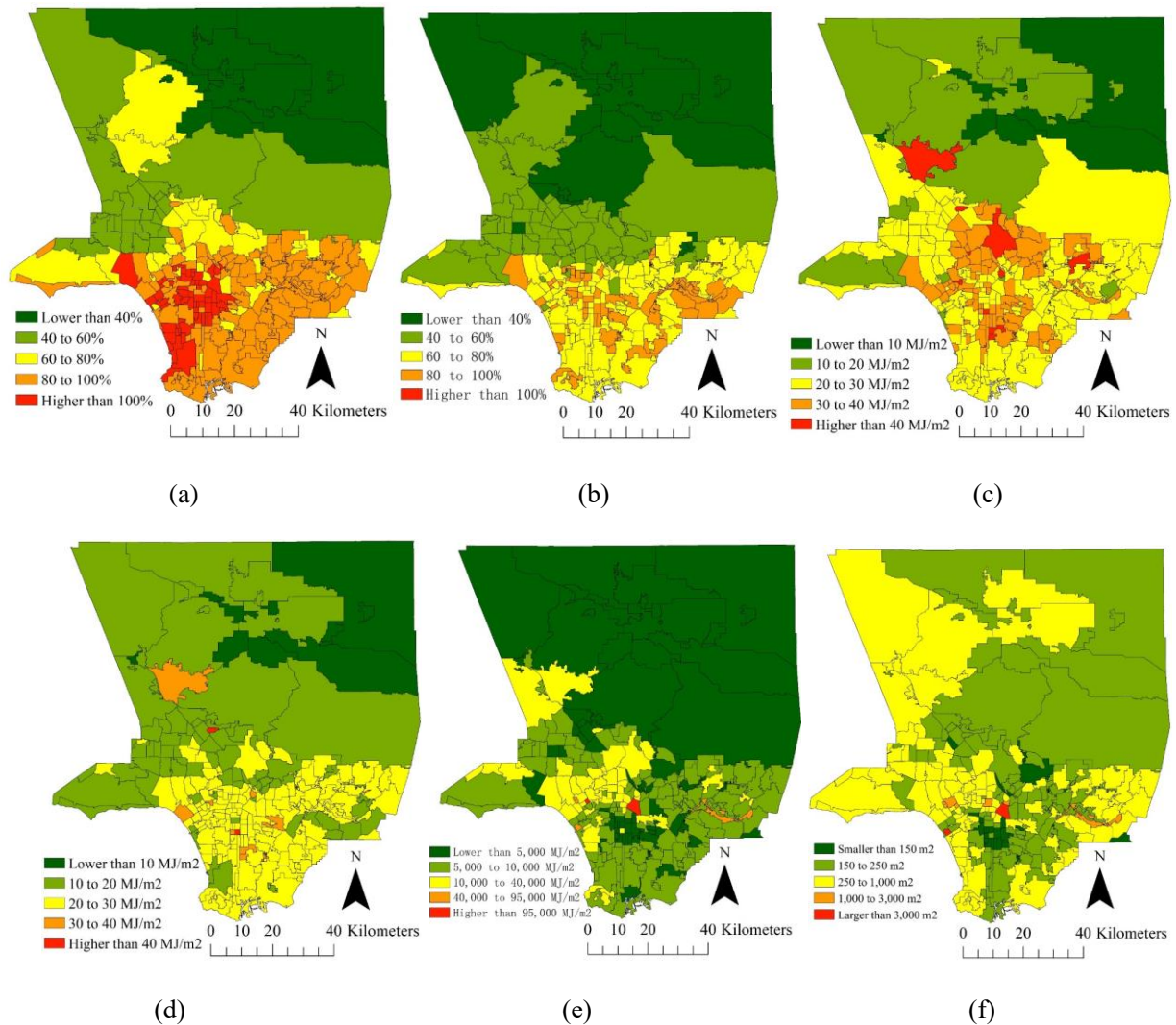


Figure 6.6. The spatial variation of cooling energy consumption changes by 2050 caused by climate change in Los Angeles County at the neighborhood scale: (a) annual relative change (%) under the RCP8.5 scenario; (b) annual relative change (%) under the RCP6.0 scenario; (c) annual energy intensity absolute difference (MJ/m²) under the RCP8.5 scenario; (d) annual energy intensity absolute difference (MJ/m²) under the RCP6.0 scenario; the spatial variation of the absolute difference in cooling energy consumption per building in 2050 caused by climate change in Los Angeles County at the neighborhood scale (MJ/m²): (e) under the RCP8.5 scenario; (f) average floor area per building (m²) (Zheng & Weng, 2019).

6.4 Discussion and Conclusions

This section discusses the major findings, implications, strengths and limitations of the approach used in this study compared to previous published studies. The results of previous studies suggest that buildings in warmer climate zones have larger annual total energy increases than those in colder climate zones. The findings of this study agree with those of previous findings, However, more importantly, this study discovered a large variation even within the same climate zone, which was caused by building types and ages. In examining the changes in energy demand at finer temporal scales (i.e., monthly and diurnal), the variation of energy demand increases across different building types were larger, suggesting that simulations at high spatial and temporal resolutions were indeed necessary. Although lighting and equipment usage were not directly affected by climate change, they can increase the internal heat gain and raise the indoor temperature, resulting in the need for more cooling energy consumption.

Unlike previous studies, which used representative buildings (Andrić et al. 2016; Berger et al. 2014; Dirks et al. 2015; Huang and Gurney 2016) or assumed that each type of building had the same floor area fraction to the total building stock (Wang and Chen, 2014), this approach linked the building energy simulation and climate change model to fine-scale urban building inventory data. Therefore, this approach allows analysts and policy makers to assess the sensitivity of different regions in a city to climate change with regard to building energy demand increases at different spatial and temporal scales. In addition, a complete database of each building in Los Angeles County was built and can be combined with other data. Policy makers can take the database as a reference to choose appropriate policies that target specific regions. At the county scale, the results in this study suggest that the likely dramatic increase in the cooling energy demand is the major driving force of total energy increases at all-time scales. Because

electricity is the main source for space cooling, the high cooling demand should exceed the current electricity generate capacity. Moreover, due to electricity being the secondary energy source, the rising cooling energy demand will also lead to the increased consumption of other energy sources, such as traditional fossil fuels, which are widely used to generate electricity. According to the California Energy Commission, only 29% of electricity was generated through renewable energy sources in 2016, and the traditional energy sources remained the major sources. As a result, more greenhouse gases have been emitted. This study found that the increase in the energy demand was not distributed evenly throughout Los Angeles County at the neighborhood scale. Regions with a high density of tall commercial buildings (downtown and major commercial zones) exhibited the largest energy demand increase. Advanced building technologies can help save large amounts of energy, as indicated by buildings built after 2004 being more energy efficient than those built before 2004 at the annual and monthly time scales. However, 188,060 commercial buildings were built before 2004 in Los Angeles County, which account for 97.84% of all existing commercial buildings. In contrast, only 4,152 (2.16%) existing commercial buildings were built after 2004. Therefore, policy makers may consider the potential of zero net energy buildings (Rey-Hernandez et al., 2018) throughout the county and give the highest priority to regions most vulnerable to climate change. To achieve this goal, the high-resolution database of building sustainability created in this study can be combined with the solar potential rate for each region in Los Angeles County. At the individual building scale, two types of restaurants were identified to have much higher energy demand increases than the other types of buildings despite their locations and ages. Given that their peak energy demand increase was during lunch and dinner times in summer, reducing the solar heat gain and the effectiveness of cooling should be considered simultaneously for all restaurants. Strategies, such as installing

solar panels, cool roofs, green roofs, cooling system update, and window retrofit, should be considered.

CHAPTER 7

MODELING THE PERFORMANCE OF GREEN ROOF SYSTEMS AND PHOTOVOLTAIC PANELS FOR BUILDING ENERGY SAVINGS

7.1 Introduction

The potential mitigation effects of green roofs and PV-green roofs on buildings that are more vulnerable to climate change in terms of increased energy demand are discussed in this chapter, which comprises four sections. The methods were presented in detail in Section 4.4. In Section 7.2, the performance of PV-green roof mitigation strategies on the potential building energy use increase due to climate change is evaluated at different temporal (annual and monthly) scales. Section 7.3 presents the result of sensitivity analysis of the green roof model to key parameters. Major findings, strengths, and limitations of the methodology used in this study compared to previously published works are discussed in Section 7.4.

7.2 Evaluation of Green Roofs and Photovoltaic Panels on building Energy Savings at Different Temporal Scales

According to the results in Chapter 6, there are large within-county spatial variations in the building energy demand increases under both climate change scenarios. However, the increased energy demand was found to be more substantial under the RCP8.5 scenario. Moreover, the increased cooling energy demand was found to be more severe than the total energy demand. To assess the potential mitigation effects of PV-green roof systems, this study

identified the neighborhoods that are expected to have the largest increase in the cooling energy demand in buildings under the RCP8.5 scenario as study sites. In the following step, buildings found to have greater energy increases were selected as the buildings for experiment.

Glendale and Koreatown were selected as the study sites because they exhibited the largest positive AD and RC in the cooling energy demand among all neighborhoods (Figure 7.1), respectively. Within the two study sites, the two types of restaurants (full-service and fast-food restaurants) were found to be more susceptible to the large increases in the cooling energy demand in both neighborhoods based on the measured AD or RC. Among the other building types, outpatient buildings showed the highest AD in Glendale, while medium offices showed the highest RC in Koreatown. Building composition was the primary factor that caused these two neighborhoods to have large increases in the cooling energy demand. The two types of restaurants made up 6.03% and 9.56% of commercial buildings in Glendale and Koreatown, which was higher than that in the entire Los Angeles County (4.26%). Table 7.1 summarizes the results for 13 selected vulnerable buildings in terms of the performance of PV-green roof mitigation on potential building energy savings. This study intended to include one building per prototype, although not all the prototypes were available in the study sites. For example, post-2004 outpatient facilities and fast-food restaurants could not be found in Glendale.

7.2.1 Evaluation of Green Roofs and Photovoltaic Panels on Building Energy Savings at the Annual Scale

The solar potential for each building roof was rated using the open-source roof solar potential data from the Google Project Sunroof database, which provides the area available for PV system installation. All 13 buildings passed the threshold of 1,405 hours of usable sunlight per year and ranked as high solar potential roofs. Therefore, in this dissertation, both green roofs

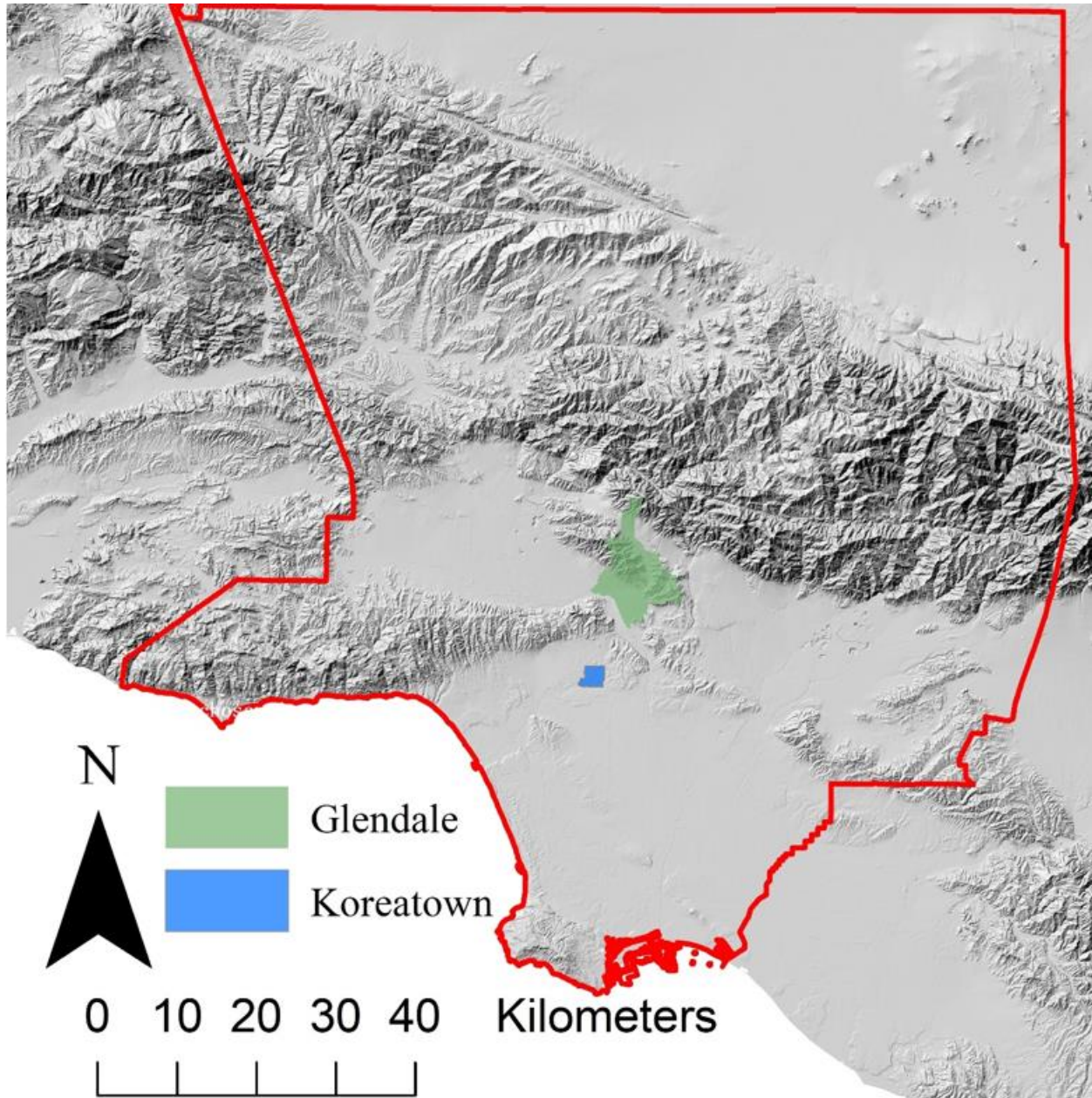


Figure 7.1. The location of the two study sites for evaluation of green roofs and photovoltaic panels on building Energy Savings: Glendale and Koreatown, Los Angeles County, California, USA.

Table 7.1

Selected buildings for performance evaluation of PV-green roof mitigation effects on potential building energy savings.

ID	Area (m ²)	Number of Floors	Type	Neighborhood	Age
1	1,057	1	Full-Service Restaurant	Glendale	Before 1980
2	304	1	Fast-Food Restaurant	Glendale	1980–2003
3	290	1	Full-Service Restaurant	Glendale	1980–2003
4	138	1	Fast-food Restaurant	Glendale	Before 1980
5	352	1	Fast-Food Restaurant	Glendale	After 2004
6	876	1	Outpatient	Glendale	1980–2003
7	186	1	Outpatient	Glendale	Before 1980
8	219	1	Fast-Food Restaurant	Koreatown	Before 1980
9	353	1	Full-Service Restaurant	Koreatown	Before 1980
10	467	1	Full-Service Restaurant	Koreatown	1980–2003
11	455	1	Fast-Food Restaurant	Koreatown	1980–2003
12	587	3	Medium Office	Koreatown	Before 1980
13	828	3	Medium Office	Koreatown	1980–2003

and PV systems were added to each tested building during the simulation. Table 7.2 presents the available area for PV system installation and simulated annual electricity produced in gigajoules (GJ) for each tested building in 2050.

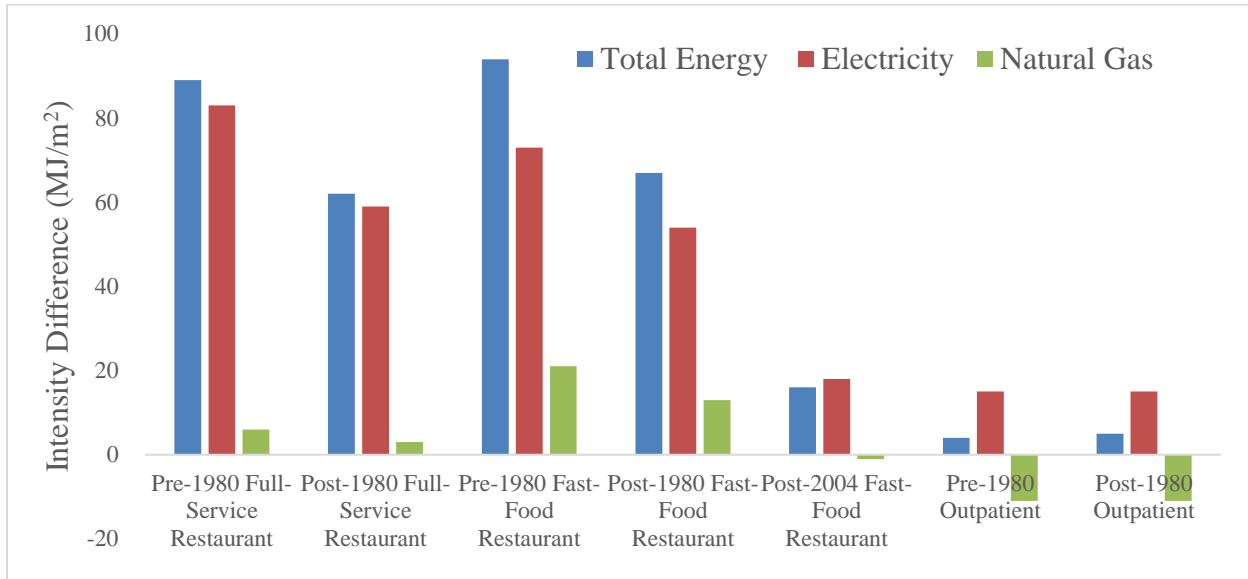
Figure 7.2 presents the annual energy savings (MJ/m²) from green roofs on the tested buildings compared to traditional roofs at two study sites under the RCP8.5 emission scenario. All buildings with green roofs showed positive energy savings with regard to both the total energy and electricity demand, although the extent of the savings differed according to building type. The majority of the total energy savings arose from electricity savings. The two types of restaurants showed a higher degree of electricity and natural gas savings than the other building categories, suggesting that they would receive the most benefits in terms of energy savings after the installation of green roofs. However, green roofs were predicted to save less energy for

Table 7.2

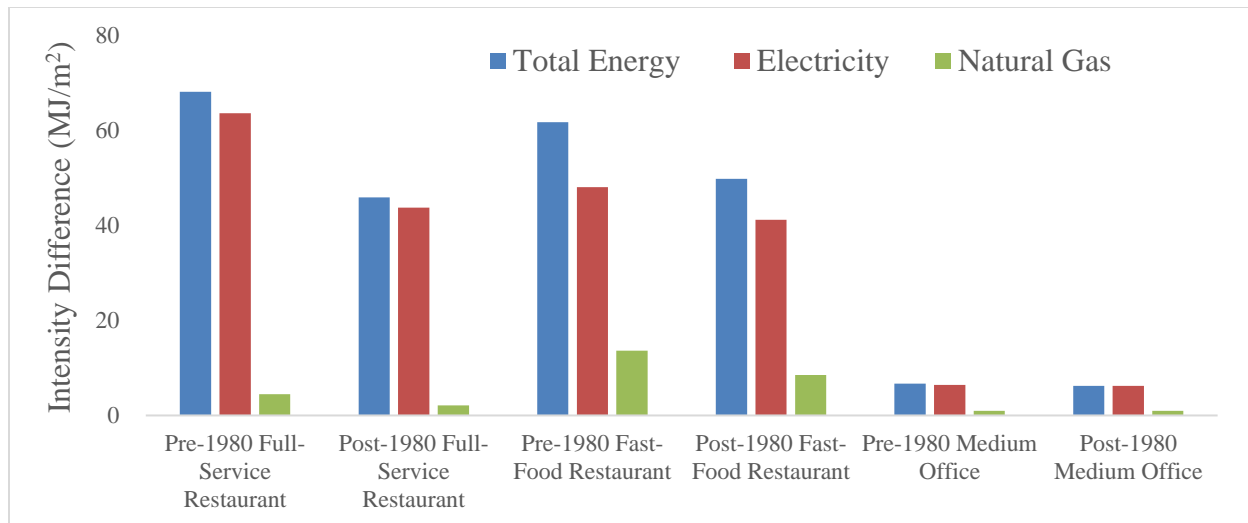
Simulation of annual electricity produced by photovoltaic panels in 2050 for the tested buildings under the RCP8.5 emission scenario.

ID	Available Area for Photovoltaic System Installation (m ²)	Simulated Annual Electricity Produced by the Photovoltaic System in Gigajoules (GJ)
1	183	55.84
2	39	11.63
3	54	16.69
4	29	8.62
5	65	19
6	425	127.02
7	57	16.62
8	42	12.82
9	73	20.52
10	99	29.62
11	139	39.55
12	253	74.4
13	549	160.34

newly constructed restaurants. Green roofs exhibited the largest energy savings for pre-1980 restaurants, but for post-2004 restaurants showed the least savings. However, this contrast was not obvious for medium offices and outpatient buildings. Figure 7.3 shows the percentage breakdown of the individual components contributing to the annual electricity savings from green roofs at the two study sites under the RCP8.5 emission scenario. Most electricity savings were derived from cooling energy savings, followed by savings on fan energy, suggesting that lower indoor temperatures can also save ventilation energy. Other savings (e.g., lighting, equipment, pumps, humidification, and refrigeration) were trivial for most of the tested buildings except for the two outpatient buildings and post-1980 medium office. One reason for this difference is that the space heating energy was supplied by electricity, which also contributed to

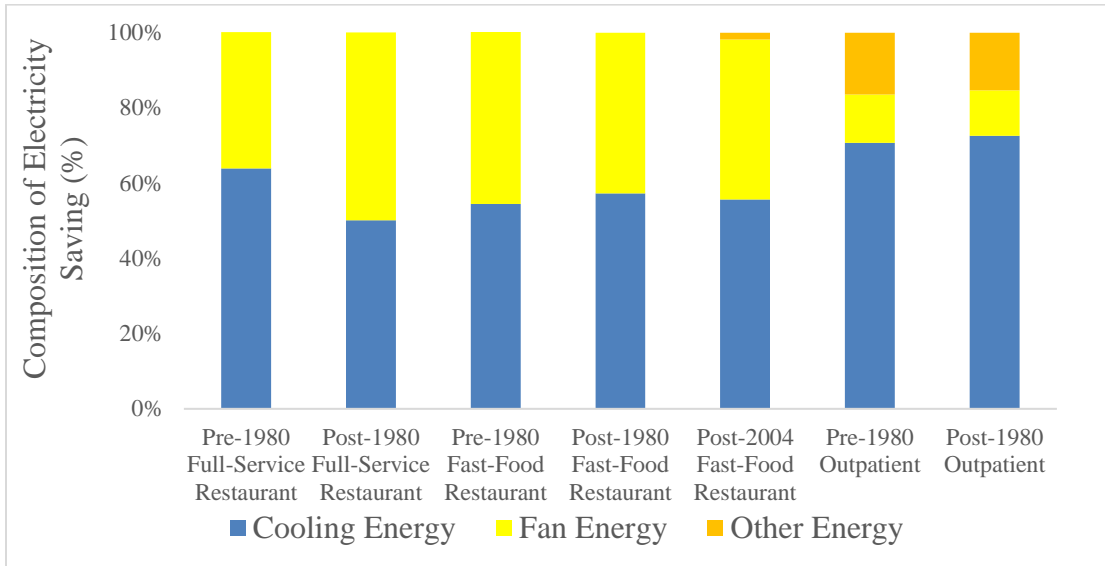


(a)

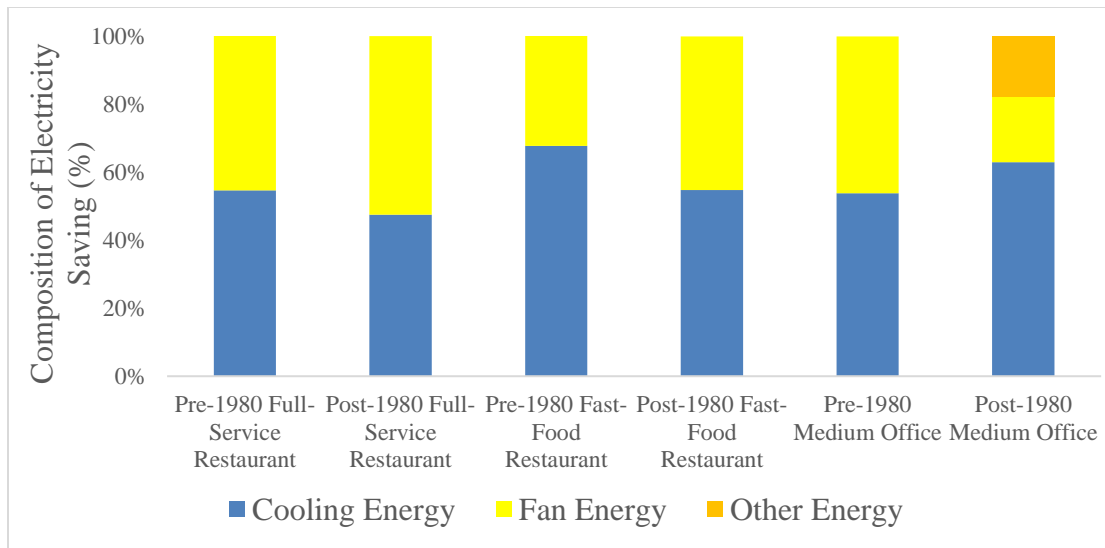


(b)

Figure 7.2. Annual energy savings (MJ/m²) for green roofs on the tested buildings compared to traditional roofs under the RCP8.5 emission scenario in 2050: (a) Glendale; (b) Koreatown.

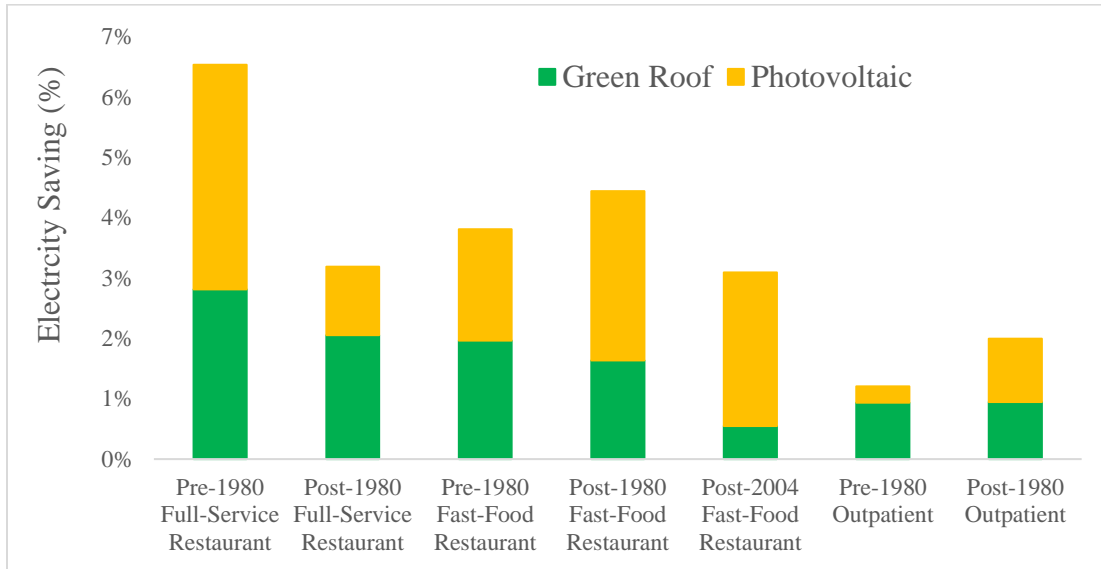


(a)

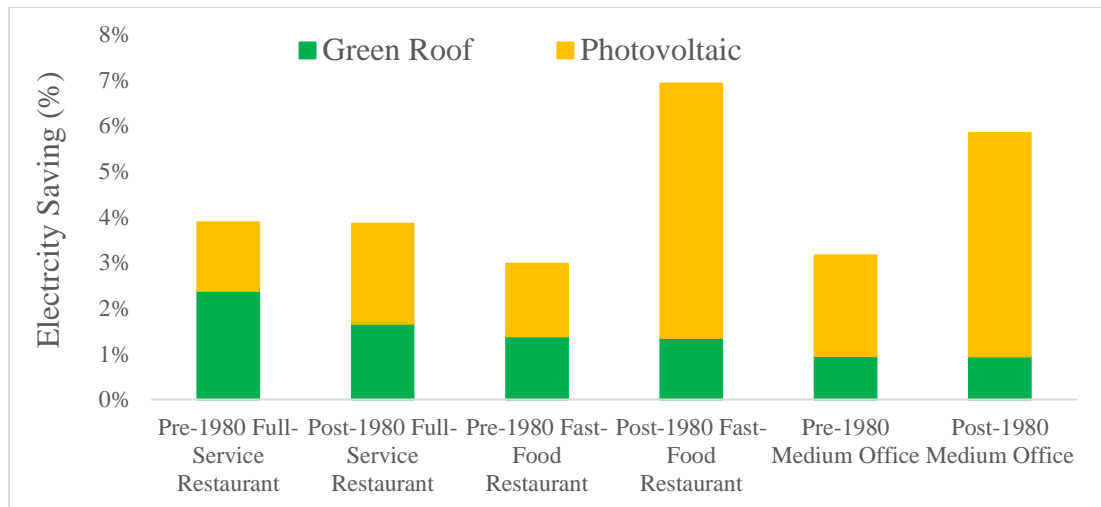


(b)

Figure 7.3. Percentage breakdown (%) of the individual components contributing to the simulated annual electricity savings from green roofs compared with traditional roofs under the RCP8.5 emission scenario in 2050: (a) Glendale; (b) Koreatown.



(a)



(b)

Figure 7.4. Percentage (%) of annual electricity savings from the integration of green roofs and photovoltaic systems compared with traditional roofs under the RCP8.5 emission scenario in 2050: (a) Glendale; (b) Koreatown.

their electricity savings. Thus, it can be concluded that all benefits of electricity savings from green roofs are from building HVAC systems. Figure 7.4 presents the annual electricity saving

percentage due to the integration of green roofs and photovoltaic systems at the two study sites under the RCP8.5 emission scenario. The annual electricity savings from the installation of PV-green roofs ranged from 1.2% (pre-1980 outpatient building) to 6.92% (post-1980 fast-food restaurant). Table 7.3 and Table 7.4 present the RC between 2050 and present (1991–2005) for all tested buildings under the RCP8.5 emission scenario with regard to the annual total energy and electricity demand, respectively. All restaurants with PV-green roofs were predicted to consume less total energy in 2050 than at present (Table 7.3), even under the high-emission scenario (RCP8.5), which indicates the robustness of PV-green roofs. The reduction in the increased net building energy demand caused by climate change ranged from 8.2% (pre-1980 outpatient building) to 299.2% (pre-1980 full-service restaurant). Although PV-green roofs cannot fully offset the increases in predicted electricity consumption in 2050 for the majority of buildings, the extent of the increase is much lower than with traditional roofs (Table 7.4).

A life-cycle approach, as adopted in Bianchini and Hewage (2012), was performed to analyze the social-economic benefits of installing PV-green roofs on all tested buildings. The parameter settings also followed the settings in Bianchini and Hewage (2012), which are listed in Table 7.5. The PV system installation cost for each building was found on the Google Project Sunroof website. The return on investment (ROI) after 20 years was found to exceed 100% in 12 of the 13 tested buildings, and the payback periods for installing PV-green roofs on all tested buildings ranged from 5.3 years (post-1980 medium office) to 14.2 years (post-1980 fast-food restaurant) (Table 7.6), suggesting that these buildings could receive considerable social-economic benefits. Compared to traditional roofs, which have a lifespan of only 20 years, the expected lifespan of a green roof varies from 30 to 55 years (Bianchini & Hewage, 2012; Chemisana & Lamnatou, 2014; Lamnatou & Chemisana, 2014, 2015). Therefore, the savings

Table 7.3

Relative change (%) in annual total energy demand between 2050 and present (1991–2005) in all tested buildings under RCP8.5 emission scenario.

Building Type	Neighborhood	RC (Traditional Roof) (%)	RC (PV-green Roof) (%)
Pre-1980 Full-Service Restaurant	Glendale	1.3%	-2.6%
Post-1980 Full-Service Restaurant	Glendale	1.7%	-0.2%
Pre-1980 Fast-Food Restaurant	Glendale	1.6%	-0.9%
Post-1980 Fast-Food Restaurant	Glendale	1.1%	-1.6%
Post-2004 Fast-Food Restaurant	Glendale	1.0%	-0.2%
Pre-1980 Outpatient	Glendale	5.1%	4.7%
Post-1980 Outpatient	Glendale	5.8%	4.7%
Pre-1980 Full-Service Restaurant	Koreatown	1.0%	-1.3%
Post-1980 Full-Service Restaurant	Koreatown	1.3%	-0.9%
Pre-1980 Fast-Food Restaurant	Koreatown	1.1%	-0.8%
Post-1980 Fast-Food Restaurant	Koreatown	0.6%	-3.2%
Pre-1980 Medium Office	Koreatown	9.5%	6.1%
Post-1980 Medium Office	Koreatown	7.8%	1.5%

Table 7.4

Relative change (%) in annual electricity energy demand between 2050 and present (1991–2005) in all tested buildings under the RCP8.5 emission scenario.

Building Type	Neighborhood	RC (Traditional Roof) (%)	RC (PV-green Roof) (%)
Pre-1980 Full-Service Restaurant	Glendale	9.9%	2.8%
Post-1980 Full-Service Restaurant	Glendale	9.5%	6.0%
Pre-1980 Fast-Food Restaurant	Glendale	7.4%	3.3%
Post-1980 Fast-Food Restaurant	Glendale	7.4%	2.7%
Post-2004 Fast-Food Restaurant	Glendale	6.8%	3.5%
Pre-1980 Outpatient	Glendale	5.8%	4.6%
Post-1980 Outpatient	Glendale	6.3%	4.2%
Pre-1980 Full-Service Restaurant	Koreatown	6.8%	2.7%
Post-1980 Full-Service Restaurant	Koreatown	6.6%	2.5%
Pre-1980 Fast-Food Restaurant	Koreatown	4.5%	1.4%
Post-1980 Fast-Food Restaurant	Koreatown	4.5%	-2.7%
Pre-1980 Medium Office	Koreatown	10.0%	6.5%
Post-1980 Medium Office	Koreatown	7.9%	1.6%

Table 7.5

Key parameters for the social-economic benefit analysis of installing green roofs (Bianchini & Hewage, 2012).

Investment/benefits	Value (\$/m ²)	Type	Time frame
Initial Construction Cost	146	Investment	One time
Maintenance Cost	2	Investment	Annual
Storm Water Retention	0.38	Benefit	Annual
Avoid Infrastructure Cost	39	Benefit	One time
Longevity Benefit	160	Benefit	After 20 years
Reduction of Infrastructure Improvement	8	Benefit	One time

Table 7.6

Return on investment (%) and payback periods (years) for installing green roofs and photovoltaic systems on all tested buildings.

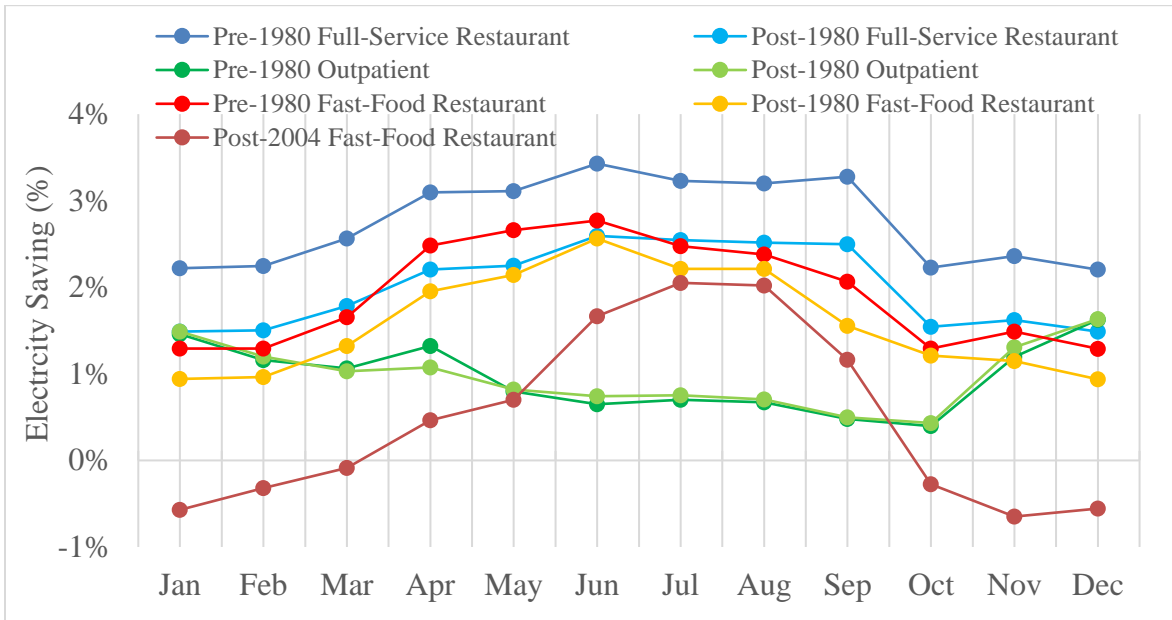
Building Type	Neighborhood	Return on Investment (ROI) after 20 years (%)	Payback Period (Years)
Pre-1980 Full-Service Restaurant	Glendale	173.9%	8.5
Post-1980 Full-Service Restaurant	Glendale	109.2%	12.7
Pre-1980 Fast-Food Restaurant	Glendale	126.8%	11.5
Post-1980 Fast-Food Restaurant	Glendale	95.2%	14.2
Post-2004 Fast-Food Restaurant	Glendale	162.8%	8.9
Pre-1980 Outpatient	Glendale	182.4%	9.0
Post-1980 Outpatient	Glendale	101.3%	13.7
Pre-1980 Full-Service Restaurant	Koreatown	104.5%	14.1
Post-1980 Full-Service Restaurant	Koreatown	124.1%	11.9
Pre-1980 Fast-Food Restaurant	Koreatown	126.8%	11.8
Post-1980 Fast-Food Restaurant	Koreatown	128.3%	11.7
Pre-1980 Medium Office	Koreatown	281.1%	5.9
Post-1980 Medium Office	Koreatown	322.1%	5.3

from re-roofing 20 years after initial construction can be counted as a longevity benefit of green roofs. In addition to the longevity benefit, installation of extensive green roofs could also increase property prices by at least 2% (Bianchini & Hewage, 2012), which could contribute to

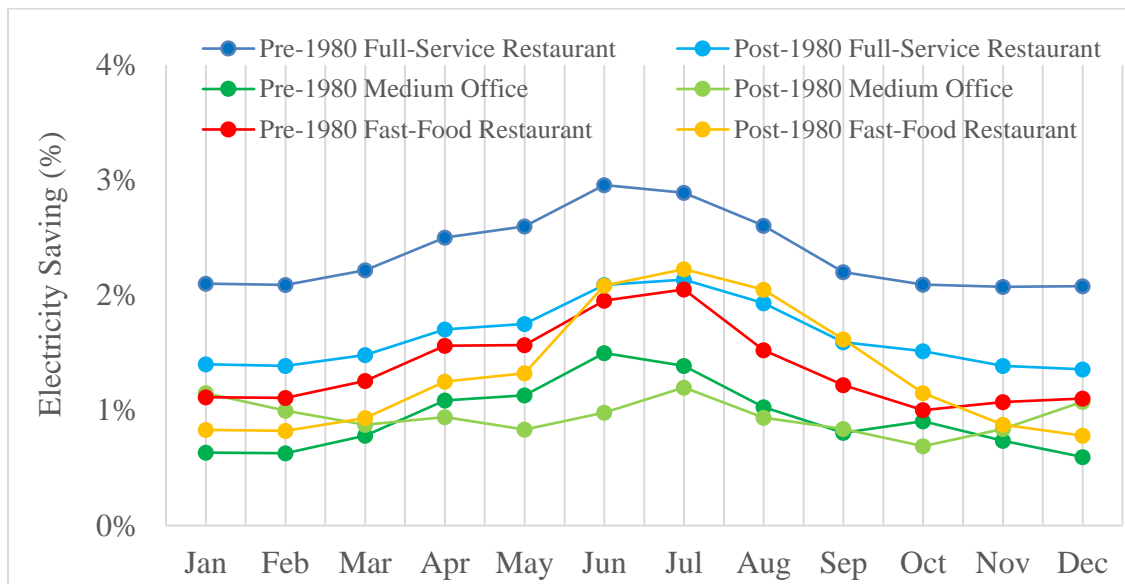
the high ROI and reasonable payback period. In this study, the estimation of projected increase in property prices was made based on the current prices of commercial buildings in Glendale and Koreatown using the LoopNet website (<https://www.loopnet.com/>).

7.2.2 Evaluation of Green Roofs and Photovoltaic Panels on Building Energy Saving at the Monthly Scale

Because larger increases in building energy demand were observed at finer time scales in Chapter 6, this section further analyzed the performance of green roofs on energy savings at the monthly scale. Because the outputs of energy generated by PV systems were only provided at the annual scale, this section focused only on the performance of green roofs on electricity savings. Figure 7.5 demonstrates the monthly electricity saving percentage from green roofs at the two study sites under the RCP8.5 emission scenario compared with traditional roofs. All buildings with green roofs showed positive electricity savings in all months except the post-2004 fast-food restaurant from October to March, although the negative electricity savings are less than 1%. Moreover, all buildings showed more electricity savings during the summer months than the winter months except for the two outpatient buildings in Glendale. All restaurants showed higher monthly electricity savings in the summer months regardless of location and building age, which indicates that green roofs can provide more benefits to restaurants when temperatures are high at the study sites. It was also observed that electricity savings were slightly higher for buildings in Glendale than those in Koreatown. The reason for this difference is that Glendale is located in the Burbank-Glendale weather zone, which has higher monthly temperatures than Koreatown, which is located in the Los Angeles International Airport weather zone (Figure 4.3). In addition, green roofs installed on older restaurants were found to save more electricity for most months, because newly built restaurants, especially the post-2004 restaurants, were found to be less



(a)



(b)

Figure 7.5. Percentage (%) of monthly electricity savings from green roofs compared with traditional roofs under the RCP8.5 emission scenario in 2050: (a) Glendale; (b) Koreatown.

sensitive to climate change as they were already equipped with advanced HVAC systems and higher insulation levels.

7.3 Evaluation of the Green Roof Model Sensitivity

In this section, the model sensitivity to key input parameters related to green roofs is evaluated. Because a detailed parametric test of all green roof parameters is beyond the scope of this dissertation, only the three most important parameters (LAI, soil depth, and irrigation), which were identified from the previous literature (Sailor, 2008; Sailor et al., 2012), are examined. The pre-1980 full-service restaurant in Glendale was selected, because it showed the highest electricity saving potential at both time scales (annual and monthly). Table 7.7 shows the matrix of seven different settings for LAI, soil depth, and irrigation saturation percentage. The base model was defined as the model used in the previous section. Soil depth and LAI variations were set to the minimum and maximum threshold values allowed by EnergyPlus. For roof irrigation systems, the “smart schedule” was used, although the irrigation saturation percentages were set differently. For the low-irrigation model, the irrigation saturation percentage was set to 5%, which means that irrigation would not be performed when the soil is considered to be “moist” (higher than 5% saturation). For the high-irrigation model, the irrigation saturation percentage was set to 95%. All other parameters were unchanged from Section 4.4.1.

Differences in monthly electricity savings for various green roof settings applied to the pre-1980 full-service restaurant under the RCP8.5 emission scenario in 2050 are presented in Figure 7.6.

The energy saving ability of the green roof was positively correlated with the three key parameters, which agrees with the results of the literature (Sailor, 2008; Sailor et al., 2012). The irrigation saturation percentage had the largest impact on electricity savings among the three key parameters for most months, and this impact reached its maximum in summer (August). This

result differs from what was found in Sailor (2008), who suggested that soil thickness had the largest impact on energy use. The reason for this difference is that Glendale is a neighborhood in the Los Angeles Basin that experiences very little precipitation throughout the year (except in winter). Therefore, irrigation is essential for the plants used for green roofs on Glendale buildings.

Table 7.7

Characteristics of different settings of green roofs simulated under the RCP8.5 emission scenario.

Simulation Model	Leaf Area Index (LAI)	Soil Depth (m)	Irrigation Saturation Percentage (%)
Base Model	2	0.2	30%
Low LAI	1	0.2	30%
High LAI	5	0.2	30%
Thin Soil	2	0.1	30%
Thick Soil	2	0.7	30%
Low-Irrigation	2	0.2	5%
High-Irrigation	2	0.2	90%

7.4 Discussion and Conclusions

This section discusses the major findings, strengths, and limitations of the methodology used in this chapter compared with previously published works. All buildings with green roofs showed positive energy savings with regard to total energy and electricity, and the savings caused by green roofs were positively correlated with three key parameters: LAI, soil depth, and irrigation saturation percentage. Moreover, the majority of the electricity saving benefits from green roofs were found in the HVAC systems. In addition, the energy saving ability of green roofs did exhibit seasonality. The above findings agree with the results of previous studies (Gargari et al., 2016; Morakinyo et al., 2017; Semaan & Pearce, 2016; Sailor, 2008; Sailor et al., 2012). However, this study further found that green roofs have different energy

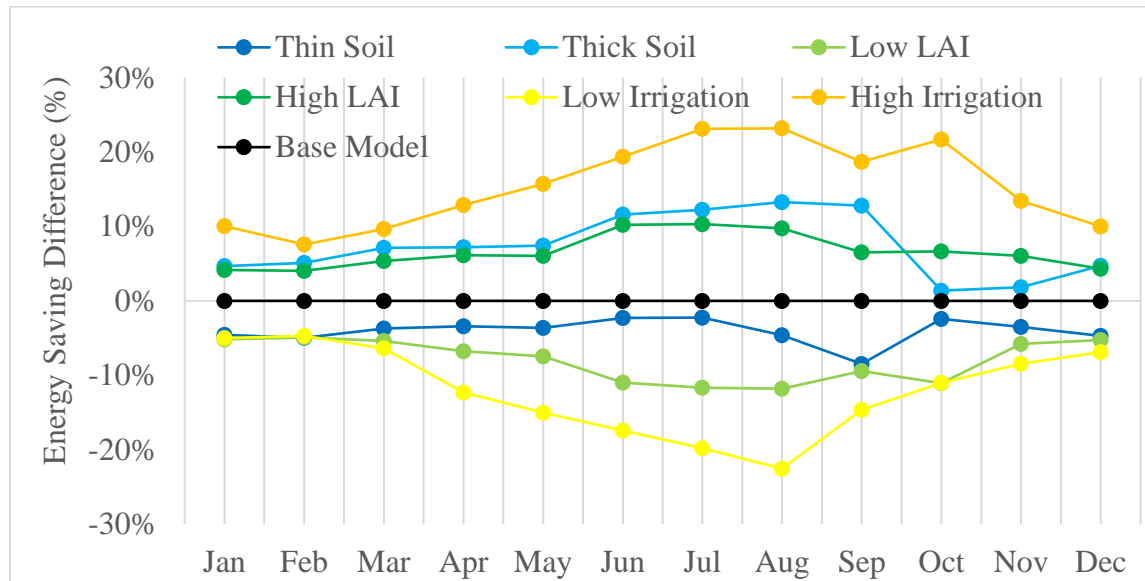


Figure 7.6. Differences (%) in monthly electricity savings for various green roof settings applied to the selected full-service restaurant constructed before 1980 under the RCP8.5 emission scenario in 2050 in Glendale, Los Angeles County, USA.

saving abilities on different types of buildings with different technologies, which has received very little attention in previous studies. The two types of restaurants showed a higher degree of electricity and natural gas savings than the other building types, and less energy savings for newly constructed restaurants was also predicted.

The uncertainties in the green roof energy saving simulation mainly arose from the limitations of the current green roof module in EnergyPlus. The latest version of the module does not have the option for users to input the plant species that are widely used in green roofs. Using the current settings in the green roof module would ignore the fact that the LAI for some species may change slightly throughout the year, although this change would not significantly affect the simulation result. Moreover, there is no indicator that shows the settings are applicable to the real environment. For example, it was demonstrated that increased depth of soil layer can promote

the energy saving ability of green roofs. However, an increase of soil thickness will also increase the weight of the green roof, which may exceed the load bearing capacity of some building roofs. Therefore, in this study followed the settings of Sailor (2008), which were based on validated data from two monitored buildings with green roofs at Portland State University, Oregon, instead of applied the optimal settings.

CHAPTER 8

CONCLUSIONS AND FUTURE DIRECTIONS

8.1 Introduction

This chapter summarizes the contributions of this dissertation, outlines the limitations of the methodology, and discusses the directions for future research. Section 8.2 summarizes the major findings and draws conclusions on the five hypotheses. Section 8.3 discusses the limitations that may lead to uncertainties in the output, and proposes some plans for further research based on these limitations.

8.2 Summary of Major Findings

This dissertation contains three interrelated studies in Los Angeles County: 1) high spatial and temporal resolution Q_f estimation; 2) modeling the effect of climate change on building energy demand using a GIS-based high spatial and temporal resolution approach; and 3) modeling the performance of PV-green roof systems on building energy savings. The first study provided a hybrid approach to Q_f modeling, as presented in Chapter 5, which combined the inventory and GIS methods to create a 365-day hourly Q_f profile at 120-m spatial resolution based on data available to the public. A high spatial and temporal Q_f profile that can be readily incorporated into urban energy balance and UHI models was developed, providing valuable information for government agencies, the energy sector, and the general public. The second study proposed an integrated approach of modeling and GIS to assess the impact of climate

change on building energy consumption for different types and ages of buildings in Los Angeles County at both high spatial and temporal resolutions, as described in Chapter 6. The third study discussed the potential mitigation effects of PV-green roofs on vulnerable buildings that are susceptible to the largest increases in energy demand under the context of climate change, as presented in Chapter 7.

Hypothesis 1 “Building energy demand is the major contributor to Q_f , and building energy demand can make the typical diurnal Q_f profiles across all four seasons appear to have different shapes due to changes in cooling and heating demands” was supported. The main findings from the first study were that the magnitudes and temporal patterns of Q_f in Los Angeles County varied on workdays and nonworkdays by season and for different land use types. Moreover, a large within-county difference in Q_f was discovered among different regions. The downtown Los Angeles area was found to have the largest mean Q_f throughout the year. Building energy consumption was identified as the dominant contributor to the overall Q_f in the downtown area. In addition, Q_f on the selected extremely hot summer workday was substantially higher than that of the average of all summer workdays from 8 am to 11 pm. The increase in building energy consumption due to higher demands for space cooling to offset the extremely hot weather was the dominant driver that caused the higher Q_f .

Hypothesis 2 “The majority of building types show an obvious annual increase in energy demand by 2050, and the variation in energy increases across different building types will be even larger at finer temporal scales (i.e., monthly and diurnal)” was supported. The results of the second study suggested that the majority of building types showed an apparent increase in energy demand under both emission scenarios, and the energy demand increase was higher with the high-emission scenario. In examining the change in energy demand at finer temporal scales (i.e.,

monthly and diurnal), it was found that the energy increase differed considerably according to the building type.

Hypothesis 3 “Areas with more commercial buildings are more vulnerable to climate change because commercial buildings have higher energy consumption intensities than residential buildings” was supported. Commercial buildings were found to have a higher energy demand increase than residential buildings. Neighborhoods with larger than 100% RC in the cooling energy demand were mostly located in the Los Angeles International Airport weather zone, because it had the highest percentage of commercial buildings. Moreover, building size and density played an important role in the energy demand AD. Neighborhoods with the largest increase in energy consumption intensity were located in the major commercial zones with a high density of tall commercial buildings.

Hypothesis 4 “The installation of PV-green roofs can reduce at least 20% of net building energy demand increase caused by climate change for all chosen types of test buildings, and the reduction extent will vary by building type” was partially supported. Reductions in the increased net building energy demand caused by climate change varied by building type, which ranged from 8.2% (pre-1980 outpatient building) to 299.2% (pre-1980 full-service restaurant). The reduction in the net building energy demand was found to exceed 20% in 11 of the 13 tested buildings.

Hypothesis 5 “Building types that are predicted to have the highest energy demand increase caused by climate change receive the most benefits in terms of energy savings” was supported. In Chapter 6, two types of restaurants (full-service and fast-food restaurants) were predicted to have the highest summer energy demand increase due to climate change. In Chapter 7, restaurants were predicted to have 112.5% to 299.5% reductions in the increased net energy

demand due to climate change, much higher than the other types of buildings examined in this study. Moreover, all restaurants with PV-green roofs were predicted to consume less total energy in 2050 than at present even under the high-emission scenario (RCP8.5), indicated that they received the most benefits in terms of energy savings.

In addition to the hypothesis testing, this dissertation also included some other major findings. When compared with previous studies (Ichinose et al., 1999; Nie et al., 2014; Quah & Roth., 2012; Wong et al., 2015), which estimated Q_f in cities or regions with higher population densities (Tokyo, Hong Kong, and Singapore), traffic emissions were found to account for a higher percentage of Q_f in Los Angeles County, while human metabolism contributed less. This finding suggests that in addition to climate conditions, social-economic factors of a city can also affect the characteristics of Q_f .

The results of the second study suggest that under the same climate conditions, the different composition, technologies, size, and density of buildings can induce large spatial variations in energy demand, even within the same city. How to control the cooling energy consumption is vital for the sustainability of Los Angeles under climate change scenarios. Advanced building technologies, including increased insulation and energy efficient equipment and materials, can all contribute significantly to cooling energy savings while maintaining the comfort level. Other strategies, such as transforming to renewable energy, should also be considered.

All buildings with green roofs showed positive energy savings with regard to total energy and electricity, and the majority of the benefits in terms of electricity savings from green roofs were found in the HVAC systems. In addition, the energy saving ability of green roofs did exhibit seasonality.

All three studies showed the innovation of the proposed methodology, filled gaps in the current literature, and indicated strong applicability. The first study developed a hybrid approach that integrated the inventory and GIS modeling approaches. The GIS modeling approach can create a time-dependent Q_f profile at high spatial and temporal resolutions with high accuracy, and the inventory approach can validate and calibrate the results estimated from the GIS modeling approach. This integration allowed for assessing the discrepancies between simulated and actual energy consumption. Compared to the approaches of previous studies that used state, county, or census levels for calibrating the simulation results, the use of neighborhood-level reference data enabled us to address local variations of energy consumption patterns by building.

The second research project designed an innovative approach to study the climate change effect on building energy consumption at fine spatial and temporal scales. By utilizing the unique capability of GIS, which integrates different types of data and organizes them based on spatial locations, the approach used in this study can capture the spatial and temporal variations of building energy use in Los Angeles County. It can generate valuable datasets and information suitable for policy makers, energy suppliers and consumers to consider adaptation and mitigation strategies. The approach used in this study has strong applicability, because it is appropriate for any area with the availability of a GIS-based building dataset and weather data at a high temporal resolution.

In the existing literature, the mitigation potential of increased building energy consumption caused by climate change have been briefly discussed, and no experiments have been conducted to test the performance of mitigation options, such as sustainable roofs (green roofs, PV roofs, or PV-green roofs). The third study filled this gap by estimating the mitigation performance of PV-green roofs on buildings that are more vulnerable to climate change in terms

of the increased energy demand. Factors that might affect the energy saving ability of PV-green roofs, such as local climate conditions, seasonal effects, building types, and building technologies, were examined, and the results provided valuable information to guide policy makers.

Based on all the findings of this dissertation, the recommendations to Los Angeles County can be summarized as follows. First, it is necessary to apply several strategies to avoid the future energy consumption path towards the high-emission scenario (RCP8.5), such as transferring more energy supply from fossil fuel sources to renewable sources, reducing the transmission loss of electricity, and increasing the awareness of the general public to reducing unnecessary cooling energy use. Second, because the majority of existing commercial buildings in Los Angeles County were built before 2004, which were found to be more sensitive to climate change in terms of the increased energy consumption potential, mitigation strategies will need to be applied. Because the majority of the energy demand increase was predicted for electricity and cooling energy, PV-green roofs are a viable mitigation option. This is especially for buildings built before 2004. To optimize the performance of PV-green roofs, experiments will need to be conducted at the individual building scale that take the local climate condition into consideration when determining the key parameters for the experiment. For example, irrigation and species selection can be essential, because Los Angeles County has very low precipitation in summer. The three potential ways to reduce irrigation cost and water usage are to use drought-tolerant plant species, to apply efficient irrigation techniques, and to store rainwater for irrigation (Heusinger et al., 2018; Shafique et al., 2018). In addition to the roofs, the sides of buildings can also be utilized for building energy mitigation, as the benefits of wall-mounted PV-green

systems, solar thermal collectors, and hybrid solar windows have been studied in previous studies (Moren & Korjenic, 2017; Ulavi, Hebrink, & Davidson, 2014).

8.3 Limitations and Future Directions

Although this dissertation fills multiple gaps in the existing literature, limitations remain. First, data availability was still a major limitation in this dissertation and caused uncertainties in each part. As discussed in Section 5.5, the uncertainties in the building energy consumption came from occupancy behaviors and building prototypes, which can only represent the most common building technologies and characteristics in the survey data in Los Angeles County. Moreover, the traffic emission simulation would be more accurate, if seasonal variations of emission factors from several types of vehicles could be included. During hot weather, vehicles tend to consume more fuel to run air conditioners. Although the Q_f simulation included the majority of its components, some other components, such as greenhouses gases emitted from pollution and solid waste process, were not included. The resolution of the weather data (TMY3) was still relatively coarse, which is not sufficient to reflect the regional differences in the Los Angeles County. More detailed information regarding residential buildings, such as building age and materials, were not readily available. Additional uncertainty was caused by the fact that data from multiple spatial scales were combined in this dissertation. For example, the actual building energy consumption at the neighborhood scale was used for the validation. Although this is much more accurate than that used in previous studies, which used coarser reference data at the state and county level, the discrepancy between simulations and actual consumption within a neighborhood cannot be addressed. Finally, the energy consumption data for individual buildings were not available for this study because they are confidential.

Future studies can achieve higher modeling accuracy if the issues of the aforementioned data can be overcome. Under the context of the development of “Geospatial big data”, the spatial and temporal scales of the data available to the public are expected to become finer in the future. Moreover, interdisciplinary research will likely be conducted more frequently. Both of these directions of development will increase the dimensions of input data. For example, Building Information Modeling (BIM) data, which is an intelligent 3D model-based building dataset, are under development in many cities. The 3D BIM data contain a greater level of detail for each individual building than the 2D building shapefile used in this dissertation. Information such as materials, structures, specific models of HVAC systems, and drainage systems will become available. The integration of BIM and GIS will increase the accuracy of energy consumption simulations and provide more options to customize PV-green roofs at the individual building level. For example, this integration would allow decision makers and designers to run sensitivity tests while considering different combinations of input parameters, such as local water availability, irrigation investments, types of blinds, and facing directions of windows to determine the best option. On the other hand, the simulation of individual building energy consumption can be made much more accurate if multistage HVAC systems and survey results of personal behaviors regarding the choice of heating and cooling temperatures in a study area into are considered.

However, the larger amount and finer scales of the input data will also bring challenges to computing, storage, and the integration of data from different sources and scales, which will become a more important issue to be addressed. In this study, the time required for the building energy simulation in Los Angeles County was approximately five and a half hours using Python. However, in the future, the time required for data processing over large areas, such as the entire

country, will likely increase dramatically due to the increased complexity of the input data.

Therefore, the development of geospatial technologies is crucial and will play an important role in solving this problem by reducing the size of data and advancing the computing algorithms. In

conclusion, the higher level of data availability, interdisciplinary research, and advanced

geospatial technologies will promote the developments in high-resolution Q_f and building energy demand modeling studies.

REFERENCES

- Alcazar, S. S., Olivieri, F., & Neila, J. (2016). Green roofs: Experimental and analytical study of its potential for urban microclimate regulation in Mediterranean-continental climates. *Urban Climate*, *17*, 304–317. doi:10.1016/j.uclim.2016.02.004
- Allen, L., Lindberg, F., & Grimmond, C. S. B. (2011). Global to city scale urban anthropogenic heat flux: model and variability. *International Journal of Climatology*, *31*(13), 1990–2005. doi:10.1002/joc.2210
- Andrić, I., Gomes, N., Pina, A., Ferrão, P., Fournier, J., Lacarrière, B., & Le Corre, O. (2016). Modeling the long-term effect of climate change on building heat demand: case study on a district level. *Energy and Buildings*, *126*, 77–93. doi:10.1016/j.enbuild.2016.04.082
- Berger, T., Amann, C., Formayer, H., Korjenic, A., Pospischal, B., Neururer, C., & Smutny, R. (2014). Impacts of climate change upon cooling and heating energy demand of office buildings in Vienna, Austria. *Energy and Buildings*, *80*, 517–530. doi:10.1016/j.enbuild.2014.03.084
- Bianchini, F., & Hewage, K. (2012). Probabilistic social cost-benefit analysis for green roofs: A lifecycle approach. *Building and Environment*, *58*, 152–162. doi:10.1016/j.buildenv.2012.07.005
- California Energy Commission. (2016). Retrieved from <http://ecdms.energy.ca.gov/elecbycounty.aspx>
- California State Board of Equalization. (2016). Retrieved from <http://www.boe.ca.gov/sptaxprog/spftrpts.htm>
- Catalano, C., Marcenò, C., Laudicina, V. A., & Guarino, R. (2016). Thirty years unmanaged green roofs: Ecological research and design implications. *Landscape and Urban Planning*, *149*, 11–19. doi:10.1016/j.landurbplan.2016.01.003

- Cellura, M., Guarino, F., Longo, S., & Tumminia, G. (2018). Climate change and the building sector: modelling and energy implications to an office building in southern Europe. *Energy for Sustainable Development, 45*, 46–65. doi:10.1016/j.esd.2018.05.001
- Chapman, S., Watson, J., & McAlpine, C. (2016). Large seasonal and diurnal anthropogenic heat flux across four Australian cities. *Journal of Southern Hemisphere Earth Systems Science, 60*(3), 342–360.
- Chemisana, D., & Lamnatou, C. (2014). Photovoltaic-green roofs: an experimental evaluation of system performance. *Applied Energy, 119*, 246–256. doi:10.1016/j.apenergy.2013.12.027
- Chow, W. T. L., Salamanca, F., Georgescu, M., Mahalov, A., Milne, J. M., & Ruddell, B. L. (2014). A multi-method and multi-scale approach for estimating city-wide anthropogenic heat fluxes. *Atmospheric Environment, 99*, 64–76. doi:10.1016/j.atmosenv.2014.09.053
- Deru, M., Field, K., Studer, D., Benne, K., Griffith, B., Torcellini, P., . . . Rosenberg, M. (2011). *US Department of Energy commercial reference building models of the national building stock* (Publication No. NREL/TP-5500-46861). Retrieved from <https://www.nrel.gov/docs/fy11osti/46861.pdf>
- Dimond, K., & Webb, A. (2017). Sustainable roof selection: Environmental and contextual factors to be considered in choosing a vegetated roof or rooftop solar photovoltaic system. *Sustainable Cities and Society, 35*, 241–249. doi:10.1016/j.scs.2017.08.015
- Dirks, J. A., Gorrissen, W. J., Hathaway, J. H., Skorski, D. C., Scott, M. J., Pulsipher, T. C., . . . Rice, J. S. (2015). Impacts of climate change on energy consumption and peak demand in buildings: A detailed regional approach. *Energy, 79*, 20–32. doi:10.1016/j.energy.2014.08.081
- Energy Atlas. (2017). Retrieved from <http://www.energyatlas.ucla.edu/>
- Fan, H., & Sailor, D. J. (2005). Modeling the impacts of anthropogenic heating on the urban climate of Philadelphia: a comparison of implementations in two PBL schemes. *Atmospheric Environment, 39*(1), 73–84. doi:10.1016/j.atmosenv.2004.09.031
- Feng, C., Zheng, H., Wang, R., Yu, X., & Su, Y. (2015). A novel solar multifunctional PV/T/D system for green building roofs. *Energy Conversion and Management, 93*, 63–71. doi:10.1016/j.enconman.2015.01.001

- Ferreira, M. J., de Oliveira, A. P., & Soares, J. (2010). Anthropogenic heat in the city of São Paulo, Brazil. *Theoretical and Applied Climatology*, *104*(1–2), 43–56.
doi:10.1007/s00704-010-0322-7
- Flanner, M. G. (2009). Integrating anthropogenic heat flux with global climate models. *Geophysical Research Letters*, *36*(2). doi:10.1029/2008gl036465
- Gargari, C., Bibbiani, C., Fantozzi, F., & Campiotti, C. A. (2016). Environmental Impact of Green Roofing: The Contribute of a Green Roof to the Sustainable use of Natural Resources in a Life Cycle Approach. *Agriculture and Agricultural Science Procedia*, *8*, 646–656. doi:10.1016/j.aaspro.2016.02.087
- Ghedamsi, R., Settou, N., Gouareh, A., Khamouli, A., Saifi, N., Reciou, B., & Dokkar, B. (2016). Modeling and forecasting energy consumption for residential buildings in Algeria using bottom-up approach. *Energy and Buildings*, *121*, 309–317.
doi:10.1016/j.enbuild.2015.12.030
- Google Project Sunroof. (2018). Retrieved from <https://www.google.com/get/sunroof>
- Grimmond, C. S. B. (1992). The suburban energy balance: Methodological considerations and results for a mid-latitude west coast city under winter and spring conditions. *International Journal of Climatology*, *12*(5), 481–497. doi:doi:10.1002/joc.3370120506
- Guneralp, B., Zhou, Y., Urge-Vorsatz, D., Gupta, M., Yu, S., Patel, P. L., . . . Seto, K. C. (2017). Global scenarios of urban density and its impacts on building energy use through 2050. *Proceedings of the National Academy of Sciences of the United States of America*, *114*(34), 8945–8950. doi:10.1073/pnas.1606035114
- Hamilton, I. G., Davies, M., Steadman, P., Stone, A., Ridley, I., & Evans, S. (2009). The significance of the anthropogenic heat emissions of London's buildings: A comparison against captured shortwave solar radiation. *Building and Environment*, *44*(4), 807–817.
doi:10.1016/j.buildenv.2008.05.024
- Hashemi, S. S. G., Mahmud, H. B., & Ashraf, M. A. (2015). Performance of green roofs with respect to water quality and reduction of energy consumption in tropics: A review. *Renewable and Sustainable Energy Reviews*, *52*, 669–679.
doi:10.1016/j.rser.2015.07.163

- Heiple, S., & Sailor, D. J. (2008). Using building energy simulation and geospatial modeling techniques to determine high resolution building sector energy consumption profiles. *Energy and Buildings*, 40(8), 1426–1436. doi:10.1016/j.enbuild.2008.01.005
- Herrando, M., Cambra, D., Navarro, M., de la Cruz, L., Millán, G., & Zabalza, I. (2016). Energy Performance Certification of Faculty Buildings in Spain: The gap between estimated and real energy consumption. *Energy Conversion and Management*, 125, 141–153. doi:10.1016/j.enconman.2016.04.037
- Herrera-Gomez, S. S., Quevedo-Nolasco, A., & Pérez-Urrestarazu, L. (2017). The role of green roofs in climate change mitigation. A case study in Seville (Spain). *Building and Environment*, 123, 575–584. doi:10.1016/j.buildenv.2017.07.036
- Heusinger, J., Sailor, D. J., & Weber, S. (2018). Modeling the reduction of urban excess heat by green roofs with respect to different irrigation scenarios. *Building and Environment*, 131, 174–183. doi:10.1016/j.buildenv.2018.01.003
- Hu, D., Yang, L., Zhou, J., & Deng, L. (2012). Estimation of urban energy heat flux and anthropogenic heat discharge using aster image and meteorological data: case study in Beijing metropolitan area. *Journal of Applied Remote Sensing*, 6(1), 1–18.
- Huang, J., & Gurney, K. R. (2016). The variation of climate change impact on building energy consumption to building type and spatiotemporal scale. *Energy*, 111, 137–153. doi:10.1016/j.energy.2016.05.118
- Ichinose, T., Shimodozono, K., & Hanaki, K. (1999). Impact of anthropogenic heat on urban climate in Tokyo. *Atmospheric Environment*, 33(24–25), 3897–3909.
- International Energy Agency. (2009). *World Energy Outlook 2009*. Retrieved from <http://www.worldenergyoutlook.org/media/weowebiste/2009/WEO2009.pdf>
- Intergovernmental Panel on Climate Change. (2014). *Climate Change 2014: Synthesis Report*. New York, NY: Cambridge University Press.
- Kato, S., & Yamaguchi, Y. (2005). Analysis of urban heat-island effect using ASTER and ETM+ Data: Separation of anthropogenic heat discharge and natural heat radiation from sensible heat flux. *Remote Sensing of Environment*, 99(1–2), 44–54. doi:10.1016/j.rse.2005.04.026

- Kato, S., Yamaguchi, Y., Liu, C. C., & Sun, C. Y. (2008). Surface Heat Balance Analysis of Tainan City on March 6, 2001 Using ASTER and Formosat-2 Data. *Sensors (Basel)*, 8(9), 6026–6044. doi:10.3390/s8096026
- Kikegawa, Y., Genchi, Y., Kondo, H., & Hanaki, K. (2006). Impacts of city-block-scale countermeasures against urban heat-island phenomena upon a building's energy-consumption for air-conditioning. *Applied Energy*, 83(6), 649–668. doi:10.1016/j.apenergy.2005.06.001
- Kikegawa, Y., Genchi, Y., Yoshikado, H., & Kondo, H. (2003). Development of a numerical simulation system toward comprehensive assessments of urban warming countermeasures including their impacts upon the urban buildings' energy-demands. *Applied Energy*, 76(4), 449–466. doi:10.1016/S0306-2619(03)00009-6
- Kłysik, K. (1996). Spatial and seasonal distribution of anthropogenic heat emissions in Lodz, Poland. *Atmospheric Environment*, 30(20), 3397–3404.
- Lamera, C., Becciu, G., Rulli, M. C., & Rosso, R. (2014). Green roofs effects on the urban water cycle components. *Procedia Engineering*, 70, 988–997. doi:10.1016/j.proeng.2014.02.110
- Lamnatou, C., & Chemisana, D. (2014). Photovoltaic-green roofs: a life cycle assessment approach with emphasis on warm months of Mediterranean climate. *Journal of Cleaner Production*, 72, 57–75. doi:10.1016/j.jclepro.2014.03.006
- Lamnatou, C., & Chemisana, D. (2015). A critical analysis of factors affecting photovoltaic-green roof performance. *Renewable and Sustainable Energy Reviews*, 43, 264–280. doi:10.1016/j.rser.2014.11.048
- Lee, S.-H., Song, C.-K., Baik, J.-J., & Park, S.-U. (2009). Estimation of anthropogenic heat emission in the Gyeong-In region of Korea. *Theoretical and Applied Climatology*, 96(3), 291–303. doi:10.1007/s00704-008-0040-6
- Li, M., Cao, J., Xiong, M., Li, J., Feng, X., & Meng, F. (2018). Different responses of cooling energy consumption in office buildings to climatic change in major climate zones of China. *Energy and Buildings*, 173, 38–44. doi:10.1016/j.enbuild.2018.05.037
- Li, X., & Ratti, C. (2018). Mapping the spatial distribution of shade provision of street trees in Boston using Google Street View panoramas. *Urban Forestry & Urban Greening*, 31, 109–119.

- LoopNet. (2019). Retrieved from <https://www.loopnet.com/>
- Los Angeles Times. (2013). *L.A. County neighborhoods*. Retrieved from <http://boundaries.latimes.com/set/la-county-neighborhoods-v6/>
- Lukač, N., & Žalik, B. (2013). GPU-based roofs' solar potential estimation using LiDAR data. *Computers & Geosciences*, 52, 34–41. doi:10.1016/j.cageo.2012.10.010
- Makar, P. A., Gravel, S., Chirkov, V., Strawbridge, K. B., Froude, F., Arnold, J., & Brook, J. (2006). Heat flux, urban properties, and regional weather. *Atmospheric Environment*, 40(15), 2750–2766. doi:10.1016/j.atmosenv.2005.11.061
- Masson, V. (2000). A physically-based scheme for the urban energy budget in atmospheric models. *Boundary-layer meteorology*, 94(3), 357–397.
- Mastrucci, A., Baume, O., Stazi, F., & Leopold, U. (2014). Estimating energy savings for the residential building stock of an entire city: A GIS-based statistical downscaling approach applied to Rotterdam. *Energy and Buildings*, 75, 358–367. doi:10.1016/j.enbuild.2014.02.032
- McFarland, J., Zhou, Y., Clarke, L., Sullivan, P., Colman, J., Jaglom, W. S., . . . Creason, J. (2015). Impacts of rising air temperatures and emissions mitigation on electricity demand and supply in the United States: a multi-model comparison. *Climatic Change*, 131(1), 111–125. doi:10.1007/s10584-015-1380-8
- Mohajerani, A., Bakaric, J., & Jeffrey-Bailey, T. (2017). The urban heat island effect, its causes, and mitigation, with reference to the thermal properties of asphalt concrete. *Journal of Environmental Management*, 197, 522–538. doi:10.1016/j.jenvman.2017.03.095
- Morakinyo, T. E., Dahanayake, K. W. D. K. C., Ng, E., & Chow, C. L. (2017). Temperature and cooling demand reduction by green-roof types in different climates and urban densities: A co-simulation parametric study. *Energy and Buildings*, 145, 226–237. doi:10.1016/j.enbuild.2017.03.066
- Moren, M. S. P., & Korjenic, A. (2017). Green buffer space influences on the temperature of photovoltaic modules: Multifunctional system: Building greening and photovoltaic. *Energy and Buildings*, 146, 364–382. doi:10.1016/j.enbuild.2017.04.051
- Nie, W.-S., Sun, T., & Ni, G.-H. (2014). Spatiotemporal characteristics of anthropogenic heat in an urban environment: A case study of Tsinghua Campus. *Building and Environment*, 82, 675–686. doi:10.1016/j.buildenv.2014.10.011

- Ohashi, Y., Genchi, Y., Kondo, H., Kikegawa, Y., Hirano, Y., & Yoshikado, H. (2003). A study of horizontal temperature distribution within urban canopy layer at the Tokyo central area. Paper presented at the Fifth International Conference on Urban Climate, Lodz, Poland.
- Ohashi, Y., Genchi, Y., Kondo, H., Kikegawa, Y., Yoshikado, H., & Hirano, Y. (2007). Influence of Air-Conditioning Waste Heat on Air Temperature in Tokyo during Summer: Numerical Experiments Using an Urban Canopy Model Coupled with a Building Energy Model. *Journal of Applied Meteorology and Climatology*, *46*(1), 66–81.
doi:10.1175/jam2441.1
- Oke, T. R. (1976). The distinction between canopy and boundary-layer urban heat islands. *Atmosphere*, *14*(4), 268–277. doi:10.1080/00046973.1976.9648422
- Oke, T. R. (1987). *Boundary Layer Climates* (2nd ed.). London, England: Routledge.
- Oke, T. R. (2006). Towards better scientific communication in urban climate. *Theoretical and Applied Climatology*, *84*(1–3), 179–190.
- Papachristos, G. (2015). Household electricity consumption and CO₂ emissions in the Netherlands: A model-based analysis. *Energy and Buildings*, *86*, 403–414.
doi:10.1016/j.enbuild.2014.09.077
- Park, C., Schade, G. W., Werner, N. D., Sailor, D. J., & Kim, C.-H. (2016). Comparative estimates of anthropogenic heat emission in relation to surface energy balance of a subtropical urban neighborhood. *Atmospheric Environment*, *126*, 182–191.
doi:10.1016/j.atmosenv.2015.11.038
- Pigeon, G., Legain, D., Durand, P., & Masson, V. (2007). Anthropogenic heat release in an old European agglomeration (Toulouse, France). *International Journal of Climatology*, *27*(14), 1969–1981. doi:10.1002/joc.1530
- Quah, A. K. L., & Roth, M. (2012). Diurnal and weekly variation of anthropogenic heat emissions in a tropical city, Singapore. *Atmospheric Environment*, *46*, 92–103.
doi:10.1016/j.atmosenv.2011.10.015
- Rey-Hernández, J. M., Yousif, C., Gatt, D., Velasco-Gómez, E., San José-Alonso, J., & Rey-Martínez, F. J. (2018). Modelling the long-term effect of climate change on a zero energy and carbon dioxide building through energy efficiency and renewables. *Energy and Buildings*, *174*, 85–96. doi:10.1016/j.enbuild.2018.06.006

- Roth, M., Oke, T. R., & Emery, W. J. (1989). Satellite-derived urban heat islands from three coastal cities and the utilization of such data in urban climatology. *International Journal of Remote Sensing*, *10*(11), 1699–1720. doi:10.1080/01431168908904002
- Rubio-Bellido, C., Pérez-Fargallo, A., & Pulido-Arcas, J. A. (2016). Optimization of annual energy demand in office buildings under the influence of climate change in Chile. *Energy*, *114*, 569–585. doi:10.1016/j.energy.2016.08.021
- Ruosteenoja, K., Carter, T. R., Jylhä, K., & Tuomenvirta, H. (2003). *Future climate in world regions: and inter comparison of model-based projections for the new IPCC emissions scenarios*. Helsinki, Finland: Finnish Environment Institute.
- Sailor, D. J. (2001). Relating residential and commercial sector electricity loads to climate—evaluating state level sensitivities and vulnerabilities. *Energy*, *26*(7), 645–657.
- Sailor, D. J. (2008). A green roof model for building energy simulation programs. *Energy and Buildings*, *40*(8), 1466–1478. doi:10.1016/j.enbuild.2008.02.001
- Sailor, D. J. (2011). A review of methods for estimating anthropogenic heat and moisture emissions in the urban environment. *International Journal of Climatology*, *31*(2), 189–199. doi:10.1002/joc.2106
- Sailor, D. J., Brooks, A., Hart, M., & Heiple, S. (2007). A bottom-up approach for estimating latent and sensible heat emissions from anthropogenic sources. Proceedings of the 7th Symposium on the Urban Environment, San Diego, CA. Retrieved from https://ams.confex.com/ams/7Coastal7Urban/techprogram/paper_127290.htm
- Sailor, D. J., Elley, T. B., & Gibson, M. (2012). Exploring the building energy impacts of green roof design decisions—a modeling study of buildings in four distinct climates. *Journal of Building Physics*, *35*(4), 372–391.
- Sailor, D. J., Georgescu, M., Milne, J. M., & Hart, M. A. (2015). Development of a national anthropogenic heating database with an extrapolation for international cities. *Atmospheric Environment*, *118*, 7–18. doi:10.1016/j.atmosenv.2015.07.016
- Sailor, D. J., & Lu, L. (2004). A top-down methodology for developing diurnal and seasonal anthropogenic heating profiles for urban areas. *Atmospheric Environment*, *38*(17), 2737–2748. doi:10.1016/j.atmosenv.2004.01.034
- Sathaye, J. A., Dale, L. L., Larsen, P. H., Fitts, G. A., Koy, K., Lewis, S. M., & de Lucena, A. F. P. (2012). *Estimating risk to California energy infrastructure form projected climate*

- change* (Publication No. CEC-500-2012-057). Retrieved from <https://eta.lbl.gov/publications/estimating-risk-california-energy>
- Sathaye, J. A., Dale, L. L., Larsen, P. H., Fitts, G. A., Koy, K., Lewis, S. M., & de Lucena, A. F. P. (2013). Estimating impacts of warming temperatures on California's electricity system. *Global Environmental Change*, *23*(2), 499–511. doi:10.1016/j.gloenvcha.2012.12.005
- Scherba, A., Sailor, D. J., Rosenstiel, T. N., & Wamser, C. C. (2011). Modeling impacts of roof reflectivity, integrated photovoltaic panels and green roof systems on sensible heat flux into the urban environment. *Building and Environment*, *46*(12), 2542–2551. doi:10.1016/j.buildenv.2011.06.012
- Schindler, B. Y., Blaustein, L., Lotan, R., Shalom, H., Kadas, G. J., & Seifan, M. (2018). Green roof and photovoltaic panel integration: Effects on plant and arthropod diversity and electricity production. *Journal of Environmental Management*, *225*, 288–299. doi:10.1016/j.jenvman.2018.08.017
- Schuffert, S. (2013). *An automatic data driven approach to derive photovoltaic-suitable roof surfaces from ALS data*. Paper presented at the Joint Urban Remote Sensing Event 2013 (pp. 267–270). Sao Paulo, Brazil.
- Scott, M. J., Daly, D. S., Hathaway, J. E., Lansing, C. S., Liu, Y., McJeon, H. C., . . . Zhou, Y. (2015). Calculating impacts of energy standards on energy demand in U.S. buildings with uncertainty in an integrated assessment model. *Energy*, *90*, 1682–1694. doi:10.1016/j.energy.2015.06.127
- Semaan, M., & Pearce, A. (2016). Assessment of the Gains and Benefits of Green Roofs in Different Climates. *Procedia Engineering*, *145*, 333–339. doi:10.1016/j.proeng.2016.04.083
- Seto, K. C., Dhakal, S., Bigio, A., Blanco, H., Delgado, G. C., Dewar, D., . . . Lwasa, S. (2014). Human settlements, infrastructure and spatial planning. In Intergovernmental Panel on Climate Change, *Climate Change 2014: Mitigation of Climate Change* (pp. 923–1000). New York, NY: Cambridge University Press.
- Shafique, M., Kim, R., & Rafiq, M. (2018). Green roof benefits, opportunities and challenges – A review. *Renewable and Sustainable Energy Reviews*, *90*, 757–773. doi:10.1016/j.rser.2018.04.006

- Shen, P. (2017). Impacts of climate change on U.S. building energy use by using downscaled hourly future weather data. *Energy and Buildings*, *134*, 61–70.
doi:10.1016/j.enbuild.2016.09.028
- Shi, Z., Fonseca, J. A., & Schlueter, A. (2017). A review of simulation-based urban form generation and optimization for energy-driven urban design. *Building and Environment*, *121*, 119–129. doi:10.1016/j.buildenv.2017.05.006
- Silva, C. M., Gomes, M. G., & Silva, M. (2016). Green roofs energy performance in Mediterranean climate. *Energy and Buildings*, *116*, 318–325.
doi:10.1016/j.enbuild.2016.01.012
- Smith, C., Lindley, S., & Levermore, G. (2009). Estimating spatial and temporal patterns of urban anthropogenic heat fluxes for UK cities: the case of Manchester. *Theoretical and Applied Climatology*, *98*(1–2), 19–35. doi:10.1007/s00704-008-0086-5
- Susca, T., Gaffin, S. R., & Dell'osso, G. R. (2011). Positive effects of vegetation: urban heat island and green roofs. *Environmental Pollution*, *159*(8–9), 2119–2126.
doi:10.1016/j.envpol.2011.03.007
- Tam, V. W. Y., Wang, J., & Le, K. N. (2016). Thermal insulation and cost effectiveness of green-roof systems: An empirical study in Hong Kong. *Building and Environment*, *110*, 46–54. doi:10.1016/j.buildenv.2016.09.032
- Tang, X., & Qu, M. (2016). Phase change and thermal performance analysis for green roofs in cold climates. *Energy and Buildings*, *121*, 165–175. doi:10.1016/j.enbuild.2016.03.069
- Taylor, J. W., de Menezes, L. M., & McSharry, P. E. (2006). A comparison of univariate methods for forecasting electricity demand up to a day ahead. *International Journal of Forecasting*, *22*(1), 1–16. doi:10.1016/j.ijforecast.2005.06.006
- Ulavi, T., Hebrink, T., & Davidson, J. H. (2014). Analysis of a Hybrid Solar Window for Building Integration. *Energy Procedia*, *57*, 1941–1950.
doi:10.1016/j.egypro.2014.10.058
- United Nations Department of Economic and Social Affairs. (2018). Retrieved from <https://www.un.org/development/desa/publications/2018-revision-of-world-urbanization-prospects.html>

- United States Census Bureau. (2017). Retrieved from <https://www.census.gov/quickfacts/fact/table/losangelescountycalifornia,ca/PST045217#PST045217>
- United States Department of Energy. (2012). *2011 Buildings Energy Data Book*. Washington, DC: United States Department of Energy.
- United States Department of Energy. (2018). Retrieved from <https://www.energy.gov/energysaver/energy-efficient-home-design/cool-roofs>
- United States Department of Transportation. (2011). *Annual Vehicle Distance Travelled in Miles and Related Data 2010 by Highway Category and Vehicle Type*. Retrieved from <https://www.fhwa.dot.gov/policyinformation/statistics/2010/vm1.cfm>
- United States Energy Information Administration. (2014). *Petroleum & Other Liquids: Gasoline and Diesel Fuel Update*. Retrieved from http://www.eia.gov/petroleum/gasdiesel/diesel_proc-methods.cfm
- Vijayaraghavan, K. (2016). Green roofs: A critical review on the role of components, benefits, limitations and trends. *Renewable and Sustainable Energy Reviews*, 57, 740–752. doi:10.1016/j.rser.2015.12.119
- Waibel, C., Evins, R., & Carmeliet, J. (2017). Efficient time-resolved 3D solar potential modelling. *Solar Energy*, 158, 960–976. doi:10.1016/j.solener.2017.10.054
- Wan, K. K. W., Li, D. H. W., Pan, W., & Lam, J. C. (2012). Impact of climate change on building energy use in different climate zones and mitigation and adaptation implications. *Applied Energy*, 97, 274–282. doi:10.1016/j.apenergy.2011.11.048
- Wang, H., & Chen, Q. (2014). Impact of climate change heating and cooling energy use in buildings in the United States. *Energy and Buildings*, 82, 428–436. doi:10.1016/j.enbuild.2014.07.034
- Wang, Y., & Akbari, H. (2016). The effects of street tree planting on Urban Heat Island mitigation in Montreal. *Sustainable Cities and Society*, 27, 122–128. doi:10.1016/j.scs.2016.04.013
- Wang, Y., Akbari, H., & Chen, B. (2016). Urban Geometry and Environmental Urban Policy Development. *Procedia Engineering*, 169, 308–315. doi:10.1016/j.proeng.2016.10.038

- Wong, M. S., Yang, J., Nichol, J., Weng, Q., Menenti, M., & Chan, P. (2015). Modeling of Anthropogenic Heat Flux Using HJ-1B Chinese Small Satellite Image: A Study of Heterogeneous Urbanized Areas in Hong Kong. *IEEE Geoscience and Remote Sensing Letters*, *12*(7), 1466–1470. doi:10.1109/LGRS.2015.2409111
- Wong, N. H., Jusuf, S. K., Syafii, N. I., Li, W. H., & Tan, A. Y. K. (2012). Simulation of the impact of climate change on the current building's residential envelope thermal transfer value (ETTV) regulation in Singapore. Proceedings of the International Conference on Sustainable Design and Construction 2011 (pp. 34–42). Kansas City, MO.
- Xu, P., Huang, Y. J., Miller, N., Schlegel, N., & Shen, P. (2012). Impacts of climate change on building heating and cooling energy patterns in California. *Energy*, *44*(1), 792–804. doi:10.1016/j.energy.2012.05.013
- Xu, W., Wooster, M. J., & Grimmond, C. S. B. (2008). Modelling of urban sensible heat flux at multiple spatial scales: A demonstration using airborne hyperspectral imagery of Shanghai and a temperature-emissivity separation approach. *Remote Sensing of Environment*, *112*(9), 3493–3510. doi:10.1016/j.rse.2008.04.009
- Yang, J., Kumar, D. L. M., Pyrgou, A., Chong, A., Santamouris, M., Kolokotsa, D., & Lee, S. E. (2018). Green and cool roofs' urban heat island mitigation potential in tropical climate. *Solar Energy*, *173*, 597–609. doi:10.1016/j.solener.2018.08.006
- Yang, W., Chen, B., & Cui, X. (2014). High-resolution mapping of anthropogenic heat in China from 1992 to 2010. *International Journal of Environmental Research and Public Health*, *11*(4), 4066–4077. doi:10.3390/ijerph110404066
- Yi, C. Y., & Peng, C. (2014). Microclimate Change Outdoor and Indoor Coupled Simulation for Passive Building Adaptation Design. *Procedia Computer Science*, *32*, 691–698. doi:10.1016/j.procs.2014.05.478
- Zhang, H., Weng, Q., Lin, H., & Zhang, Y. (2015). *Remote sensing of impervious surfaces in tropical and subtropical areas*. Boca Raton, FL: CRC Press.
- Zheng, Y., & Weng, Q., (2014). Assessing solar potential of commercial and residential buildings in Indianapolis using LiDAR and GIS modeling. Proceedings of the 2014 3rd International Workshop on Earth Observation and Remote Sensing Applications (pp. 398–402). Changsha, China.

- Zheng, Y., & Weng, Q., (2018). High spatial- and temporal- resolution anthropogenic heat discharge estimation in Los Angeles County, California. *Journal of Environmental Management*, 206, 1274–1286. doi:10.1016/j.jenvman.2017.07.047
- Zheng, Y., & Weng, Q., (2019). Modeling the effect of climate change on building energy demand in Los Angeles County by using a GIS-based high spatial- and temporal- resolution approach. *Energy*, 176, 641–655. doi:10.1016/j.energy.2019.04.052
- Zhou, Y., Clarke, L., Eom, J., Kyle, P., Patel, P., Kim, S. H., . . . Seiple, T. (2014). Modeling the effect of climate change on U.S. state-level buildings energy demands in an integrated assessment framework. *Applied Energy*, 113, 1077–1088. doi:10.1016/j.apenergy.2013.08.034
- Zhou, Y., Eom, J., & Clarke, L. (2013). The effect of global climate change, population distribution, and climate mitigation on building energy use in the U.S. and China. *Climatic Change*, 119(3–4), 979–992. doi:10.1007/s10584-013-0772-x
- Zhou, Y., & Gurney, K. (2010). A new methodology for quantifying on-site residential and commercial fossil fuel CO₂ emissions at the building spatial scale and hourly time scale. *Carbon Management*, 1(1), 45–56. doi:10.4155/cmt.10.7
- Zhou, Y., Weng, Q., Gurney, K. R., Shuai, Y., & Hu, X. (2012). Estimation of the relationship between remotely sensed anthropogenic heat discharge and building energy use. *ISPRS Journal of Photogrammetry and Remote Sensing*, 67, 65–72. doi:10.1016/j.isprsjprs.2011.10.007
- Zhu, M., Pan, Y., Huang, Z., & Xu, P. (2016). An alternative method to predict future weather data for building energy demand simulation under global climate change. *Energy and Buildings*, 113, 74–86. doi:10.1016/j.enbuild.2015.12.020

APPENDIX A: FULL ARTICLE OF PUBLICATION (ZHENG & WENG, 2018)



RightsLink®

Home

Create
Account

Help



Title: High spatial- and temporal-resolution anthropogenic heat discharge estimation in Los Angeles County, California

Author: Yuanfan Zheng, Qihao Weng

Publication: Journal of Environmental Management

Publisher: Elsevier

Date: 15 January 2018

© 2017 Elsevier Ltd. All rights reserved.

If you're a **copyright.com user**, you can login to RightsLink using your copyright.com credentials.

Already a **RightsLink user** or want to [learn more?](#)

Please note that, as the author of this Elsevier article, you retain the right to include it in a thesis or dissertation, provided it is not published commercially. Permission is not required, but please ensure that you reference the journal as the original source. For more information on this and on your other retained rights, please visit: <https://www.elsevier.com/about/our-business/policies/copyright#Author-rights>



Contents lists available at ScienceDirect

Journal of Environmental Management

journal homepage: www.elsevier.com/locate/jenvman

Research article

High spatial- and temporal-resolution anthropogenic heat discharge estimation in Los Angeles County, California

Yuanfan Zheng^b, Qihao Weng^{a, b, *}^a School of Geography, South China Normal University, Guangzhou, 510631, PR China^b Center for Urban and Environmental Change, Department of Earth and Environmental Systems, Indiana State University, Terre Haute, IN, 47802, USA

ARTICLE INFO

Article history:

Received 30 April 2017

Received in revised form

16 July 2017

Accepted 17 July 2017

Available online 22 July 2017

Keywords:

Anthropogenic heat flux

High resolution

Building energy

Traffic emission

Urban areas

Los Angeles

ABSTRACT

Anthropogenic heat flux (Q_f), which originates through energy consumption from buildings, industrial plants, vehicle exhausts, and human metabolism releases, is an important component in the urban Surface Energy Balance (SEB) system, and is key to understanding of many urban environmental issues. The present study provided a hybrid Q_f modeling approach, which combined the inventory and GIS approach to create a 365-day hourly Q_f profile at 120 m spatial resolution in Los Angeles County, California, USA. Q_f was estimated by separate calculation of heat release from buildings, traffics, and human metabolism, respectively. The results indicated that Q_f showed different magnitudes and diurnal patterns between workdays (dual-peak shape) and weekends/holidays, and also varied with seasons, and land use types. Q_f yielded the highest values in the summer workdays, with its maximum value of 7.76 w/m^2 . Q_f in hot summer workdays was obviously higher than that in the average summer workdays, which caused by higher demands for space cooling in buildings, and can reach 8.14 w/m^2 at maximum. Building energy consumption was identified as the dominant contributor to the Q_f in Downtown Los Angeles, which was found to have the largest mean Q_f throughout the year among all neighborhoods. It can be concluded that Q_f in the downtown was more significant in workdays than that in non-workdays, and its maximum value can reach 100 w/m^2 . It is suggested that our approach may have wider applicability for Q_f estimation in large areas compared with the existing studies, as all the data used were available to the public. A high spatial and temporal Q_f profile, which can readily be incorporated into urban energy balance and Urban Heat Island (UHI) studies, provides valuable data and information for pertinent government agencies and researchers.

© 2017 Elsevier Ltd. All rights reserved.

1. Introduction

Although urbanized areas cover about 2% of the global land area, they account for 67–76% of global final energy consumption and 71–76% of fossil fuel-related CO_2 emissions (Gunalp et al., 2017; Seto and Shakal, 2014). Energy demanding in cities is predicted to increase over the next 20 years and probably beyond (International Energy Agency, 2009; Quah and Roth, 2012), because of reduction of rural development (Valipour, 2016, 2017;

Yannopoulos et al., 2015) and urbanized areas will expand to provide homes for 81% of the world's population, with the majority of the population increase coming from developing countries (Weng, 2015). Continued urbanization will bring an impact to urban climate, as the increasing anthropogenic heat flux (Q_f) associated with growing energy consumption in cities can directly affect the urban boundary layer (UBL) and urban canopy layer (UCL) over different spatial and temporal scales (Oke, 2006). The Q_f can originate through energy consumption from buildings, industrial plants, vehicle exhausts, and human metabolism releases within cities. It is an important component in the urban Surface Energy Balance (SEB) system, which is a key to understand urban environmental issues and can be quantified by the following equation (Oke, 1987):

* Corresponding author. Center for Urban and Environmental Change, Department of Earth and Environmental Systems, Indiana State University, Terre Haute, IN, 47802, USA.

E-mail address: qweng@indstate.edu (Q. Weng).

<http://dx.doi.org/10.1016/j.jenvman.2017.07.047>

0301-4797/© 2017 Elsevier Ltd. All rights reserved.

$$R_n + Q_f = H + LE + G \quad (1)$$

where R_n is net radiation, Q_f is anthropogenic heat, H is sensible heat, LE is latent heat, and G is ground heat. The sum of net radiation and anthropogenic heat denotes the total available energy in urban environments, whereas the sum of sensible heat, latent heat, and ground heat is the dissipation of available energy through turbulent transport, conduction, and advection (Nie et al., 2014).

For dense cities with high energy demands, Q_f can potentially be an important or even dominant component of the SEB (Hamilton et al., 2009; Hu et al., 2012; Nie et al., 2014). Comparison between Q_f and solar radiation in previous studies indicated that Q_f can be equal to or even greater than the incident solar radiation during winter days (Nie et al., 2014; Hamilton et al., 2009). Moreover, Q_f was proved to be a major contributor to urban heat island (UHI) formation (Fan and Sailor, 2005; Hu et al., 2012; Ohashi et al., 2003; Wong et al., 2015). The notion of an UHI effect can be characterized by a large stretch of non-evaporating impervious materials covering urban areas, with a consequent rise in sensible heat flux at the expense of latent heat flux (Oke, 1987).

Because of the significance of Q_f in understanding the urban surface energy balance, urban energy transfer, and its effect to urban climate, numerous researches had been conducted to estimate Q_f in mid-latitude cities (Chapman et al., 2016; Ferreira and Oliveira, 2011; Grimmond, 1992; Hamilton et al., 2009; Ichinose et al., 1999; Nie et al., 2014; Sailor and Lu, 2004; Smith et al., 2009; Zhou et al., 2012), subtropical cities (Chow et al., 2014; Park et al., 2016; Wong et al., 2015), tropical cities (Quah and Roth, 2012), and at global scale (Allen et al., 2011; Flanner, 2009). The winter Q_f profile is generally greater in magnitude than the corresponding summer profile in mid-latitude cities (Sailor and Lu, 2004). However, in subtropical or tropical cities, Q_f in the warmer months is found equal to or larger than Q_f in the cooler months (Ichinose et al., 1999; Quah and Roth, 2012; Wong et al., 2015). Besides the climate effect, the density of population also contributes to the differences of Q_f between cities (Ichinose et al., 1999; Wong et al., 2015). The magnitude of Q_f varies greatly not only between cities but also within cities, which depended on per capita energy use, building density, and meteorological conditions (Chapman et al., 2016; Chow et al., 2014; Hamilton et al., 2009; Ichinose et al., 1999; Quah and Roth, 2012; Smith et al., 2009).

The majority of previous studies used three categories of approaches to estimate Q_f : (1) inventory approach, (2) energy budget residual approach, and (3) GIS modeling approach. The inventory approaches, which also called the top-down approach, estimate the anthropogenic heat based on population density and energy consumption statistics data from buildings and vehicles (Grimmond, 1992; Ichinose et al., 1999; Klysiak, 1996; Pigeon et al., 2007; Sailor and Lu, 2004; Sailor et al., 2015; Smith et al., 2009). It requires data at large aggregate scales (e.g. annual), and down-scales them into smaller scales of interest (e.g. hourly) (Quah and Roth, 2012). Since the energy consumption data at large scales are available, this approach has been applied to estimate Q_f at cities throughout the world, for example, in Vancouver, Canada (Grimmond, 1992), Lodz, Poland (Klysiak, 1996), Tokyo, Japan (Ichinose et al., 1999), Toulouse, France (Pigeon et al., 2007), and Manchester, UK (Smith et al., 2009). One study that made a significant impact was conducted by Sailor and Lu (2004), which proposed a method to downscale data at coarser scales to individual census tract to estimate season-specific diurnal profiles of Q_f for six major cities in the U.S.A. Sailor et al. (2015) applied this method to develop a national database of seasonally and diurnally varying Q_f for 61 largest cities in 2015.

The energy balance residual approach estimates Q_f through Equation (1) by measuring net radiation, sensible heat, latent heat, and ground heat using remote sensing meteorological data (Hu et al., 2012; Kato and Yamaguchi, 2005; Kato et al., 2008; Wong et al., 2015; Xu et al., 2008; Yang et al., 2014; Zhou et al., 2012), and long-term eddy covariance flux tower (Chow et al., 2014; Park et al., 2016). Kato and Yamaguchi (2005) was the first to separate Q_f from natural heat radiation from sensible heat flux, based on the energy balance model using Advanced Spaceborne Thermal Emission and Reflection Radiometer (ASTER) imagery and ground meteorological data. Xu et al. (2008) modeled the urban sensible heat in the city of Shanghai, China, at multiple spatial scales. Hu et al. (2012) used a continuous layer of meteorological data and ASTER image to estimate Q_f and their seasonal and spatial variations in Beijing, China. Wong et al. (2015) developed a novel algorithm to model Q_f for mixed pixels, which decomposed image pixels of HJ-1B satellite imagery into fractions of impervious-surfaces and vegetation.

The GIS modeling approaches (Hamilton et al., 2009; Quah and Roth, 2012; Sailor et al., 2007; Zhou et al., 2012), which also called the bottom-up approach. Unlike the inventory approach, it uses energy consumption modeled at small scales (e.g. individual buildings) to scale the information up to larger scales of interest (Quah and Roth, 2012). Earlier studies (Kikegawa et al., 2003, 2006; Masson, 2000; Ohashi et al., 2007) simply estimated Q_f by integrating building energy simulation results with urban canopy meteorological model. Later on, researchers (Hamilton et al., 2009; Sailor et al., 2007; Zhou et al., 2012) started to integrated more detailed building energy simulations for prototypical buildings with GIS database containing attributes such as types, ages, and sizes. Researches in recent years (Chapman et al., 2016; Ferreira and Oliveira, 2011; Quah and Roth, 2012) added traffic emissions and human metabolism into the Q_f estimation.

The above three approaches have their respective advantages and disadvantages. The limitation of inventory approach is the estimation accuracy relies on the data availability and quality. Moreover, it would be difficult to quantify Q_f at fine scales due to the limitation on spatial (usually County or Statewide) and temporal (usually annual or monthly) resolution of data. The energy balance residual approach is simpler and more straightforward, but each component in the model can introduce uncertainties and propagates errors towards the final estimated result (Zhou et al., 2012). The accumulation of errors in the measurements of sensible heat, latent heat, and ground heat can result in under- or over-estimation of Q_f (Park et al., 2016). It can also be limited by the spatial and temporal resolution of remote sensing satellite images and meteorological data, as it is difficult to account for hourly variations of Q_f emission. The GIS approach is the only approach that can measure Q_f in any temporal (annual, monthly, weekly, daily, and diurnal) and spatial resolution. Moreover, it has been considered to be much reliable when compared to the other two approaches since it measure Q_f directly from each of the contributing sources. But this approach is time consuming and requires large volume of data. A common drawback in the existing studies is the absence of validation for the estimated Q_f at a fine scale.

Since Q_f has large spatial and temporal variations, there is a need for high spatial and temporal resolution simulations. However, such simulations of Q_f are subject to the availability of data from multiple sources and robustness of time-dependent simulation models, and are difficult to be conducted by using a single approach (Sailor, 2011). Although the majority of previous studies were restricted to a single approach, there were a few studies in recent years combined multiple approaches to estimate Q_f (Chow et al., 2014; Nie et al., 2014; Park et al., 2016; Zhou et al.,

2012). Zhou et al. (2012) examined the similarity of spatial patterns of Q_f estimated by the energy balanced residual approach and the GIS modeling approach. However, the GIS modeling approach only included building energy consumption modeling and ignored the emission from traffic, human metabolism, and industrial plants. Other studies (Chow et al., 2014; Nie et al., 2014; Park et al., 2016) were restricted to small study areas at local spatial scale. The data required by energy balanced residual approach by Chow et al. (2014) and Park et al. (2016) were measured by a long-term eddy covariance flux tower built near the study area, which is not available in every part of the city. The inventory approach adopted by Nie et al. (2014) was based on an on-campus survey, which might also be unfeasible for larger spatial scales due to the unavailability of such data. In addition, the differences of weekday and weekend were all ignored due to lack of high temporal Q_f simulation. From the discussion above, it can be concluded that there still remain some gaps in the current literature for Q_f estimation with high spatial and temporal resolutions in large areas even with hybrid approaches were applied. This study intends to fill this gap by proposing a novel hybrid Q_f modeling approach, which combines the inventory and GIS approach to create a 365 day hourly Q_f profile at 120 meter resolution in Los Angeles County, California, USA, based on data that available to the public. Since this approach can provide more detail information of Q_f in a larger area of spatial varieties for both workdays and weekends, it would be valuable for city government agencies, energy sector, and the general public. The specific objectives are: 1) to develop a high spatial and temporal Q_f profile that can readily be incorporated into urban energy balance and UHI modeling; and 2) to analyze Q_f across multiple spatial and temporal scales. We attempt to answer the following research questions: 1) what are the typical diurnal Q_f profiles in four seasons during workdays and weekends across different land use types; 2) whether extremely hot days in the summer can lead to notable increase in Q_f when compared to averaged summer days; and 3) why some areas have obvious higher Q_f than others and what are the major contributors?

2. Study area and data

The Los Angeles County, California, USA, was chosen as the study area. As of the 2010 U.S. Census, the county has a population of 9,818,605 (State & County QuickFacts, 2014), making it the most populous county in the nation. Los Angeles has a Subtropical-Mediterranean climate (Koppen climate classification), which is a type of dry subtropical climate, with dry and hot summers and moist winters. Los Angeles County is also subject to microclimates due to its topography, with a large variation in temperature between areas closed to each other. For example, during the summer the average temperature at the Santa Monica Coast is below 27° C, but at the inland areas can above 32° C.

Major datasets used in this study area are listed in Table 1. In order to simulate the 365 day hourly building energy consumption, datasets included Los Angeles Countywide building outlines, building prototypes, Los Angeles County Parcel shapefiles, and Typical Meteorological Year records. Building outlines provided information of building height, building area, type, and year of construction. They were captured from stereo imagery as part of the LAR-IAC2 Project (2008 acquisition) and updated as part of the LARIAC4 (2014) imagery acquisition. The Los Angeles County parcel data, on the other hand, contained information on land use types, which were collected from Los Angeles County Enterprise GIS website. Building prototypes and Typical Meteorological Year were obtained from US Department of Energy (DOE) and National Solar Radiation Data Base, respectively. The Census Transportation Planning Products (CTPP) shapefiles were used for hourly human metabolism estimation. Annual Average Daily Traffic (AADT) data and County road shapefiles were acquired to estimate the hourly traffic emissions. Finally, the annual county energy consumption data was downloaded from the website of LA Energy Atlas, which recorded historical energy consumption data from different sectors (commercial, residential, and industrial) by year, and were used for validation and calibration.

3. Methodology

The sources of Q_f can be divided into three major categories of waste heat (Sailor and Lu, 2004):

$$Q_f = Q_b + Q_v + Q_m \quad (2)$$

where Q_b , Q_v , and Q_m represent heat fluxes emitted by buildings, transportation, and human metabolism, respectively. In this paper, Q_m was determined by the inventory approach, while Q_b and Q_v were simulated by using a combined GIS modeling and inventory approach.

3.1. Human metabolism simulation

Human metabolism (Q_m) is the heat released by human bodies during their daily activities, which varies with population density, activity phase, and time of the day. This study offered a diurnal time-dependent population density based method to simulate the human metabolism in Los Angeles County. The Census Transportation Planning Products (CTPP) shapefiles created by US Census Bureau, which contained information of total population, number of workers in working place, time of arrival at work place, school enrollment population, and employment status, were used to simulate hourly population density. In working days, population density can be estimated by using the following equation:

$$PD = (WPI + WP2 + UE + S) / A \quad (3)$$

Table 1
Datasets used in this study and their sources.

Data	Source
Census Transportation Planning Products (CTPP) Shapefiles	U.S. Census Website
Los Angeles Countywide Building Outline Dataset	Los Angeles County Data Portal
Building Prototypes	US Department of Energy (DOE)
Los Angeles County Parcel shapefiles	Los Angeles County Enterprise GIS
Typical Meteorological Year (TMY3) weather data	National Solar Radiation Data Base
Annual Average Daily Traffic (AADT) data	California Department of Transportation Website
Los Angeles County Road Shapefiles	U.S. Census Website
Annual County Energy Consumption Statistics	LA Energy Atlas

Table 2
Schedule of working population during working day.

Time arriving work place/time leaving home	Time return to home from work
5:00–5:59 a.m.	3:00–3:59 p.m.
6:00–6:59 a.m.	4:00–4:59 p.m.
7:00–7:59 a.m.	5:00–5:59 p.m.
8:00–8:59 a.m.	6:00–6:59 p.m.
9:00–9:59 a.m.	7:00–7:59 p.m.
10:00–10:59 a.m.	8:00–8:59 p.m.
11:00–11:59 a.m.	9:00–9:59 a.m.

where WP1 is working population in the work place; WP2 is the population of people work at home; UE is unemployment population; S is student population; A is the area of census tract.

In the next step, a diurnal human metabolism simulation model was created from the time-dependent population distribution within each hour, which was based on data of 1) working/student population arriving workplace/school and 2) working/student population leaving home at each time interval. Table 2 presents the schedule of typical working population would likely to be at. The schedule was designed based on several assumptions: 1) the average daily working hour was 8 h; 2) there was a 1-hour lunch break; 3) average time needed for daily commute was 1 hour. Therefore, the time between people leaves their home to work and back home from work was set to 10 h. The commuter flow for each census tract was estimated based on the following two cases:

Case 1: If population at working place (working hours) > residential population, it meant there were more workers and students from other census tracts coming into this census tract than going out. Thus, the time dependent population can be calculated as:

$$5 \text{ am} - 11 \text{ am}: \text{Pop}(t) = PP2 + \sum_{t=5}^n (PP1 - PP2) \times AR(t)/AR(\text{total}) \quad (4)$$

$$12 \text{ pm} - 2 \text{ pm}: \text{Pop}(t) = PP1 \quad (5)$$

$$3 \text{ pm} - 8 \text{ pm}: \text{Pop}(t) = PP1 - \sum_{t=15}^n (PP1 - PP2) \times AR(t - 10)/AR(\text{total}) \quad (6)$$

$$9 \text{ pm} - 4 \text{ am}: \text{Pop}(t) = PP2 \quad (7)$$

where PP1 is population at working day during working hours; PP2 is total population (residential) in each census tract; AR(t) is population of workers and students arrive at work place during time interval "t", and AR(total) is total population of workers and students arrive at work place in entire day.

Case 2: If population at working day during working hours < residential population, workers and students from other place to this census tract were less than workers and student going to other census tract during working hours, so time dependent population at each census tract can be calculated as:

$$5 \text{ am} - 11 \text{ am}: \text{Pop}(t) = PP2 - \sum_{t=5}^n (PP2 - PP1) \times L(t)/L(\text{total}) \quad (8)$$

$$12 \text{ pm} - 2 \text{ pm}: \text{Pop}(t) = PP1 \quad (9)$$

$$3 \text{ pm} - 8 \text{ pm}: \text{Pop}(t) = PP1 + \sum_{t=15}^n (PP2 - PP1) \times L(t - 10)/L(\text{total}) \quad (10)$$

$$9 \text{ pm} - 4 \text{ am}: \text{Pop}(t) = PP2 \quad (11)$$

where L(t) is population of workers and students leaving home during time interval "t" and L(total) is total population of workers and students leaving home.

In the final step, human metabolism was calculated as:

$$Q_m = PD \times Mt \quad (12)$$

where PD is population density per square meter, Mt is amount of energy released per person as a function of day (W). In this study, 175 W was set for Mt to represent the daytime metabolic rates in the urban area, according to Sailor and Lu (2004). Table 3 lists the energy released per person as a function of hour of the day (W).

3.2. Building energy consumption simulation

Q_b was simulated as the sum of energy consumption from industrial plants, commercial, and residential buildings. Although there is a time lag between energy consumption and heat emission into the atmosphere, detailed information on the ventilation systems and fabric of buildings for the estimation of the time delay is not generally available (Smith et al., 2009). Moreover, it is also difficult to determine how many percentage of consumed energy was rejected as waste heat because it depended on varying insulation levels and heat exchange rates in different buildings (Sailor and Lu, 2004). Therefore, this study assumed that all energy consumed within buildings was fully and instantaneously emitted into the environment as waste heat.

Building energy consumption includes space heating, cooling, lighting, ventilation, and equipment use. The amount of energy consumption for individual building can be varied, which depends on its physical parameters, prototype, operation schedule, occupant behaviors, and regional climate conditions. For example, space heating and cooling accounted for about 50% of the building energy consumption (U.S. Department of Energy, 2011), but it can be much higher during extreme weather conditions. Therefore, there is a need for high resolution simulation of building energy consumption, especially for large areas like Los Angeles County, which has microclimates and heterogeneous land covers. In this case, the bottom-up GIS modeling approach is more suitable than the top-down inventory approach, which based on the simulation of individual building by considering its attributes.

EnergyPlus, a well-known building energy simulation tool, developed by the U.S. Department of Energy (DOE), was used to simulate 365-day building energy consumption with hourly interval in this study. This software has been extensively tested and validated for the ANSI/ASHRAE standards and widely used by engineers and scientists to model building energy consumption (Huang and Gurney, 2016). Local climate datasets and building

Table 3
Energy released per person as function of hour of the day (W).

Time Period	Time dependent energy release per hour
12–4:59 a.m.	75 W
5–7:59 a.m.	125 W
8 a.m.–7:59 p.m.	175 W
8 p.m.–11:59 p.m.	125 W

prototypes (Table 1) were two required data sources as the input. Its simulation models allowed the customization of occupancy behaviors by providing setting for attributes like daylighting schedule, balanced point temperature, HVAC operation hours, and the number of equipment, which directly determined the energy demand of buildings. The output included hourly site energy consumption by end-use and fuel type for a building prototype under a given weather condition.

3.2.1. Local climate datasets and building prototypes

The hourly weather data files (Table 1) used in EnergyPlus was retrieved from the third (and the latest) Typical Meteorological Year (TMY3) collection. Each TMY3 files included hourly weather data (temperature, solar radiation, precipitation, relative humidity, etc.) in one year duration for a specific location, which is developed based on 1991–2005 weather data or 1976–2005 weather data, if the later existed (Huang and Gurney, 2016). Since Los Angeles County covered a large area, the climate can be different due to urban island effect and the influences from different topographic and land uses. Hourly TMY3 data from 7 weather locations that distributed throughout the entire County were used to simulate the hourly building energy consumption.

Sixteen commercial building prototypes, developed by U.S. DOE, were used for simulation. The DOE created these building prototypes based on Commercial Buildings Energy Consumption Survey (CBECS) data by the U.S. Energy Information Administration (EIA), which provided information on building characteristics, including thermal properties, operation schedules, and three different age categories (pre-1980, post-1980, and new-2004). The age categories reflected differences in the technologies of building insulation, envelope, heating, ventilation, and cooling (HVAC) systems, lighting, and equipment for each type of building, which led to different abilities in energy saving under the same out-door environment. Buildings with newer technology had more energy-efficient equipment, better insulation to mitigate the impact of non-optimal outside temperature, smaller energy intensity of lighting, and more energy-efficient HVAC system (Deru et al., 2011; Huang and Gurney, 2016).

Two prototypes of residential buildings, i.e., multi-families low-rise apartment buildings and single-family detached houses, were developed by DOE in 2009 based on building codes specified in the International Energy Conservation Code (IECC) and Residential Energy Consumption Survey (RECS). Each of these prototypes was modified to represent three types of heating systems (electric resistance, gas furnace, and heat pump), resulting in six residential sub-prototypes residential houses (Huang and Gurney, 2016).

Industry plants, which were ignored by many of the existing studies, were considered as a type of building. However it cannot be simulated using EnergyPlus because it was not included in the building prototypes. Therefore, we used inventory approach to disaggregate the industrial energy consumption data at coarse scale to finer scale. The details were discussed in the following sections.

3.2.2. Schedules of building and occupant behavior

This study designed separate profiles for workdays and weekends/holidays in order to obtain an accurate 365-day building energy use simulation, which usually ignored by previous studies. The differences in operation hours and occupancy status between workdays and weekends/holidays can result in a difference of energy use to certain extent. The DOE generated building prototypes contained specific operation hours for each type of building in workdays, weekends, and public holidays in Los Angeles area based on the CBECS survey. Office buildings, school

buildings, outpatient service buildings were set as closed during the weekend and public holidays, while buildings like quick service restaurants, hospitals, and hotels were set as opening 7 days a week, 24 h a day.

Residential buildings did not have routine operation hours as commercial buildings, and their energy consumption status totally depended on the occupancy behaviors. Therefore, during the workdays, a population distribution based modeling method was used. The hourly profile of population work at home, unemployed population, and time leaving/returning home that used to calculate human metabolism was applied to determine whether or not a residential house was occupied. The occupancy number in residential house in each census district can be calculated by divide the time-dependent population by the number of residential house. If population number lower than house number, it can be assumed that some houses were vacant during that particular time period, and the energy consumption for vacant houses was then set to zero. For occupied houses, lighting load was determined by time of the sun set, and time of the sun rise, which was based on the assumption that lights turned on during sunset in the evening, and turn off during the sleep time, which set to 12pm; and lights turned on again before sunrise in the morning. On weekends and public holidays, all residential buildings were set as occupied at all times.

For commercial and residential buildings, heating and cooling energy consumption was simulated depending on the comparison between indoor temperature and the balanced point temperature at which no cooling or heating was required. If indoor temperature was higher than the set up temperature, it can be assumed that the cooling system was working to maintain the set up temperature; if indoor temperature was lower than the comfort temperature, the heating system assumed to be turn on. The balanced point temperature was usually assumed to be 18.3 °C (65 °F) in previous studies (Wang and Chen, 2014). In this study, we assigned 20 °C as the temperature that set up by the occupants in thermostats, which was close to the balanced point temperature.

The energy use in the industrial sector did not have a large difference from that in the commercial and residential buildings due to its relatively insensitivity to variations in weather and a much more uniform diurnal and seasonal distribution (Sailor, 2011). It is fairly common that energy consumption of industrial sector was assumed uniformly distributed among the 8760 h of the year (Sailor and Lu, 2004; Sailor, 2011).

3.2.3. Initial annual building energy consumption simulation and calibration

We categorized the 365-day building energy consumption simulation into 8 different “seasonal and day type” profiles: (1) spring workdays; (2) spring weekends/holidays; (3) summer workdays; (4) summer weekends/holidays; (5) fall workdays; (6) fall weekends/holidays; (7) winter workdays; and (8) winter weekends/holidays. The annual building energy consumption from commercial and residential sectors was calculated based on the aggregation of energy consumed in each particular hour, day, and season. First, the hourly building Energy Use Intensity (EUI), defined as the hourly energy use per square meter, was simulated using the EnergyPlus. For commercial buildings, there were 2688 different values of EUIs, which resulted from the combination of 8 “seasonal and day type” profiles, 7 weather zones, 16 building prototypes, and 3 age groups. Residential buildings exhibited 366 different values of EUIs, which resulted from the combination of 8 “seasonal and day type” profiles, 7 weather zones, and 6 prototypes.

The energy consumption for an individual building (BE) i within

a particular hour j can be calculated by the following equation:

$$BE_{hour(i,j)} = EUI_{ij} \times A_{building(i)} \times FN_{building(i)} \quad (13)$$

where $A_{building(i)}$ is the footprint area of building i , $FN_{building(i)}$ is the floor number, which was estimated based on building height. The daily energy consumption of building i for day j was calculated as follows:

$$BE_{day(i,j)} = \sum_{j=1}^{24} BE_{hour(i,j)} \quad (14)$$

The building energy consumption within a season k was calculated as follows:

$$BE_{season(k)} = \sum_{j=1}^{t1} BE_{workday(i,j,k)} + \sum_{j=1}^{t2} BE_{non-workday(i,j,k)} \quad (15)$$

where $BE_{workday(i,j,k)}$ and $BE_{non-workday(i,j,k)}$ are the EUI at a particular hour i within the day j during the season k in workday and non-workdays (weekends and holidays), respectively; $t1$ and $t2$ are the number of workdays and non-workdays within season k , respectively. The annual building energy consumption for sector l was calculated as:

$$BE_{annual(l)} = \sum_{k=1}^4 BE_{season(k)} \quad (16)$$

Although the GIS modeling approach can simulate building energy consumption at much finer spatial (individual building level) and temporal scales (hourly) when compared to the inventory approach, there were still discrepancies between simulation results and the actual energy consumption, which can be caused by uncertainties between the simulation and the truth. Therefore, annual energy consumption data from California Energy Commission (CEC) (<http://ecdms.energy.ca.gov/electbycounty.aspx>) and LA Energy Atlas (<http://www.energyatlas.ucla.edu/>) were used as reference to calibrate the simulation model. The Energy Atlas provides detailed historical annual energy consumption data from all building energy sectors, including commercial, residential and industrial sector at a finer scale of city neighborhood level. Compared to previous studies that used the county, state, or census division level energy consumption data to calibrate the simulation, the use of neighborhood level reference data allowed us to address the regional variation of energy consumption patterns in each building sector.

The annual energy consumption of commercial buildings and residential buildings in each neighborhood were calculated and compared to the reference energy consumption data. In the next step, the EUI of each type of commercial and residential building was calibrated by using the ratio between simulated results and the reference energy consumption data. The energy consumption data for industrial sector in some neighborhoods were masked out, because of many industrial consumers did not share their data to the public. Therefore, we used the percentage of countywide consumption to obtain the total volume of industrial energy consumption in those neighborhoods, and applied the metrics of median consumption per square meter and the total floor areas of industrial plants in each neighborhood to curve the EUI of industrial plant in each neighborhood.

3.2.4. Final building energy consumption simulation

After the calibration of EUI for each type of building, we adopted a gridded algorithm (Smith et al., 2009; Zhou et al., 2012) to

quantify building energy consumption in LA County in 8760 individual hour throughout the year. A 120-m resolution grid was created in the shapefile format and its spatial extent was matched with the Landsat imagery. The grid layer was overlaid with building footprint layer and each grid cell contains 0, 1, or multiple fractions of buildings. Building energy consumption in a grid cell can be estimated using the following equation:

$$BE_{grid(i)} = \frac{\sum_{j=1}^n EUI(j) \times A(j) \times FN(j)}{A2} \quad (17)$$

where $EUI(j)$, $A(j)$, $FN(j)$ are the hourly energy intensity index, floor areas, and floor numbers of building prototype j , respectively. The algorithm summed up hourly energy consumption from all the building prototypes in the given grid cell and divided by the grid area $A2$, which equals to 14400 square meters.

3.3. Traffic emission simulation

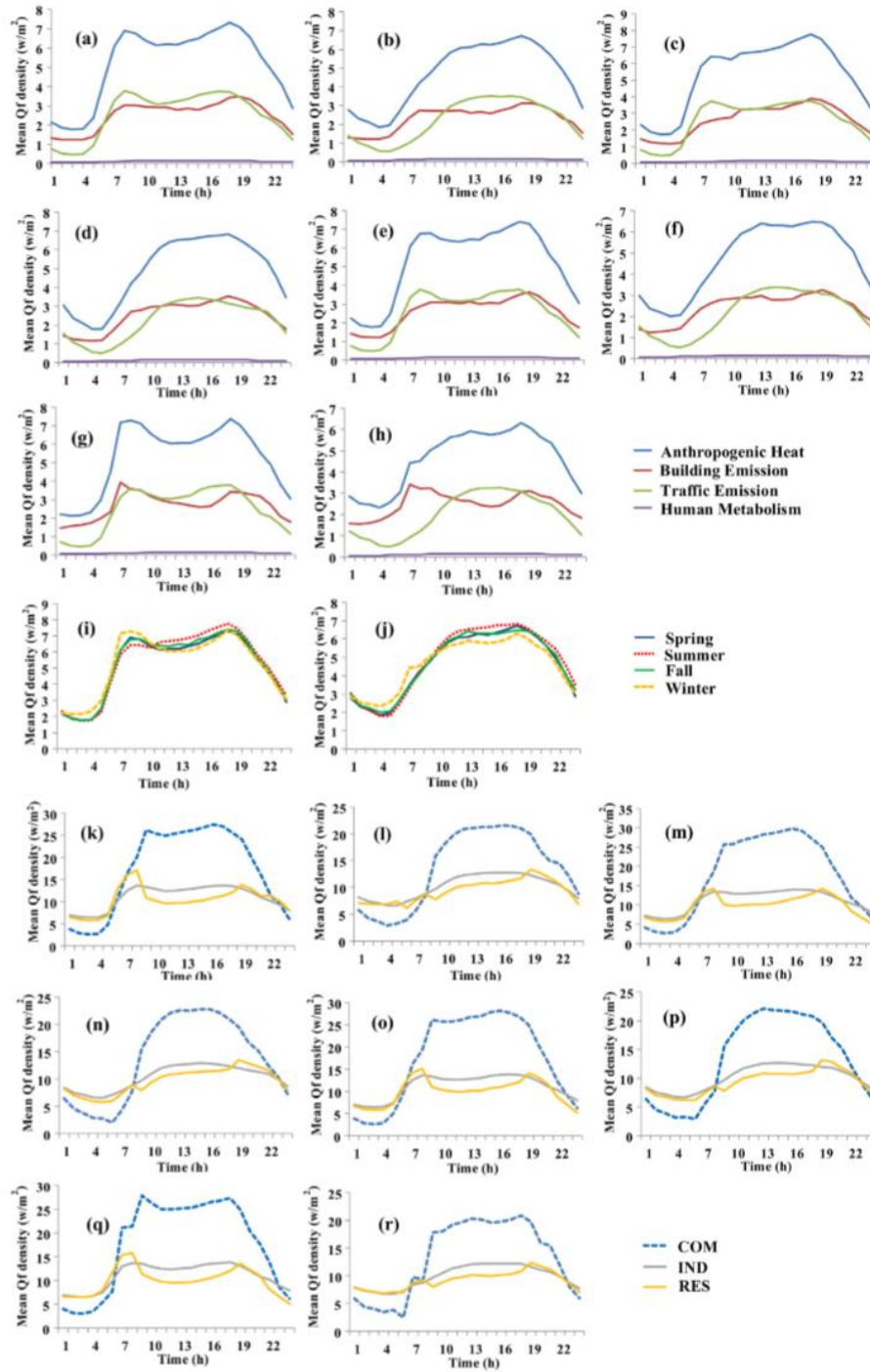
Hourly traffic emission within a particular day were simulated based on normalized annual average daily traffic (AADT) data which adjusted by seasonal scaling factor, weekday scaling factor, and diurnal scaling factor. The 2010 AADT data, which calculated by dividing 365 from the total volume of traffic of a road for a calendar year, were collected as point shapefiles from California Traffic Census Program in 808 traffic count stations. They were distributed throughout major roads in the study area. The 120-m grid, AADT traffic counts, and road shapefiles were overlaid together. The hourly traffic count values from AADT were directly assigned to the major road segments if they were located within the same grid cell with AADT points. For grid cells not containing the AADT points, the average values of traffic volume for all the points in the same neighborhood were assigned. The traffic volume in the minor roads was calculated by multiplying the traffic volume in major roads with 0.1.

We also created profiles for 8 different types of days as we did for building energy simulation. The temporal traffic variations for each day type were calculated through applying the seasonal scaling factors and the diurnal variation factors for the hourly traffic volume calculated by AADT traffic counts. The seasonal scaling factors and the diurnal variation factors were calculated using the metric of hourly vehicle miles traveled (VMT), which was available in Caltrans Performance Measurement System (PeMS) Database established by California Department of Transportation (DOT). The PeMS database contains historical hourly VMT data in each individual day from 1993 to the present. We used the VMT data from the year of 2010 to construct the diurnal vehicle volume profiles for 8 different types of days. The hourly vehicle volume factor was simulated by averaging all the VMT values from the same time during the days that in the same category.

The traffic emission in each grid square was calculated using the formula similar as Smith et al. (2009), which is:

$$Q_{FT} = \sum (N_{mxi}(t) \times L_{xi}) \times EF_m / A_i \quad (18)$$

where Q_{FT} is the vehicle emission in W/m^2 , N_{mxi} is the normalized traffic count number for vehicle type m on road x in grid square i , t is the hour of the day, L_{xi} is the length of all the roads x within the grid square i , EF_m is the fuel consumption emission factor ($J \ m^{-1}$), which can be calculated as and A_i is the area of grid square (for each grid, the area A_i can be calculated as $120 \times 120 = 14400 \ m^2$). The fuel consumption emission factor (W/m) was calculated using the equation by Sailor and Lu (2004):



$$EF_m = NHC \times \rho_{fuel} / FE (J m^{-1}) \quad (19)$$

where NHC is mean net heat of vehicle gasoline and diesel combustion ($J kg^{-1}$), which is $45.85 kJ g^{-1}$ for petrol and $46 kJ g^{-1}$ for diesel (Smith et al., 2009); ρ_{fuel} is the mean density of gasoline ($0.75 kg l^{-1}$) and diesel ($0.832 kg l^{-1}$) (U.S. Energy Information Administration, 2014; Chow et al., 2014); FE is mean fuel efficiency of all vehicles ($7.5 km l^{-1}$ in 2010) (U.S. Department of Transportation, 2011; Chow et al., 2014). Based on annually gasoline and diesel sold data from California State Board of Equalization (<http://www.boe.ca.gov/sptaxprog/spftrpts.htm>), the ratio between number of gasoline vehicles and diesel vehicles in Los Angeles County was set to 5.25:1, and mean fuel consumption emission factor (EV) was estimated to be $4668 J m^{-1}$.

4. Results

4.1. Temporal variations of anthropogenic heat flux

The diurnal variation of mean hourly Q_f and its components in spring workday, spring non-workday, summer workday, summer non-workday, fall workday, fall non-workday, winter workday, and winter non-workday in Los Angeles County are presented in Fig. 1. In general, Q_b and Q_v contributed similar proportions to Q_f but differently in time, and Q_m contributed the least proportion to Q_f despite workdays or non-workdays. In all profiles, the workday diurnal profiles of Q_f exhibited a dual-peak shape with the morning and evening peak, while the non-workday diurnal profiles of Q_f exhibited parabola shapes with only the peak in the evening hours. Because the traffic emissions reached their peak values not only in the evening rush hours but also in the morning rush hours in workdays. Peak values in the workdays were higher than that in the non-workdays, because many buildings were not in operation hours during non-workdays. The lowest values of Q_f were found at 4AM in workdays and 5AM in non-workdays.

Fig. 1 also shows the comparison of diurnal variation of Q_f among different seasons in (i) workdays and (j) non-workdays. The diurnal variations of Q_f exhibited similar shapes but small differences in magnitude. Q_f profiles in the summer possessed higher values during the noon and evening time in workdays and non-workdays than that of other seasons. The reason is that building energy consumption was the highest during the summer noon and evening hours (Fig. 1c and d) due to extra energy consumed for cooling. It can also be observed that Q_f values in the winter mornings in workdays and non-workdays were higher than in other seasons. This was caused by higher amount of building energy consumption (Fig. 1h and i) as extra energy were consumed for heating to offset the larger difference between indoor and outdoor temperatures in winter morning. It can also explain why winter was the only season that detected the highest workday Q_f value in the morning peak, instead of the evening peak.

The diurnal variations of Q_f in different land use types from 8 types of days are shown in Fig. 1k through Fig. 1r. It can be found that Q_f in commercial areas (COM) were higher than that in residential (RES) and industrial (IND) areas from 8:00 h to 21:00 h, which coincided with the fact that during the daytime population flowed into the commercial areas. Compared to Q_f in COM which displayed a parabolic shape with the peak value in 17:00 h, Q_f in RES exhibited a dual-peak shape in workdays with one peak in the

morning and the other in the evening. That was because during the working hours between morning and evening, many residential houses were not occupied. Q_f in IND discovered the lowest variation in different times, regardless of workdays and non-workdays.

4.2. Anthropogenic heat fluxes in extremely hot summer days

Q_f appeared to have the highest values in the summer workdays in Los Angeles County, with its maximum value reaching $7.76 w/m^2$ (Fig. 1g). Since traffic emission and human metabolism did not have obvious seasonal variations, the most significant driver of the increased energy use in summer came from the building sector, which required higher amount of cooling energy consumption. We performed an analysis by a comparison between Q_f in an extremely hot summer workday and that in the averaged summer workday to examine if there was an obvious increase in building energy demand in the extremely hot day and to what extent the energy use was increased.

We selected August 25th, 2015 as the extremely hot summer workday for the comparison, as its daily high temperature reached $37^\circ C$ ($98.6^\circ F$) at 13:00 h. Temperature in that day also maintained over $30^\circ C$ for 10 h from 10:00 h to 19:00 h. Fig. 2a presents the comparison result between Q_f in the extremely hot summer workday (Aug. 25, 2015) and the average summer workdays. It can be found that Q_f in the extremely hot summer workday was obviously higher than that in the average summer workdays from 8:00 h to 23:00 h, with its maximum value reach $8.14 w/m^2$. Further, the percentage breakdown of all components contributing to Q_f from 8:00 h to 23:00 h is illustrated in Fig. 2b. The building related energy use and traffic emissions were two dominant components of anthropogenic heat in both average summer workdays and the extremely hot workday. The building energy consumption contributed slightly higher percentages of Q_f (50.34%) in the extremely hot summer workday than that in average summer workdays (49.27%). It can also be discovered that for most of the time during the day (9:00 h to 21:00 h) the increase of building energy consumption due to the extremely hot weather was the dominant driver to cause a higher Q_f in the extremely hot summer workday.

Fig. 2c shows that time series of ratio between anthropogenic heat fluxes (blue solid), building emissions (red dash), traffic emissions (green dash) in the extremely hot summer workday and the average summer workdays. If heat fluxes in the extremely hot summer workday were larger than those in the averaged summer workdays, the ratio was larger than 1. Higher ratio indicated more extra heat fluxes were produced in the extremely hot summer day. It can be found that the major contributor of higher anthropogenic heat fluxes in the extremely hot summer day varied with time periods in a day. According to Fig. 2c, building emission was the major contributor for majority of the day (from 9:00 h to 18:00 h and from 20:00 h to 21:00 h), as its ratio was significantly higher than that of the traffic emission and anthropogenic heat fluxes during these time periods. The building ratio raised gradually from 8:00 h to 11:00 h, as the temperature difference between the extremely hot summer day and average summer workdays increased. This ratio remained high from 12:00 h to 16:00 h because the temperature difference reached its maximum during the daytime, and air condition systems consumed more energy to offset the larger indoor/outdoor temperature difference in the

Fig. 1. Diurnal variation of Q_b , Q_v , Q_m , and Q_m in Los Angeles, U.S.A., based on the average value of from all (a) spring workdays, (b) spring non-workdays, (c) summer workdays, (d) summer non-workdays, (e) fall workdays, (f) fall non-workdays, (g) winter workdays, and (h) winter non-workdays; comparison of diurnal variation of Q_f in different seasons in (i) workdays and (j) non-workdays in Los Angeles, U.S.A.; diurnal variation of Q_f in commercial (COM), residential (RES), and industrial (IND) areas in Los Angeles, U.S.A., based on the average value from all (k) spring workdays, (l) spring non-workdays, (m) summer workdays, (n) summer non-workdays, (o) fall workdays, (p) fall non-workdays, (q) winter workdays, and (r) winter non-workdays.

extremely hot summer day. During the daytime (8:00 h to 18:00 h), traffic emission contributed less to the higher Q_f in the extremely hot summer day as the traffic ratio was overall lower than the building ratio. However, at nighttime the traffic ratio increased dramatically while building ratio remained high, which combined to lead to the larger Q_f increment in the extremely hot summer workday. The reason that there was a significant larger traffic volume in the particular day we selected as the example of an extremely hot summer workday must be further studied to determine. Possible factors included traffic congestion or nighttime activities.

4.3. Anthropogenic heat fluxes in the urban core area

Although the daily maximum value of Q_f estimated in Los Angeles County during the extremely hot summer workday did not exceed over the average summer workday by 10 w/m^2 , there was a large within-county variation in Q_f among different regions. Fig. 3 presents the spatial distribution of Q_f estimated at 5pm during the summer workdays in Los Angeles County, when Q_f exhibited the highest value compared to other time periods (Fig. 2). It can be observed that Q_f was spatially unevenly distributed, with high values (larger than 100 w/m^2) being located in some clusters, such as the Downtown area, Korean Town, Beverly Hills, Hollywood, West Los Angeles, Long Beach, and Santa Monica, which were characterized as commercial and industrial zones. Moreover, high Q_f values can be found in major freeways, which was caused by heavy traffic emissions during the evening rush hours. The moderate Q_f values ($20\text{--}100 \text{ w/m}^2$) were detected in residential zones with high density of houses and population, while low Q_f values (less than 20 w/m^2) were located in cities with small population (Palmdale and Lancaster), low density residential zones, and minor roads. The downtown area was found to have the largest mean Q_f throughout the year, compared to other neighborhoods, because there were more densely distributed tall commercial buildings. Fig. 3 (b) shows the spatial distribution of Q_f in the downtown at 17:00 h during summer workdays. Spatial variation of Q_f values can be discovered as low values located in the southeast part of the downtown; and the values increased dramatically towards northwest. The reason was the most majority of tall commercial buildings were located in northwest part of the downtown. While the low commercial buildings, historical office buildings, apartment complexes, and warehouses were located in the southeast part, contributing to a relatively lower Q_f value. Some cells with high Q_f values in this region were located in the freeway.

Fig. 4a to Fig. 4h presents the diurnal variation of mean hourly Q_f in spring workday, spring non-workday, summer workday, summer non-workday, fall workday, fall non-workday, winter workday, and winter non-workday in the downtown area of Los Angeles. The times series of diurnal variations of Q_f exhibited a parabola shapes with the maximum value appears in the afternoon, except for Q_f in the winter workdays, which displayed a dual-peak shape. It can be concluded that Q_f in the downtown was more significant in workdays than that in non-workdays, and its maximum value can reach 100 w/m^2 (16:00 h in summer workdays). The patterns of diurnal variation were quite consistent among different types of days, which promoted us to conduct a polynomial fitting. All resultant models appeared to generate a good fit with R^2 ranging from 0.8 to 0.9.

Fig. 4 shows a comparison of diurnal variation of Q_f in the Downtown Los Angeles among different seasons in (i) workdays and (j) non-workdays. It can be found that during 9:00 h to 17:00 h, Q_f in summer workdays was higher than in other workdays (Fig. 4i), while during 5:00 h to 9:00 h, Q_f in winter weekends was the highest. Building energy consumption was the most important

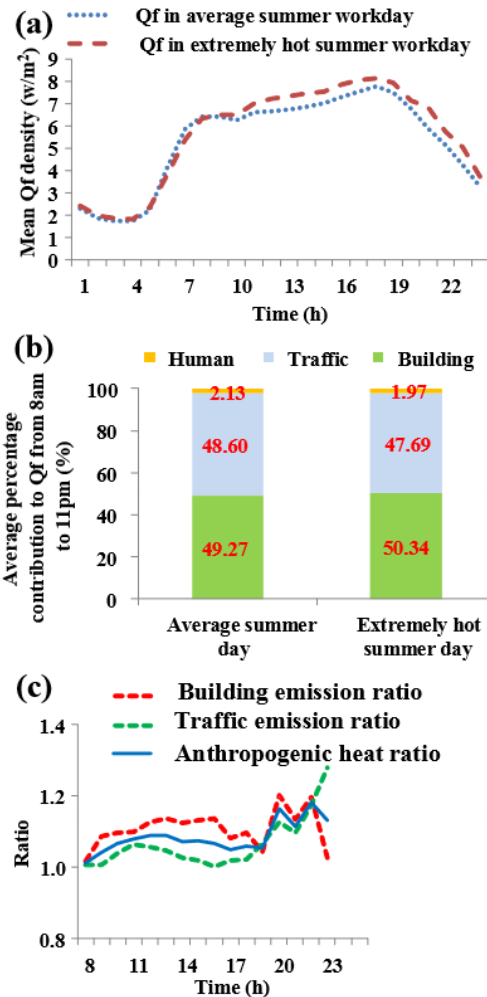


Fig. 2. Comparison between Q_f in an extremely hot summer workday (Aug. 25, 2005) and the average summer workdays (a); percentage breakdown of the individual components contributing to Q_f for average summer workdays and the extremely hot summer day from 8:00 h to 23:00 h (August 25, 2005) (b); time series of ratio between anthropogenic heat fluxes, building emissions, traffic emissions in the extremely hot summer workday and the average summer workdays (c).

factor that contributed to Q_f (Fig. 5). Fig. 6 shows that building energy consumption and traffic emission from 9:00 h to 17:00 h during workdays and 5:00 h to 9:00 h during non-workdays. Building energy consumption can be identified as the dominant factor that contributed to the higher Q_f values in summer workdays and winter non-workdays, as the traffic emissions from different seasons during these time periods were similar.

5. Discussion

This section discussed the significance of the proposed work

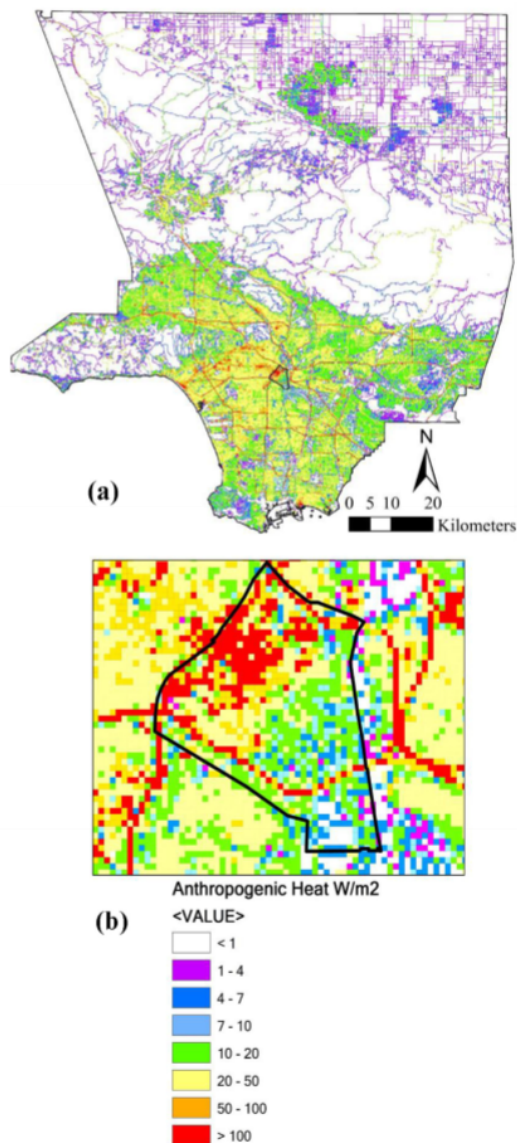


Fig. 3. Spatial distribution of Q_f in (a) Los Angeles County and (b) Downtown Los Angeles.

and a comparison between it and previously published work based on the results and the applicability of the methodology. From the existing studies, it can be found that the difference in Q_f profile in cities of different climates is obvious. For example, Chicago, San Francisco, and Philadelphia had the largest wintertime anthropogenic heating with values ranging 70 to 75 w/m^2

(averaged over the entire city), but during the summer they had peak values of anthropogenic heating in the range 30–60 w/m^2 (Sailor and Lu, 2004). The city of Seoul, South Korea, detected the largest heat emission in winter, ranging from about 35–75 w/m^2 , while in summer from 5 to 10 w/m^2 . However, in subtropical or tropical cities, Q_f in the warmer months is found equal to or larger than Q_f in the cooler months. Quah and Roth (2012) suggested that Q_f in tropical city like Singapore can be substantially higher in summer and remain high throughout the year owing to strong demands for air-conditioning. For Los Angeles, which has a Subtropical-Mediterranean climate (Köppen climate classification), no significant difference can be found when compared the summer Q_f profile with that of the winter in Sailor and Lu (2004) because of the relatively mild weather compared to the tropical or mid-latitude cities. Compared to the existing studies, the advantage of our approach is the design of separate profiles for workdays and weekends. In this way, a higher value of Q_f in the winter mornings and the summer evenings in workdays can be identified. These contrasts will be less significant if workday and weekend Q_f profiles were not separated from each other.

In addition, a large within-county difference in Q_f was discovered among different regions and land use types, which agree with the results from many previous studies (Chapman et al., 2016; Chow et al., 2014; Hamilton et al., 2009; Ichinose et al., 1999; Quah and Roth, 2012; Smith et al., 2009). The Downtown Los Angeles was found to have the largest mean Q_f throughout the year, among all the neighborhoods. Building energy consumption was identified as the dominant contributor to the overall Q_f in the downtown area. When compared with previous studies (Ichinose et al., 1999; Nie et al., 2014; Quah and Roth, 2012; Wong et al., 2015) which estimated Q_f in the cities or regions with higher population density (Tokyo, Hong Kong, Singapore), traffic emissions was found to account for a higher percentage of Q_f in Los Angeles County, while human metabolism contributed less.

The proposed approach has a higher degree of applicability for Q_f estimation in the large areas compared with previous studies, as all the data used were available to the public. Because compared to the existing studies in recent years (Chow et al., 2014; Nie et al., 2014; Park et al., 2016), which relied on data that were only available for local regions, this research was not restricted to small study areas as all data used were available for the entire Los Angeles County. Due to this reason, it can be readily applied to similar studies in different study areas with different climates. Compared to the city of Los Angeles, we may observe a larger contrast of Q_f among different seasons in mid-latitude cities with colder winter and tropical cities with hotter summer, because buildings typically consume more energy during the extreme weather conditions, which was proved in this study. Q_f in the mid-latitude cities should have its peak value during winter mornings when the offset between the indoor and outdoor temperature reaches its maximum value, especially in workdays, because more buildings would be in operation than in weekends. On the other hand, cities with similar climate as Los Angeles may not have the similar Q_f profile, because other contributors, such as social-economic factors, traffic emission and human metabolism, and building thermal envelope all impact the characteristics of Q_f . Moreover, it is the first anthropogenic heat study that designed to separate profiles for workdays and weekends/holidays in different seasons in order to obtain an accurate 365-day building energy use simulation, which explored its application on cross-examination of Q_f by using GIS-based modeling approach and the energy balance residual approach from a series of time with fine scales.

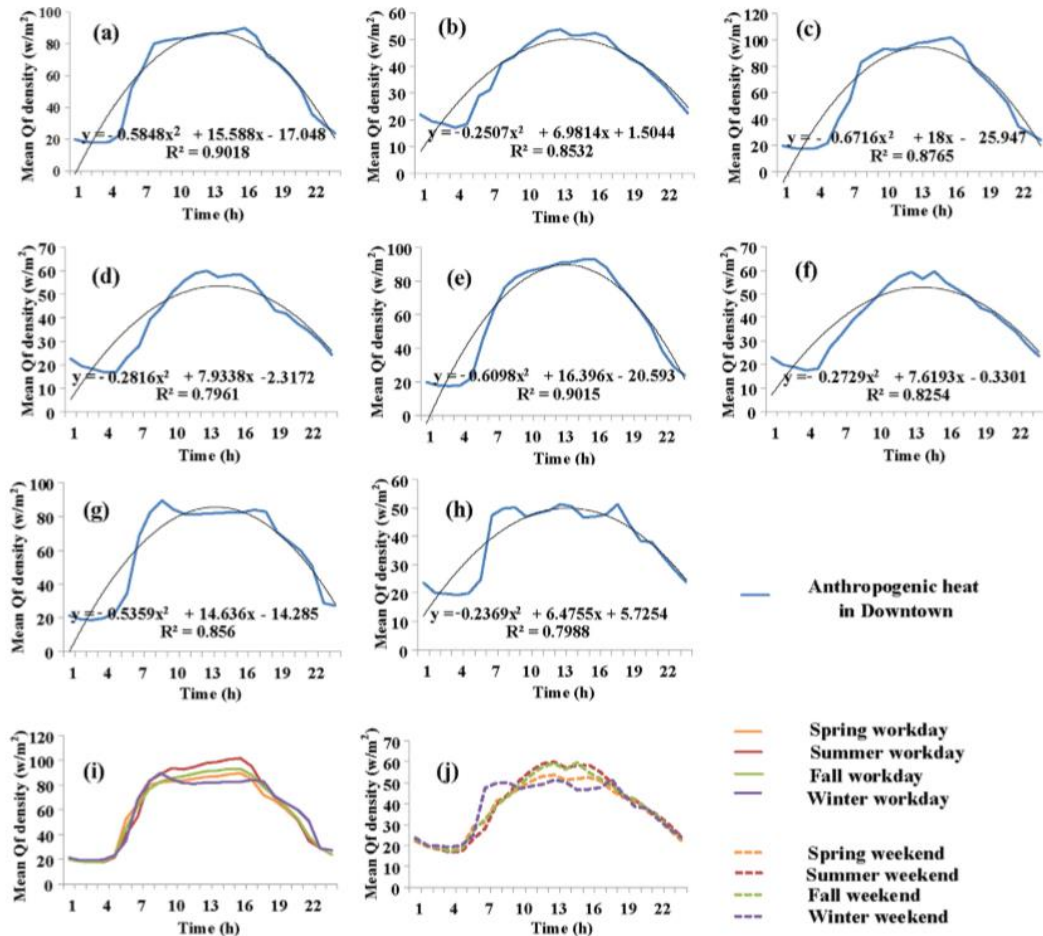


Fig. 4. Time series of diurnal variations of Q_f in the Downtown Los Angeles in 8 day types: (a) spring workdays, (b) spring non-workdays, (c) summer workdays, (d) summer non-workdays, (e) fall workdays, (f) fall non-workdays, (g) winter workdays, and (h) winter non-workdays; comparison of diurnal variation of Q_f in the Downtown Los Angeles among different seasons in (i) workdays and (j) non-workdays.

6. Conclusions

This study provided a hybrid approach to Q_f modeling, which combined the inventory and GIS methods to create a 365-day hourly Q_f profile at 120-m spatial resolution in Los Angeles County, California, USA, based on data available to the public. A high spatial and temporal Q_f profile that can be readily incorporated into urban energy balance and UHI models has been developed, which provided valuable information for city government agencies, energy sector, and the general public. The main findings from this study are the magnitudes and temporal patterns of Q_f in Los Angeles County which varied in workdays and non-workdays, seasons, and land use types. Moreover, Q_f in

the extremely hot summer workday was found obviously higher than that in the average summer workdays from 8:00 h to 23:00 h. The increase of building energy consumption due to higher demands for space cooling to offset the extremely hot weather was the dominant driver that caused the higher Q_f in the extremely hot summer workday. In addition, a large within-county difference in Q_f was discovered among different regions. The Downtown Los Angeles was found to have the largest mean Q_f throughout the year, among all the neighborhoods. Building energy consumption was identified as the dominant contributor to the overall Q_f in the downtown area. When compared with previous studies (Ichinose et al., 1999; Nie et al., 2014; Quah and Roth, 2012; Wong et al., 2015) which estimated Q_f in the cities or

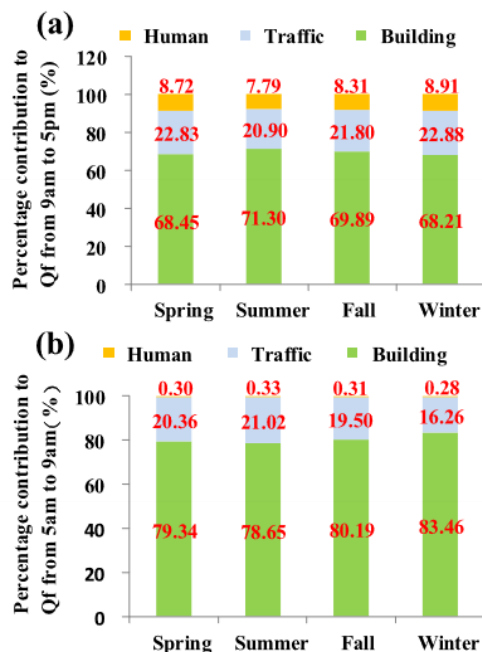


Fig. 5. Percentage breakdown of the individual component contributing to Q_f during (a) 9:00 h to 17:00 h on workdays and (b) 5:00 h to 9:00 h on non-workdays in the Downtown Los Angeles.

regions with higher population density (Tokyo, Hong Kong, Singapore), traffic emissions was found to account for a higher percentage of Q_f in Los Angeles County, while human metabolism contributed less.

The major innovation of this study is that it developed a hybrid approach which integrated the inventory and GIS modeling approaches. The GIS modeling approach can create a time-dependent Q_f profile in high spatial-temporal resolutions with a higher accuracy, and the inventory approach can validate and calibrate the results estimated from the GIS modeling approach. This integration allowed for assessing the discrepancies between simulated energy use and the actual energy consumption. Compared to previous studies that used county, state, or census levels for calibrating the simulation result, the use of neighborhood level reference data enabled to address the regional variation of energy consumption patterns by building.

Overall, this study proposed an approach to estimate Q_f at high spatial- and temporal-resolution for a large metropolitan area of diverse geographic settings. However, the data availability is still a major limitation in this study. First of all building energy consumption simulation would be more accurate if cooling and heating system for each building can become available in residential building polygon or county assessor parcel. The traffic emission simulation would be more meaningful if seasonal variation of emission factor from several types of vehicles can be included, as during cold or hot seasons, vehicles tended to consume more fuels when air condition systems were working.

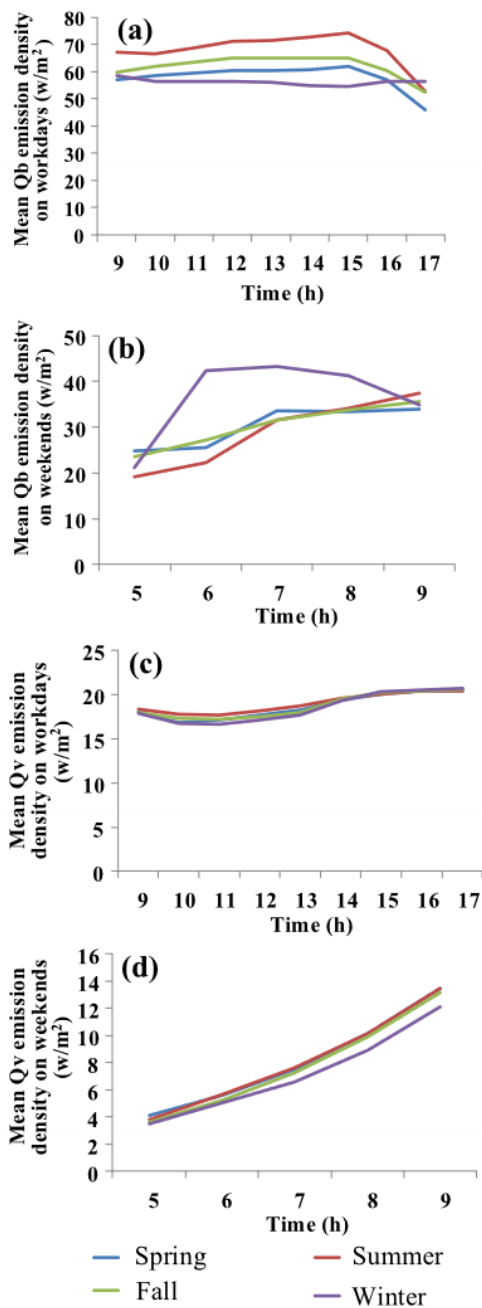


Fig. 6. Building energy consumption (Q_b) during (a) 9:00 h to 17:00 h on workdays and (b) 5:00 h to 9:00 h on non-workdays, traffic emissions (Q_v) during (c) 9:00 h to 17:00 h on workdays and (d) 5:00 h to 9:00 h on non-workdays in the Downtown Los Angeles.

Acknowledgements

We thank anonymous reviewers and editors for their constructive comments and suggestions, which improved the manuscript. Weng acknowledges a visiting chair professorship from by South China Normal University during his sabbatical leave.

References

- Allen, L., Lindberg, F., Grimmond, C.S.B., 2011. Global to city scale urban anthropogenic heat flux: model and variability. *Int. J. Climatol.* 31, 1990–2005.
- California Energy Commission (CEC), <http://ecdms.energy.ca.gov/electbycounty.aspx> (accessed 28.12.2016).
- California State Board of Equalization, <http://www.boe.ca.gov/sptaxprog/spftrpts.htm> (accessed 02.12.2016).
- Chapman, S., Watson, J.E.M., McAlpine, C.A., 2016. Large seasonal and diurnal anthropogenic heat flux across four Australian cities. *J. South. Hemisphere Earth Syst. Sci.* 60, 342–360.
- Chow, W.T.L., Salamanca, F., Georgescu, M., Mahalov, A., 2014. A multi-method and multi-scale approach for estimating city-wide anthropogenic heat fluxes. *Atmos. Environ.* 99, 64–76.
- Deru, M., Field, K., Studer, D., Benne, K., Griffith, B., Torcellini, P., Liu, B., Halverson, M., Winiarski, D., Rosenberg, M., Yazdani, M., Huang, J., Crawley, D., 2011. US Department of Energy Commercial Reference Building Models of the National Building Stock. U.S. Department of Energy, Oak Ridge.
- Fan, H., Sailor, D.J., 2005. Modeling the impacts of anthropogenic heating on the urban climate of Philadelphia: a comparison of implementations in two PBL schemes. *Atmos. Environ.* 39, 73–84.
- Ferreira, M.J., Oliveira, A.P., 2011. Anthropogenic heat in the city of Sao Paulo, Brazil. *Theor. Appl. Climatol.* 104, 43–56.
- Flanner, M.G., 2009. Integrating anthropogenic heat flux with global climate models. *Geophys. Res. Lett.* 36, <http://dx.doi.org/10.1029/2008GL036465>.
- Grimmond, C.S.B., 1992. The suburban energy balance: methodological considerations and results for a mid-latitude west coast city under winter and spring conditions. *Int. J. Climatol.* 12, 481–497.
- Guneralp, B., Zhou, Y., Urge, D., Gupta, M., Yu, S., Patel, P.L., Fragkias, M., Li, X., Seto, K., 2017. Global scenarios of urban density and its impacts on building energy use through 2050. *Proc. Natl. Acad. Sci. U. S. A. P. Nat. A. Sci.* <http://dx.doi.org/10.1073/pnas.1606035114>.
- Hamilton, I.G., Davies, M., Steadman, P., Stone, A., Ridley, I., Evans, S., 2009. The significance of the anthropogenic heat emissions of London's buildings: a comparison against captured shortwave solar radiation. *Build. Environ.* 44, 807–817.
- Hu, D., Yang, L., Zhou, J., Deng, L., 2012. Estimation of urban energy heat flux and anthropogenic heat discharge using aster image and meteorological data: case study in Beijing metropolitan area. *J. Appl. Remote. Sens.* 6.
- Huang, J., Gurney, K.R., 2016. The variation of climate change impact on building energy consumption to building type and spatiotemporal scale. *Energy* 111, 137–153.
- Ichinose, T., Shimodono, K., Hanaki, K., 1999. Impact of anthropogenic heat on urban climate in Tokyo. *Atmos. Environ.* 33, 3897–3909.
- International Energy Agency, 2009. *World Energy Outlook 2009*. <http://www.worldenergyoutlook.org/media/weowebsite/2009/WEO2009.pdf>. (Accessed 6 January 2017).
- Kato, S., Yamaguchi, Y., 2005. Analysis of urban heat island effect using ASTER and ETM+ data: separation of anthropogenic heat discharge and natural heat radiation from sensible heat flux. *Proc. Spie* 99, 44–54.
- Kato, S., Yamaguchi, Y., Liu, C., Sun, C., 2008. Surface heat balance analysis of Tainan City on March 6, 2001 using ASTER and Formosat-2 data. *Sensors* 8, 6026–6044.
- Kikegawa, Y., Genchi, Y., Yoshikado, H., Kondo, H., 2003. Development of a numerical simulation system toward comprehensive assessments of urban warming countermeasures including their impacts upon the urban buildings energy demands. *Appl. Energy* 76, 449–466.
- Kikegawa, Y., Genchi, Y., Kondo, H., Hanaki, K., 2006. Impacts of cityblock-scale countermeasures against urban heat-island phenomena upon a building's energy-consumption for air-conditioning. *Appl. Energy* 83, 649–668.
- Klysis, K., 1996. Spatial and seasonal distribution of anthropogenic heat emissions in Lodz, Poland. *Atmos. Environ.* 30, 3397–3404.
- IA Energy Atlas, <http://www.energyatlas.ucla.edu/> (accessed 22.01.2017).
- Masson, V., 2000. A physically-based scheme for the urban energy budget in atmospheric models. *Bound.-lay. Meteorol.* 94, 357–397.
- Nie, W., Sun, T., Ni, G., 2014. Spatiotemporal characteristics of anthropogenic heat in an urban environment: a case study of Tsinghua Campus. *Build. Environ.* 82, 675–686.
- Ohashi, M., Genchi, Y., Kondo, H., Kikegawa, Y., Hirano, Y., Yoshikado, H., 2003. A study of horizontal temperature distribution within urban canopy layer at the Tokyo central area. In: Fifth International Conference on Urban Climate, Lodz, Poland.
- Ohashi, Y., Genchi, Y., Kondo, H., Kikegawa, Y., Yoshikado, H., Hirano, Y., 2007. Influence of air-conditioning waste heat on air temperature in Tokyo during summer: numerical experiments using an urban canopy model coupled with a building energy model. *J. Appl. Meteorol. Clim.* 46, 66–81.
- Oke, T.R., 1987. *Boundary Layer Climates*, second ed. Taylor & Francis, Abingdon-on-Thames.
- Oke, T.R., 2006. Towards better scientific communication in urban climate. *Theor. Appl. Climatol.* 84, 179–190.
- Park, C., Schade, G.W., Werner, N.D., Sailor, D.J., Kim, C., 2016. Comparative estimates of anthropogenic heat emission in relation to surface energy balance of a subtropical urban neighborhood. *Atmos. Environ.* 126, 182–191.
- Pigeon, G., Legain, D., Durand, P., Masson, V., 2007. Anthropogenic heat release in an old European agglomeration (Toulouse, France). *Int. J. Climatol.* 27, 1969–1981.
- Quah, A.K.L., Roth, M., 2012. Diurnal and weekly variation of anthropogenic heat emissions in a tropical city, Singapore. *Atmos. Environ.* 46, 92–103.
- Sailor, D.J., 2011. A review of methods for estimating anthropogenic heat and moisture emissions in the urban environment. *Int. J. Climatol.* 31, 189–199.
- Sailor, D.J., Lu, L., 2004. A top-down methodology for developing diurnal and seasonal anthropogenic heating profiles for urban areas. *Atmos. Environ.* 38, 2737–2748.
- Sailor, D.J., Brooks, A., Hart, M., Heiple, S., 2007. A bottom-up approach for estimating latent and sensible heat emissions from anthropogenic sources. In: 7th Symposium on the Urban Environment, San Diego.
- Sailor, D.J., Georgescu, M., Milne, J.M., Hart, M.A., 2015. Development of a national anthropogenic heating database with an extrapolation for international cities. *Atmos. Environ.* 118, 7–18.
- Seto, C.K., Shalal, S., 2014. Human settlements, infrastructure and spatial planning. In: *Climate Change 2014: Mitigation of Climate Change*, IPCC Working Group III Contribution to the Fifth Assessment Report of the Intergovernmental Panel on Climate Change. Cambridge University Press, pp. 923–1000.
- Smith, C., Lindley, S., Levermore, G., 2009. Estimating spatial and temporal patterns of urban anthropogenic heat fluxes for UK cities: the case of Manchester. *Theor. Appl. Climatol.* 98, 19–35.
- United States Department of Transportation, 2011. *Annual Vehicle Distance Traveled in Miles and Related Data 2010 by Highway Category and Vehicle Type*. <http://www.fhwa.dot.gov/policyinformation/statistics/2010/pdf/vm1.pdf>. (Accessed 3 December 2016).
- United States Energy Information Administration, 2014. *Petroleum & Other Liquids: Gasoline and Diesel Fuel Update*. In: http://www.eia.gov/petroleum/gasdiesel/diesel_proc-methods.cfm. (Accessed 3 December 2016).
- U.S. Department of Energy, 2011. <https://energy.gov/> (accessed 08.01.2017).
- Valipour, M., 2016. Variations of land use and irrigation for next decades under different scenarios. *Irriga* 1, 262–288.
- Valipour, M., 2017. Global experience on irrigation management under different scenarios. *J. Water Land Dev.* 32, 95–102.
- Wang, H., Chen, Q., 2014. Impact of climate change heating and cooling energy use in Buildings in the United States. *Energ. Build.* 82, 428–436.
- Weng, Q., 2015. *Remote Sensing of Impervious Surfaces in Tropical and Subtropical Areas*. CRC Press, Boca Raton, FL.
- Wong, M.S., Yang, J., Nichol, J., Weng, Q., Menenti, M., Chan, P., 2015. Modeling of anthropogenic heat flux using HJ-1B Chinese small satellite image: a study of heterogeneous urbanized areas in Hong Kong. *IEEE. Geosci. Remote. S* 12, 1466–1470.
- Xu, W., Wooster, M.J., Grimmond, C.S.B., 2008. Modeling of urban sensible heat flux at multiple spatial scales: a demonstration using airborne hyperspectral imagery of Shanghai and a temperature-emissivity separation approach. *Proc. Spie* 112, 3493–3510.
- Yang, W., Chen, B., Cui, X., 2014. High-resolution mapping of anthropogenic heat in China from 1992 to 2010. *Int. J. Environ. Res. S. PU* 11, 4066–4077.
- Yannopoulos, S.I., Lyberatos, G., Theodossiou, N., Li, W., Valipour, M., Tamburrino, A., Angelakis, A.N., 2015. Evolution of water lifting devices (pumps) over the centuries worldwide. *Water-SUI* 7, 5031–5060.
- Zhou, Y., Weng, Q., Gurney, K.R., Shuai, Y., Hu, X., 2012. Estimation of the relationship between remotely sensed anthropogenic heat discharge and building energy use. *ISPRS. J. Photogramm.* 67, 65–72.

APPENDIX B: FULL ARTICLE OF PUBLICATION (ZHENG & WENG, 2019)



RightsLink®

Home

Create Account

Help



Title: Modeling the effect of climate change on building energy demand in Los Angeles county by using a GIS-based high spatial- and temporal-resolution approach

Author: Yuanfan Zheng, Qihao Weng

Publication: Energy

Publisher: Elsevier

Date: 1 June 2019

© 2019 Elsevier Ltd. All rights reserved.

LOGIN

If you're a **copyright.com user**, you can login to RightsLink using your copyright.com credentials.

Already a **RightsLink user** or want to [learn more?](#)

Please note that, as the author of this Elsevier article, you retain the right to include it in a thesis or dissertation, provided it is not published commercially. Permission is not required, but please ensure that you reference the journal as the original source. For more information on this and on your other retained rights, please visit: <https://www.elsevier.com/about/our-business/policies/copyright#Author-rights>



Contents lists available at ScienceDirect

Energy

journal homepage: www.elsevier.com/locate/energy

Modeling the effect of climate change on building energy demand in Los Angeles county by using a GIS-based high spatial- and temporal-resolution approach

Yuanfan Zheng, Qihao Weng*

Center for Urban and Environmental Change, Department of Earth and Environmental Systems, Indiana State University, Terre Haute, IN, 47802, USA



ARTICLE INFO

Article history:

Received 1 October 2018
 Received in revised form
 14 February 2019
 Accepted 8 April 2019
 Available online 9 April 2019

Keywords:

Buildings
 Energy demand
 Climate change
 High resolution modeling
 Urban sustainability
 Los Angeles

ABSTRACT

Climate change affects the demands for heating and cooling in buildings. This study proposed a GIS-based approach to combine climate modeling, building energy simulation, and inventory of building characteristics to quantify climate change's effect on building energy demand in Los Angeles, California. The impact was assessed by comparing building energy demands under current and future climate conditions through two metrics: relative change (RC) and absolute difference (AD), in annual, monthly, and diurnal scales under A1F1 and A2 emission scenarios. A spatial analysis was performed to assess neighborhoods vulnerable to climate change. Results suggest that most building types showed an apparent increase of energy demands under both scenarios. The increase of cooling energy demand resulted in great changes in RC and AD. Larger changes were observed at finer time scales. The energy demand for buildings increased from April to October, but decreased from November to March. The largest positive AD of total energy for all building types occurred in August, ranging 1.8–30.9 MJ/sqm, but the characteristics of diurnal AD varied with building types. Areas with dense tall commercial buildings would foresee the largest increase in energy demand. Our approach can foresee the sensitivity of building energy demands at different spatio-temporal scales.

© 2019 Elsevier Ltd. All rights reserved.

1. Introduction

Energy consumption in commercial and residential buildings accounts for 41% of U.S. primary energy consumption in 2010, and about 50% of the building energy consumption is for space heating and cooling [1,2]. Climate change will affect the energy system in a number of ways, one of which is through changes in demands for heating and cooling in buildings [3–5]. Tropical, sub-tropical, and some mid-latitude cities will expect different levels of increase in annual building energy usage, as the increase of cooling energy consumption cannot be offset by the decrease of heating energy consumption. The increase of annual energy usage in these cities will cause more carbon emissions, as coal and natural gas are still the major resources to produce electricity that used for cooling in buildings. Since buildings account for the major parts of a city's energy consumption, it is vital to assess this sector fully to develop measures and methods towards urban sustainability [6,7],

especially under the context of global warming.

In developing urban sustainability strategies, policy-makers need to consider a more sustainable way of building energy supply and consumption. These may include the efforts to transfer building energy sources from traditional fossil fuels to renewable energy sources [8–10], increasing the efficiency of energy transport ([11,43], and advancing the energy saving ability in new and existing buildings [12–14]. For example, some studies analyzed the potential to enhance the solar energy utilization by design photovoltaic (PV) roofs [9], combine PV panel with green roofs [8], and analysis 3D solar potential for individual building. Other studies discussed the way to mitigate the increasing energy demand under climate change. Sathaye et al. [11] studied the climate change impacts on California's energy infrastructure and transmission line carrying capacity. Herrera-Gomez et al. [13], conducted a case study in Mediterranean climate to discuss the role of green roofs in climate change mitigation. Tang and Qu [14] addresses the similar research question, but in cold climates. Dimond and Webb [12] compared the green roof with solar panel system for sustainable roof selection and suggested the decision should be made by fitting the type and scale of project goals. The Previous researchers have

* Corresponding author.

E-mail address: qweng@indstate.edu (Q. Weng).

applied different approaches to study the impact of climate change on building energy demand, given that this impact can be affected by many environmental and social-economic factors, such as current local climate conditions, function of the city, economic status, population density, and building thermal characteristics. Approaches used in the existing studies can be grouped into two categories: the top-down and bottom-up strategies. The top down strategy focuses on the broader spatial (global, national, and state levels) and temporal scales (annual), which compare the climate change's impact on heating and cooling energy across different states and countries. There are two types of widely used approaches in the top-down strategy: observation-based regression/prediction [15,43,4,11]; and global/regional energy modeling [16–18]. The observation-based approach uses the historical relationship of energy consumption and climate data to predict future energy consumption under a changing climate. Although this approach makes prediction based on the reference data, resolution of the output is determined by the resolution of input historical data and the accuracy of the estimation depends on the quality of the selected regression model [1]. Moreover, this approach ignores the effect of the changing building technologies, which may play an important role in energy consumption change. The global/regional energy modeling uses a numerical model to estimate the nation/state level building energy consumption by combining building technologies, policy, economy, population growth, and climate. The impact of global warming on building energy consumption is based on simulation of different IPCC scenarios. For example, Zhou et al. [17] presented a detailed building energy model with U.S. state-level representation, nested in an integrated assessment framework of the Global Change Assessment Model (GCAM). They revealed the spatially heterogeneity of global warming' impact on heating and cooling energy and fuels uses in building sector across 50 states in the United States.

The bottom-up strategy, on the other hand, focuses on finer spatial (district, neighborhood, and individual building) and temporal (hourly) scales [1,3,19–26]. This strategy typically simulates the future energy demands for individual buildings based on the detailed information in building or building prototype and the projected future climate. The simulated energy demands are then compared with the current energy demands to quantify the differences. Vidrih and Medved [25] simulated the indoor climate and energy consumption for heating and cooling of four buildings with different cooling techniques to quantify the effect of climate change on energy demands of buildings. They concluded that it is crucial to include free-cooling techniques in the planning process of the buildings, as they are more efficient in easing the overheating problem and reduce the cooling energy demand. Berger et al. [20] calculated and compared heating and cooling demands from nine selected office buildings under current and future conditions in Vienna, Australia. They discovered distinct differences in energy performance of buildings from different periods of construction, which adopted various building technologies. Andri et al. [19] compared the energy simulation results from a district of buildings in Lisbon, Portugal, from 2010 to 2050, and discovered heat demand density could decrease in the range of 22.3–52.4% in 2050. Huang and Gurney [1] used the building prototypes developed by U.S. Department of Energy (DOE), which included 18 types and 3 age groups, and the weather data from different climate zones to assess the variations of climate change's impact on different spatial and temporal scales. Their results suggested that the variation of impact within climate zones can be larger than the variation between climate zones, and that the potential bias may be substantial when estimating climate-zone scale changes with a small number of representative buildings. Shen [24] downscaled the future climate data into hourly scale using a “morphing” method to

predict future energy use for residential buildings in the United States.

In order to develop a sustainable city under the context of climate change, policy makers may need information at different spatial scales. Existing studies either combined climate change modeling with the broad scales (annual and state level) inventory data of buildings and social-economic activities or used representative building prototypes to assess the climate change's effect in different climate zones. However, cities, especially megacities, are mixed with different types of buildings, which were constructed in different periods of time, and with different technologies, functions, and schedules. Therefore, to the city government the sustainable development goals can be different even among neighborhoods. In developing “green and sustainable” communities, they would need disaggregated data to understand the current and future energy demands at local scales and choose appropriate measures that are targeted to specific locations. Clearly, the approaches in the existing studies cannot help them to achieve these goals. In other words, an approach essential to the city government which assesses the impact of climate change on building energy demand at fine scales (sub-city level) are lacking.

The GIS modeling technique has strong ability to capture, manipulate, analyze, and manage large amount of inventory data with geographic attributes at a high spatial and temporal resolution. This study proposed a GIS-based approach to combine climate change modeling, building energy simulation, and fine-scale (individual building level) inventory data of building characteristics to quantify the climate change's effect on building energy demand, which is the projected need of energy services, at the sub-city scale in Los Angeles, California, United States. Specific research questions to be addressed in this research are: 1) What changes in annual building energy demand of buildings would occur by 2050 by our prediction? 2) Do the trends of change remain the same when they are examined at the finer spatial and temporal scales? And 3) Which areas in the city are more vulnerable to climate change and what are the driving forces? It is expected through this research a useful approach can be developed for the city government to work towards a sustainable city through tailoring adaption and mitigation strategies for buildings in different districts.

2. Methodology

2.1. Study area

This study selected Los Angeles County, California, USA, as the study area. The county has an estimated population of 10,163,507 in July 2017 according to the U.S. Census, making it the most populous county in the nation. Los Angeles County occupies three climate zones according to the Koppen climate classification. The coastal area has “Warm Summer Mediterranean” (Csb) climate with dry and warm summers and moist winters. Its inland area, on the other hand, has the “Hot Summer Mediterranean” (Csa) climate with hotter summer compared to the coastal area. Its northern part has the “Cold Semi-Arid” (Bsk) climate, which has warm to hot summers and cold winters. The micro-climate, caused by topography, makes the county special as there is a large variation in temperature between nearby areas.

The 2010 inventory data provided by Los Angeles Energy Atlas shows that the building sector emitted the largest amount of greenhouse gases, which accounted for 39.2% of the annual total greenhouse gases emission (Table 1). Therefore, coping with the energy consumption in buildings under the context of climate change is important for developing sustainable urban environment in the Los Angeles County.

Table 1
Greenhouse gas (GHG) emissions in Los Angeles County by sector.

Sector	Emissions (MT CO ₂ e)	Percent of Inventory
Building Energy	38,900,762	39.2%
On-Road Transportation	33,226,317	33.5%
Stationary Sources	19,516,169	19.7%
Solid Waste	4,327,123	4.4%
Water Conveyance	1,117,283	1.1%
Ports	1,059,131	1.1%
Off-Road Transportation	515,044	0.5%
Wastewater Treatment	443,832	0.4%
Agriculture	26,105	0.0%
Los Angeles Worlds Airport	2760	0.0%
Total	99,134,526	

Source: <http://www.energyatlas.ucla.edu/strategies/>

2.2. Simulation model

EnergyPlus, a well-known building energy simulation tool developed by the U.S. Department of Energy (DOE), was used to simulate building energy consumption. It has been tested and validated for the ANSI/ASHRAE standards, and is widely used by engineers and scientists to model building energy consumption [27]. It requires hourly weather data and building characteristics associated with specific building prototypes to derive hourly energy simulations.

In order to test the climate change's impact on building energy demand, this study simulated the building energy consumption for all buildings using both the current and the future hourly weather data. The current hourly weather data used in EnergyPlus was retrieved from the third (and the latest) Typical Meteorological Year (TMY3) collection. Each TMY3 file contained 8760 hourly record of climate for the specific location, which was developed based on the 1991–2005 weather data. Los Angeles County consisted of seven weather zones in the TMY3 dataset (Fig. 1), including: Burbank-Glendale, Los Angeles International airport, Long Beach, Van Nuys, Lancaster, Palmdale, and Point Mugu. Each of them contained different hourly weather data collected from 1991 to 2005. Fig. 2 shows the current average monthly temperature (°C) in seven TMY3 locations in Los Angeles County. Long Beach, Los Angeles International Airport, and Point Mugu weather zones had a

relatively smaller range of monthly temperature as they are located in the coastal areas and have the “Warm Summer Mediterranean” (Csb) climate. Lancaster and Palmdale weather zones had the highest temperature during summer months but lowest temperature during the winter months due to their “Cold Semi-Arid” climate. The Burbank-Glendale and Van Nuys weather zones, with the “Hot Summer Mediterranean” (Csa) climate, had similar temperature during the wintertime as the coastal areas but higher temperature during the summer months.

The future hourly weather data was projected by using the HadCM3. Among all the future weather data construction models, the HadCM3 has a relatively smaller grid spacing, which means the simulation resolution is higher than other models and results in higher precision [24]. This model coupled the atmospheric model HadAM3, with a horizontal resolution of 2.5° latitude by 3.75° longitude, and oceanic model HadOM3 with horizontal resolution of 1.25° by 1.25°. It provides monthly change in dry-bulb temperature, diurnal temperature variation, relative humidity, wind speed, and solar radiation, which have a major impact on the building heating and cooling load.

There are various carbon dioxide emission scenarios projected by IPCC http://www.ipcc-data.org/sres/hadcm3_download.html, which are associated with the likely happened global development directions by the year of 2100, including technologies, climate and energy policies, and social-economic developments. Among all these scenarios, three of them are widely used by the current literature: A1 (high emission), A2 (medium emission), and B1 (low emission). The A1 scenario describes a future world of very rapid economic growth, global population that peaks in mid-century and then declines, and the rapid introduction of new and more efficient technologies. The A1 scenario family can be further developed into three groups that describe alternative directions of technological change in the energy system, and is distinguished by their technological emphasis: fossil intensive (A1FI), non-fossil energy sources (A1T), and a balance across all sources (A1B). The A2 (medium emission) scenario family describes a very heterogeneous world. Fertility patterns across regions converge very slowly, which results in continuously increasing global population. Economic development is primarily regionally oriented and per capita economic growth and technological change are more fragmented and

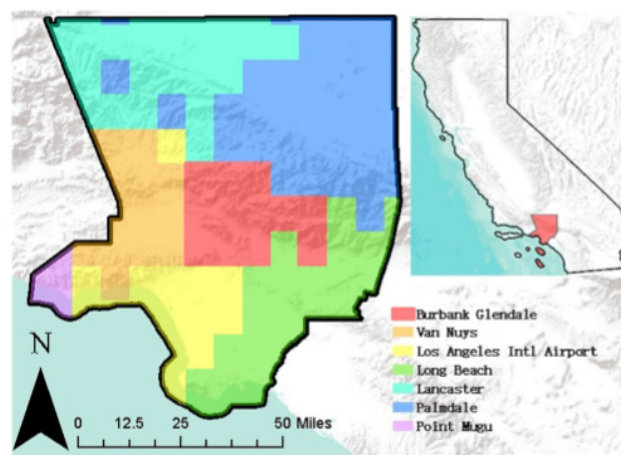


Fig. 1. TMY3 weather zones in Los Angeles County.

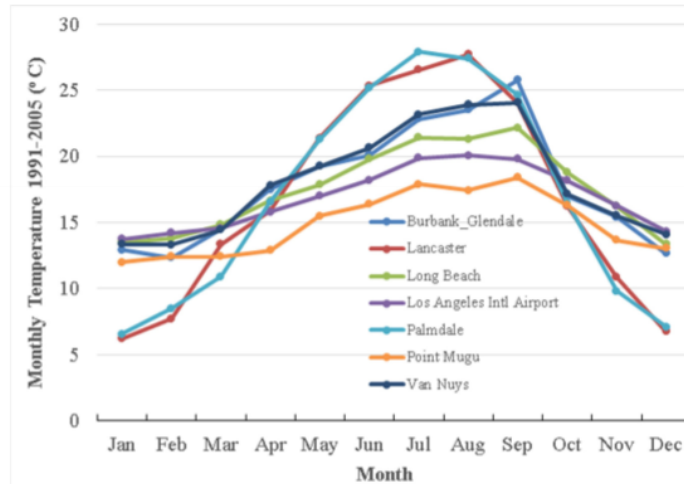


Fig. 2. Current monthly temperature (°C) in seven TMY3 locations in Los Angeles County.

slower than in other scenarios. The B1 (low emission) scenario family describes a convergent world with the same global population that peaks in mid-century and declines thereafter, as in A1, but with rapid changes in economic structures toward a service and information economy, with reductions in material intensity, and the introduction of clean and resource-efficient technologies.

This study chose A1F1 (high emission) and A2 (medium emission) for simulation. The reason is A2 scenario fits the current energy policies and emphasized the regional differences, which is suitable for the County/City level examination. The A1F1 scenario, on the other hand, represented the worst case and it can be used for the hazard assessment purpose. The low emission scenario (B1) was not chosen because it is assuming the world develops equally with the evenly distribution population, rapid economic structure change, and adoption of clean resource-efficient technologies, which is over optimistic according to the current trend and unlikely to happen in the near future. In order to create the hourly data for the year of 2050, Climate Change World Weather File Generator (CCWorldWeatherGen) tool developed by Sustainable Energy Research Group (University of Southampton) was used. This tool used hourly historical weather data (TMY2 and TMY3) as a primary input and applied the HadCM3 model to construct the future hourly data. This tool has been widely adopted by a large number of researchers [19,24,28,29,44,30]; in recent years. Since the HadCM3 model only provides monthly weather variation data, which is insufficient for hourly energy simulation, the CCWorldWeatherGen tool applies a morphing method to down-scale the monthly weather data to hourly weather data. The algorithm to calculate future hourly weather data uses the following equation:

$$X = X_0 + \Delta x_m + a_m(X_0 - (X_0)_m)$$

where $x0$ is hourly weather data from the existing historical data (TMY2 or TMY3), Δx_m the predicted monthly mean change obtained from HadCM3, a_m is the stretching factor calculated based on the changes of monthly mean value of a specific variable from future weather files relative to the existing reference weather file, and $(x0)_m$ is the monthly mean of current weather data. Since the CCWorldWeatherGen tool can only simulate the future weather

data under A2 carbon emission scenario, a pattern scaling method, which developed by the Finnish Environment Institute [31], was adopted to calculate the future weather data under A1F1 carbon emission scenario. This pattern scaling method can provide the magnitude for the future temperature changes under different IPCC scenarios based on a series of factors, which also varies with locations in the world. The idea in this technique is that the geographical pattern of the response is assumed independent of the forcing, while the amplitude of the response at each location is linearly proportional to the global mean change in the weather data [31]. For example, after the temperature response to forcing scenario A2 has been calculated by HadCM3 model, the response to scenario A1F1 can be calculated as follows:

$$\Delta T_{A1F1,s} = (\Delta T_{A1F1} / \Delta T_{A2}) \Delta T_{A2,g}$$

Where $(\Delta T_{A1F1} / \Delta T_{A2})$ is the ratio between global mean change in air temperature under A1F1 and A2 scenarios. $\Delta T_{A2,g}$ is the monthly regional change of air temperature under A2 scenario, which calculated by HadCM3 model. After the monthly weather data change under A1F1 scenario was calculated, the morphing method was applied again to down-scale them into hourly weather data. Fig. 3 presents the result of annual average hourly air temperature in 2050 in Los Angeles County under A1F1 and A2 scenarios. The values of average temperature were expected to rise by 2.7°C and 2°C at the mid-century compared to that of current temperature (1991–2005) under the A1F1 and A2 scenarios, respectively.

2.3. Building prototypes

Sixteen commercial building prototypes, developed by U.S. DOE, were used for the simulation. The DOE created these building prototypes based on Commercial Buildings Energy Consumption Survey (CBECS) data by the U.S. Energy Information Administration (EIA), and provided information on building characteristics and three age categories: pre-1980, post-1980, and new-2004. The age categories reflected differences in the technologies of building insulation, envelope, heating, ventilation, and cooling (HVAC)

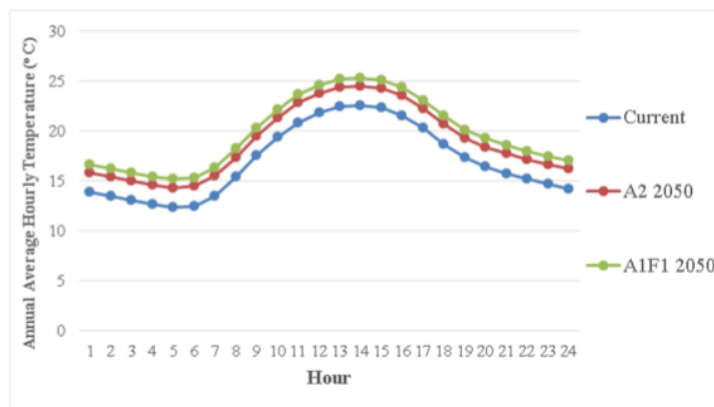


Fig. 3. Current and future hourly temperature ($^{\circ}$ C) in Los Angeles County in 2050 under A1F1 and A2 scenarios.

systems, lighting, and equipment for each type of building, which led to different abilities in energy consumption under the same outdoor environment. Buildings with newer technologies had more energy efficient equipment, better insulation to mitigate the impact of non-optimal outside temperature, smaller energy intensity of lighting, and more energy-efficient HVAC system [1,32,33]. Two prototypes of residential buildings, i.e., multi-family low-rise apartment buildings and single-family detached houses, were developed by DOE in 2009 based on building codes specified in the International Energy Conservation Code (IECC) and Residential Energy Consumption Survey (RECS). The Hourly Building Energy Use Intensity (EUI), which is the energy used per unit floor area – was simulated using the EnergyPlus taken building prototypes and TMY3 hourly local climate data in Los Angeles County as inputs.

In order to simulate the 365 day hourly energy use for individual building in Los Angeles County, a building energy modeling method was used. First, datasets included Los Angeles Countywide building outlines and Los Angeles County Parcel shapefiles were acquired. Building outlines were captured from stereo imagery as part of the LARIAC4 (2014) imagery acquisition. They provided information on building height, area, types, and year of construction. The Los Angeles County parcel data contained information on land use types, which were collected from Los Angeles County Enterprise GIS website. Second, the building shapefile and Los Angeles County parcel data were overlaid to define the typology for each building, which determined by matching with the closet prototype in CBECs or RECS based on building types, land use types, and ages.

The energy consumption for buildings were estimated based on a modeling method adopted in Zheng and Weng [33]; which combined building floor area and the number of floors in each building from GIS-based building outlines, building prototype extracted from Los Angeles County Assessor's parcel data, and energy use intensity for each building prototype simulated in EnergyPlus. The energy consumption for an individual building (BE) i within a particular hour h can be calculated by the following equation:

$$BE_{hour(i, h)} = EUI_{i, h} \times A_{building(i)} \times FN_{building(i)}$$

where $A_{building(i)}$ is the footprint area of building i , $FN_{building(i)}$ is the floor number, which was estimated based on building height. The daily energy consumption of building i for day d was calculated as follows:

$$BE_{day(i, d)} = \sum_{h=1}^{24} BE_{hour(i, h)}$$

The building energy consumption within a season s was calculated as follows:

$$BE_{season(s)} = \sum_{d=1}^{t1} BE_{workday(h, d, s)} + \sum_{d=1}^{t2} BE_{non-workday(h, d, s)}$$

where $BE_{workday(i, d, s)}$ and $BE_{non-workday(i, d, s)}$ are the EUI at a particular hour h within the day d during the season s in workday and non-workdays (weekends and holidays), respectively; $t1$ and $t2$ are the number of workdays and non-workdays within season s , respectively. The annual building energy consumption for sector a was calculated as:

$$BE_{annual(a)} = \sum_{k=1}^4 BE_{season(s)}$$

Energy use at the broader spatial scales can also be estimated at a given time period (hourly, daily, seasonally, and annually) by aggregating the energy use from individual building within the boundaries of neighborhood, city, and county GIS shapefile layers. In this study, we assumed that the building stock structure in Los Angeles County remained unchanged throughout the simulation period. In this study, we assumed that the building stock structure in Los Angeles County remained unchanged throughout the simulation period.

2.4. Calibration to reference data

Although the simulated building energy consumption contained the hourly energy usage for individual building, discrepancies existed between the simulated results and the actual energy consumption. The discrepancies between the EnergyPlus model output and the actual energy consumption can be caused by many factors. First, the simulation model used in EnergyPlus cannot account for all the factors that determined actual building energy consumption, such as the occupancy status and behaviors. Second, the simulated results only represented the end-use energy consumption, which ignored the energy loss during transport and production. Finally,

the building prototypes were developed based on the most common building technologies/characteristics in the survey data in Los Angeles County, which may not represent all the buildings in reality. Therefore, the calibration was necessary and the method used by Zheng and Weng [33]; was adopted in this research to calibrate the simulated current building energy consumption. The referenced data were obtained from California Energy Commission [34] (<http://ecdms.energy.ca.gov/electbycounty.aspx>) and LA Energy Atlas [35] (<http://www.energyatlas.ucla.edu/>). The Energy Atlas provided detailed historical annual energy consumption data from all building energy sectors, including commercial, residential and industrial sector at the neighborhood level. The simulated energy consumption from all buildings within each neighborhood and each sector were aggregated to compare with the corresponding sector in each neighborhood in the referenced data. Compared to the existing study that calibrated building energy consumption at a coarser scale, such as census division [1], the neighborhood level reference data in our study allowed us to address the regional variation of energy consumption patterns in both commercial and residential sectors, which was essential for the purpose of a local-scale study. Moreover, it can overcome the limitation on the spatial resolution, which was caused by the spatial resolution of weather data (TMY3 data). Fig. 4 presents the calibrated annual building energy consumption intensity for 16 types of commercial buildings in Los Angeles County, which was the simulation result based on the historical TMY3 data (1991–2005). The two types of restaurants (full service and quick service) consumed the largest amount of energy per square meter in the entire year. The ratio between the before- and after-calibrated building energy consumption results was computed to calibrate the simulated future building energy consumption under the two emission scenarios (A1F1 and A2). After the calibration, potential bias and uncertainty in the simulated results can be corrected at the scale of neighborhood while the differences among individual sectors and buildings within the neighborhood at a given time period can still be reflected, which is essential for city government to work towards a sustainable city through tailoring adaption and mitigation strategies at the regional level.

3. Results

The impact of climate change on buildings can be influenced by multiple factors. The analysis of each factor was given for seven TMY weather zones, three building technologies, eighteen building prototypes, and two IPCC carbon dioxide emission scenarios. This section analyzes the climate impact in three different temporal scales (annual, monthly, and hourly) and assesses changes in the spatial pattern of the building energy demand across the entire Los

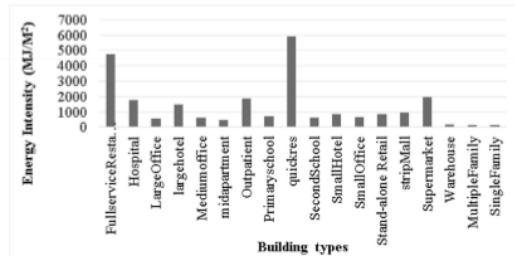


Fig. 4. The calibrated annual building energy consumption intensity for 16 types of commercial buildings in Los Angeles County. Simulation was based on the historical TMY3 data (1991–2005).

Angeles County using the metric of Relative Change (RC) and Absolute Difference (AD). The RC can be calculated by the following formula:

$$RC = (Ef - Ep)/Ep*100\%$$

It shows the difference in energy consumption between the calibrated current energy consumption (Ep) and projected future energy consumption (Ef). The AD represents the difference in energy consumption intensity, which can be calculated as follows:

$$AD = (Ef - Ep)/FA$$

where FA is the building floor area, which is the product of building floor number and area.

3.1. Impact of climate change on building energy demand at different temporal scales

3.1.1. Variation at annual scale

Variation across building types, ages, and weather zones at annual scale was first analyzed. Tables 2 and 3 show the annual average building energy demand, as measured by RC and AD, between 2050 and the present time (1991–2005) in Los Angeles County for the commercial and residential buildings. The majority of building types showed an apparent increase in energy demand under both emission scenarios, and the energy demand increase was higher with the high emission scenario. There existed a large variation regarding to energy consumption change across different types of buildings. For example, AD value ranged from –28.7 MJ/sqm (warehouse) to 68.2 MJ/sqm (Outpatient), and the RC value ranged from –11.8% (warehouse) to 7.9% (medium office) under the A1F1 scenario. Due to the higher energy consumption intensity under current climate, the majority of commercial buildings showed higher AD than two types of residential houses. Besides of the Outpatient buildings, all types of hotel, office, and school buildings presented higher AD than the rest of building categories, because of the increases in their annual cooling energy consumptions are much larger than the decreases in their heating energy consumptions. Although the two types of residential houses showed less AD increases in total energy, their RC increases were

Table 2
Relative change (%) and absolute difference (MJ/Sqm) in average annual building energy demand between 2050 and the present time (1991–2005) in Los Angeles County under A1F1 emission scenario.

Building Type	Total		Cooling	Heating
	AD	RC	AD	AD
Commercial				
Full Restaurant	1.3	0.1%	166.8	-169.2
Hospital	14	1.0%	44.6	-38
Large Hotel	51.5	3.5%	74.1	-30.6
Large Office	24.4	4.8%	29.5	-12.8
Mid-rise Apartment	30.45	4.5%	49.8	-25.15
Medium Office	46.9	7.9%	55	-12.3
Outpatient	68.2	4.0%	102.9	-36.3
Primary School	31.5	4.8%	51.5	-24.6
Quick Restaurant	18.3	0.3%	151	-142.9
Secondary School	36.7	6.2%	68	-38.9
Small Hotel	40.7	5.2%	45.8	-9.2
Small Office	31	4.9%	43.3	-13.8
Stand-alone Retail	6.8	1.0%	54.6	-47.5
Strip Mall	4.1	0.4%	57.7	-53.2
Supermarket	-18.1	-0.9%	34.7	-114.1
Warehouse	-28.7	-11.8%	5.9	-34.1
Residential: Multiple Family	7.2	4.1%	10.9	-5.9
Residential: Single Family	2.8	2.3%	10.4	-9.5

Table 3
Relative change (%) and absolute difference (MJ/Sqm) in average annual building energy demand between 2050 and the present time (1991–2005) in Los Angeles County under A2 emission scenario.

Building Type	Total		Cooling		Heating	
	AC	RC	AC	RC	AC	RC
Commercial						
Full Restaurant	-20.4	-0.4%	119.7		-137.4	
Hospital	8.6	0.5%	31.2		-29.3	
Large Hotel	34.4	2.2%	53.4		-24.9	
Large Office	16.7	3.1%	21.6		-10.5	
Mid-rise Apartment	20.75	3.0%	36.05		-19.3	
Medium Office	32.9	5.5%	40.9		-9.3	
Outpatient	53.1	3.1%	75.8		-25.3	
Primary School	20.4	3.1%	37.5		-20	
Quick Restaurant	-6.9	0.0%	107.6		-116.4	
Secondary School	21.7	3.7%	48.8		-31.6	
Small Hotel	28.5	3.5%	33		-7.4	
Small Office	20.7	3.4%	31.4		-11.2	
Stand-alone Retail	-0.1	0.1%	40.7		-38.5	
Strip Mall	-2.5	-0.2%	42.8		-43.1	
Supermarket	-24.1	-1.1%	25		-90.3	
Warehouse	-23.9	-9.8%	4.2		-27.4	
Residential: Multiple Family	4.8	2.7%	8.3		-4.9	
Residential: Single Family	1.3	1.1%	7.8		-7.7	

high. This high RC increase indicated that the residential houses were also sensitive to climate change.

Because of global warming, the cooling energy intensity for all types of buildings would increase under both emission scenarios, while the energy intensity for heating in all types of buildings would decrease. The change in the cooling and heating energy demand in the future showed even greater extent than the total energy demand change. The RC for cooling energy increase ranged from 5.9 MJ/sqm (warehouse) to 166.8 MJ/sqm (full service restaurant) under the A1F1 scenario. However, the dramatic changes in cooling and heating energy demand can easily be ignored due to the smaller changes in total energy demand, if no further analysis was performed. For example, under A1F1 scenario, the full-service restaurant category showed much larger AD than the hospital category in both cooling and heating energy intensity, but the increase of cooling would nearly be offset by the decrease of heating which made its total energy AD even smaller than that of the hospital. The two types of restaurants showed the largest AD in cooling and heating energy intensity among all types of buildings, which might be attributed to their large exposure to the outdoor environment and air intake in addition to the need for regulating the waste heat from cooking. According to our results, non-restaurant buildings had mechanical ventilation rates ranging

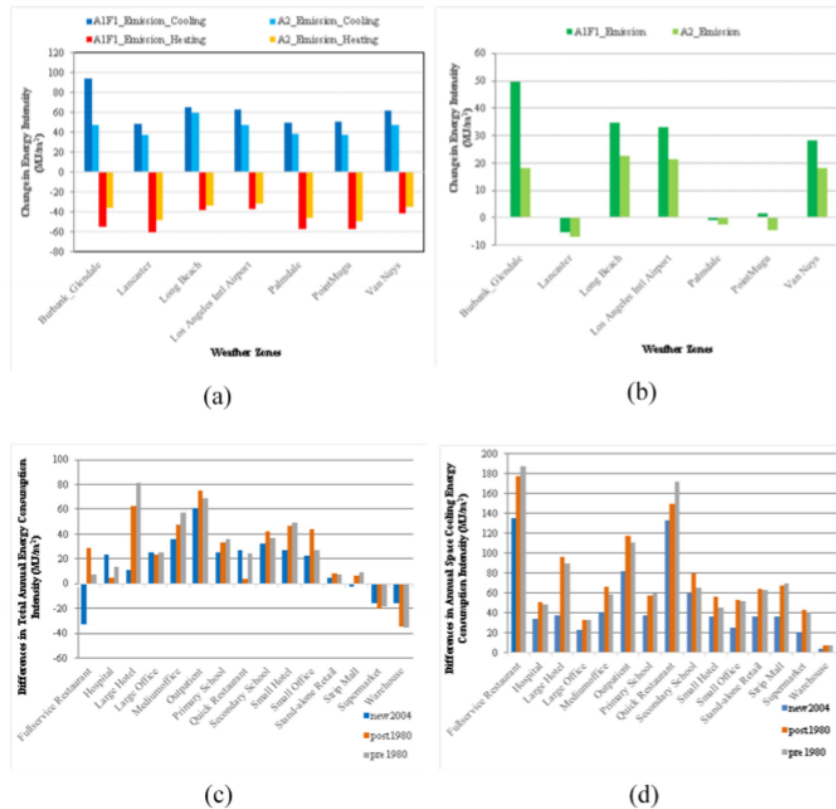


Fig. 5. Change in annual energy intensity under the two emission scenarios across different TMY3 weather zones in Los Angeles County: (a) annual energy intensity in heating and in cooling; (b) annual energy intensity consumed by buildings. Differences in total annual energy consumption intensity (c) and space cooling (d) (MJ/m²) for commercial buildings between 2050s and the 1991–2005 time period under A1F1 emission scenario.

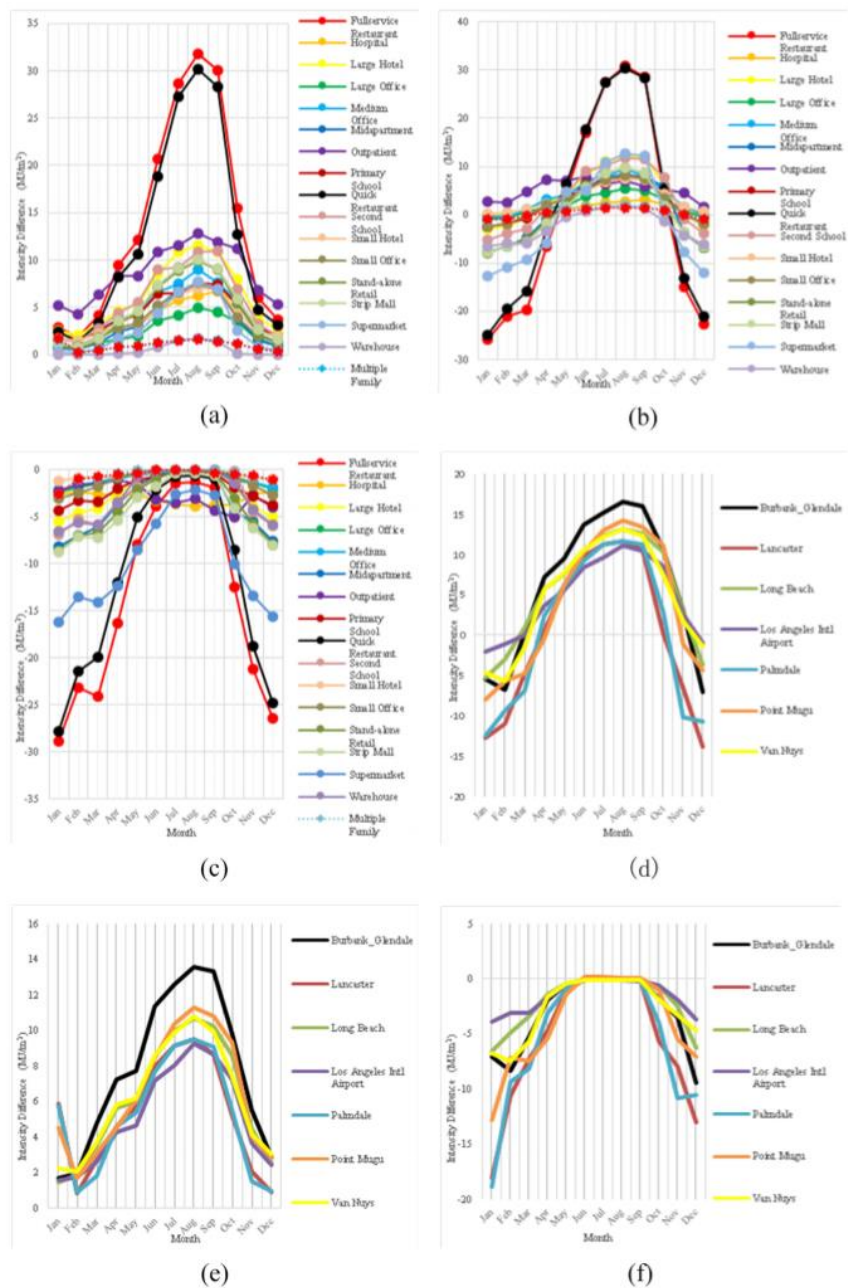


Fig. 6. Absolute difference in average monthly building energy intensity (a) total, (b) cooling, and heating (c) between 2050 and the 1991–2005 time period under the A1F1 emission scenario across building types; change in monthly energy intensity under the A1F1 emission scenarios across different TMY3 weather zones in Los Angeles County: (d) monthly total energy intensity change; (e) monthly cooling energy intensity change; and (f) monthly heating energy intensity change.

from 0.66 air changes per hour (ACH) (warehouse) to 5.51 ACH (outpatient). In comparison, the two types of restaurants had significantly higher annual average mechanical ventilation rates, which are 8.01 ACH for full-service restaurants and 9.06 ACH for quick-service restaurants, to remove the exhaust gases caused by high-intensity cooking. The warmer climate increased more ventilation energy consumption in restaurants than others in summer months. On the other hand, restaurants would experience a larger decline in heating energy demand under warmer climate because the internal heat gain through high-intensity cooking can compensate part of space heating energy in winter months. Therefore, restaurants would expect to be more sensitive to climate change. Hospitals showed the small change in cooling energy because they possessed large building internal load, such as interior equipment and lighting, which can remain constant regardless of outdoor climate change. Moreover, the strict ventilation requirements for healthcare buildings can also weaken the impact of outside temperature change [1].

Fig. 5 (a) and (b) shows the mean value of changes in energy intensity over buildings under high (A1F1) and medium (A2) emission scenarios for cooling and heating by 2050, as compared to the present time across all TMY weather zones in Los Angeles County. Due to the warmer climate in the future, the cooling energy demand within all zones would increase, while the heating energy demand would decrease. However, the extent of change varied across different weather zones. In Lancaster, Palmdale and Point Mugu, the amount of increased annual cooling energy can almost be offset by the decrease of heating energy, so no obvious change can be observed in the annual total building energy demand. But in Burbank-Glendale, Long Beach, Los Angeles International Airport, and Van Nuys, the increase of cooling energies would be much larger than the decrease in heating energy, so there would be dramatic increase in the annual total building energy demand in these weather zones.

The effect of building technologies on its energy performance was further analyzed. Fig. 5 further presented the differences in total annual energy consumption intensity (c), in space cooling (d) for commercial buildings between the year 2050 and the 1991–2005 time period under A1F1 emission scenario, which were built in three periods of time: post-2004 (new-2004), 1980 to 2004

(post-1980), and before 1980 (pre-1980). Although no substantial difference can be discovered between the pre-1980 and post-1980 buildings regarding to the energy consumption caused by global warming, it can be observed that the post-2004 buildings exhibited the smallest increase of annual total energy for the majority of building types. As Fig. 5 (d) showed, the post-2004 buildings had the smallest increase in space cooling energy demand for all types of buildings. It can be concluded that the newly constructed buildings in Los Angeles County would be less sensitive to the warmer outdoor temperature in the future. They could have the ability to maintain a comfortable indoor environment more efficiently due to their better insulation and advanced energy-saving building technologies [32], such as the installation of air conditioning systems with higher coefficient of performance (COP) to decrease the demand on energy consumption, especially electricity demand in hot summer days.

3.1.2. Variation at monthly scale

Since the impact of global warming on building energy demand may have larger variations at smaller geographical scales, this study further analyzed the impact at monthly and diurnal scales. The A1F1 scenario was assessed at smaller time scales as we want to test the vulnerability of buildings under extreme hot weathers. Although the majority of buildings had positive annual AD values, all of them had both positive and negative monthly AD values throughout the year. Moreover, all buildings showed increased cooling energy and decreased heating energy in all months (Fig. 6b and c). The largest positive AD of total energy for all buildings occurred in August (Fig. 6a), when the increase of cooling reached its peak and there was little heating demand. From April to October, the total energy demand increased because the increase of cooling energy exceeded the decreased heating energy; and from November to March, the total energy demand declined because the increase of heating demand cannot be offset by the decrease of cooling demand. The residential buildings showed less AD changes than the commercial buildings, regardless of months and energy types. The total energy AD varied from -1.09 MJ/sqm (January) to 2.02 MJ/sqm (August) for multiple-family apartments, which showed slightly larger variation than single-family houses. The commercial buildings not only showed larger monthly AD values,

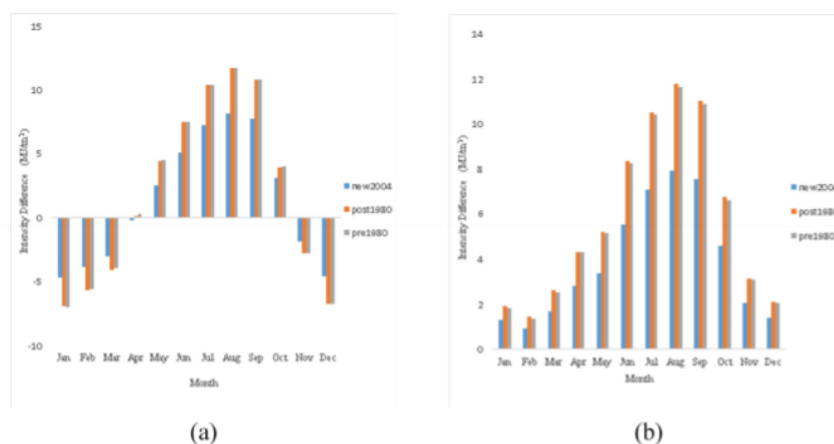
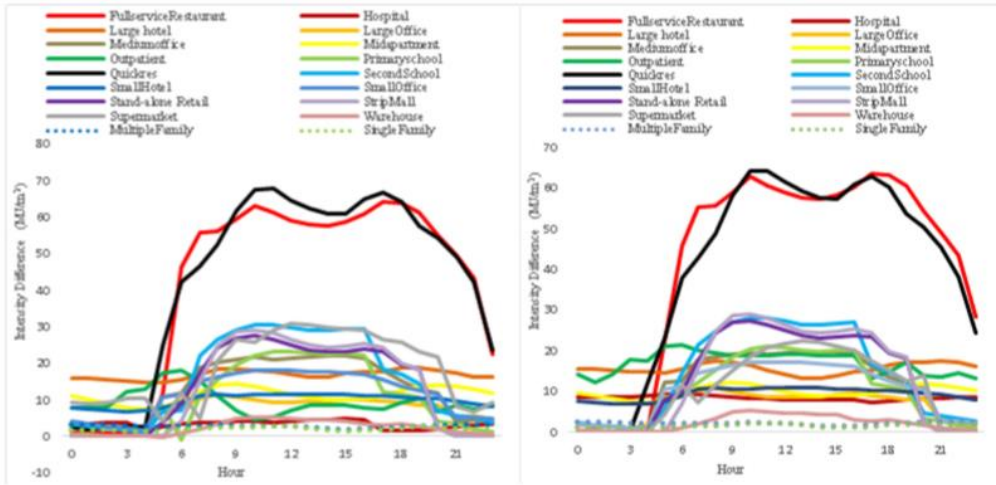
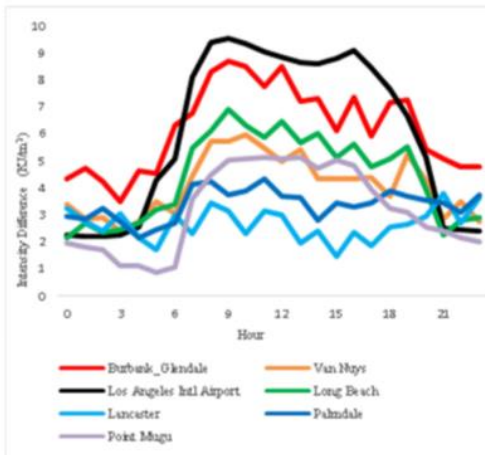


Fig. 7. Energy consumption intensity differences (MJ/m^2) by month for commercial buildings between 2050s and the 1991–2005 time period under A1F1 emission scenario. (a) Total energy consumption, (b) space cooling.

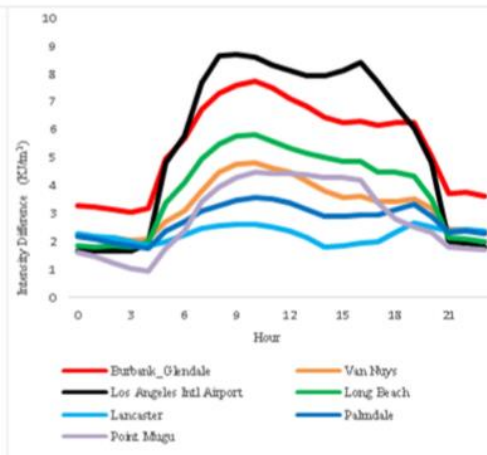


(a)

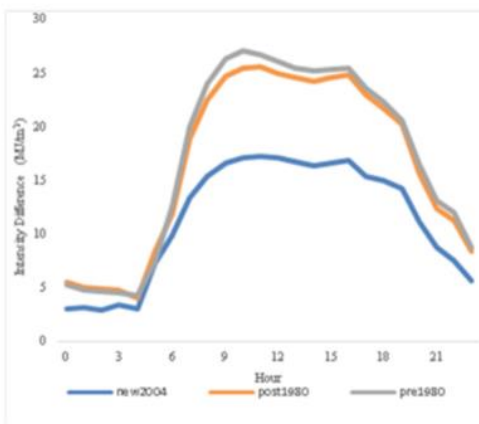
(b)



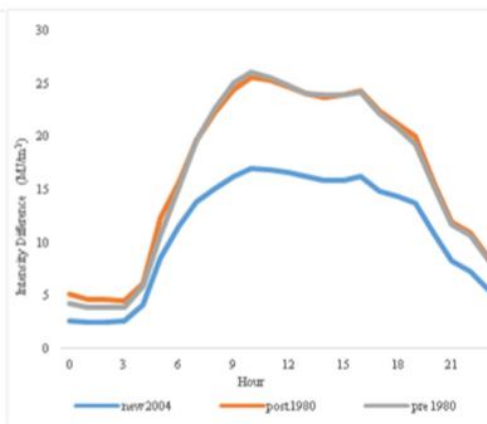
(c)



(d)



(e)



(d)

but also a greater variation among different building types. In January, the AD of total energy ranged from -25.8 MJ/sqm (full service restaurant) to 2.9 MJ/sqm (outpatient buildings), and the increase of heating energy use was the major driver. In August, as the increase of cooling energy reached its peak value in the year, the AD of total energy ranged from 1.8 MJ/sqm (warehouse) to 30.9 MJ/sqm (full service restaurant).

Fig. 6d showed the AD value of monthly energy intensity under the A1F1 emission scenarios across different TMY3 weather zones. The Burbank-Glendale weather zone presented the largest increase of total energy intensity AD from April to October among all weather zones. Because the Burbank-Glendale weather zone had the largest cooling energy increase (Fig. 6e), which caused by its basin topography, there would likely be a larger temperature increase than other weather zones. The Lancaster and Palmdale weather zones detected the largest decrease of AD for total energy from October to March because they had the largest heating energy AD decrease. It could be caused by their cold semi-arid steppe climate, which had the colder and windier winter than other weather zones. These weather zones did not have larger increase of AD for cooling. Because their average temperature in summer under the current climate is already much higher than the comfort temperature (18.3°C) (Fig. 2), they already have high cooling demand. Fig. 7 presented the total (a), space cooling (b), and space heating (c) monthly energy consumption intensity differences (MJ/sqm) between the year 2050 and the 1991–2005 time-period under A1F1 emission scenario for commercial buildings constructed in different times. The post-2004 buildings exhibited the smallest increase of cooling energy and decrease of heating energy in all months, which contributed to the least change in total energy throughout the year.

3.1.3. Variation at hourly scale

It was discovered that the largest total energy increase occurred in the summer months, especially in August. This section presented a more detailed analysis of hourly AD change across different building types, weather zones, and ages in August. The diurnal time series profiles were created to explain the hourly energy consumption change. For each specific time period, the average value of the energy consumption during the same hour in 31 days in August was used. Since there is usually little heating energy demand in August, the analysis here was based on total and cooling energy only. Fig. 8 (a) and (b) showed the average hourly building total and cooling energy intensity AD between 2050 and 1991–2005 time period under the A1F1 emission scenario across building types. Although all buildings increased total and cooling energy throughout the day, it can be observed that all commercial buildings showed a larger AD increase and a greater variation. The restaurants showed a considerably larger AD increase in total energy than others, with the maximum AD value of 67.5 KJ/sqm (quick service restaurant at 12pm), while the warehouses showed the smallest AD increase in total energy (only 5.31 KJ/sqm daily peak increase). Unlike the monthly AD changes in which all buildings had the same trend of changes in colder or warmer months, the characteristics of diurnal AD varied with types of buildings. All commercial buildings showed a larger increase of AD at daytime than at nighttime, but the time of peak AD increase in some buildings was different. The majority of commercial buildings showed highest AD increase from 9am to 5pm, but the hotel and

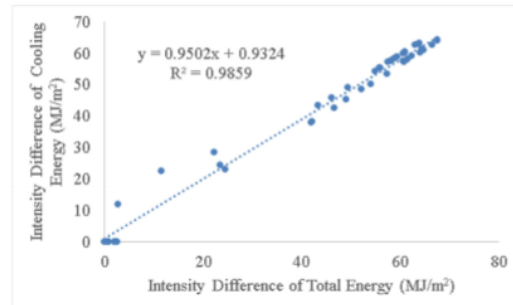


Fig. 9. Relationship between the increase of hourly cooling energy intensity difference and the increase of hourly total energy intensity difference for the restaurants in August.

residential buildings showed more increase of AD in early morning and at nighttime. It can be concluded that more human activities brought about larger increase of energy. The restaurants observed two peaks of AD increase during the daytime, corresponding to lunch and dinner time. Fig. 9 presented the relationship between the increase of hourly cooling energy AD and the increase of hourly total energy AD for the restaurants in August. The high positive correlation indicated that the cooling was the main driver for the total energy increase. Although the most increase of outdoor temperature may not correspond well with the maximum daily increase during lunch and dinner time, cooking and human metabolism produced more internal heat gain during these two periods and thus contributed to the higher cooling demand.

Fig. 8 (c) and 8 (d) showed the diurnal variation of AD in total and cooling energy intensity under the A1F1 emission scenarios across the TMY3 weather zones in Los Angeles. The variation of diurnal cooling energy was much smoother than that of the total energy, as the total energy demand was affected by additional factors in addition to the diurnal temperature variation. It can be observed that the diurnal variation of total and cooling energy AD in the Los Angeles International Airport was much closer to that of the commercial buildings. This was surprising because the Los Angeles International Airport weather zone possessed the highest percentage of commercial building floor area (30.82%) (Table 4). The diurnal variation patterns of total and cooling energy AD in Lancaster weather zone appeared similar to that of the residential buildings because it had the highest percentage of residential building floor area (91.10%). Fig. 8 (e) and (f) presented the total and space cooling diurnal energy consumption AD (KJ/sqm) between 2050s and the 1991–2005 time period in August for three age groups of commercial buildings under A1F1 emission scenario. The post-2004 buildings again displayed a higher level of energy efficiency for all time periods throughout the day.

3.2. Spatial variations of energy demand change at neighborhood scale

This section presented the spatial variation of energy demand change in 2050 due to climate change at the neighborhood scale. Fig. 10 presents the spatial variation of total and cooling energy

Fig. 8. Diurnal change in absolute difference of average building energy intensity between 2050 and 1991–2005 time period under the A1F1 emission scenario across building types in Los Angeles in August: (a) total energy, and (b) cooling energy; change in energy intensity under the A1F1 emission scenario across different TMY3 weather zones in Los Angeles in August: (c) diurnal total energy intensity change and (d) diurnal cooling energy intensity change; the diurnal energy consumption intensity differences (KJ/m²) for commercial buildings between 2050s and the 1991–2005 time period under A1F1 emission scenario across different building ages in August: (e) total energy; and (f) space cooling.

Table 4
The percentage of residential and commercial buildings floor areas in 7 weather zones in Los Angeles County.

	Percentage of Residential Building	Percentage of Commercial Building
Burbank_Glendale	81.66%	18.34%
Van Nuys	85.51%	14.49%
Los Angeles Intl Airport	69.18%	30.82%
Long Beach	80.27%	19.73%
Lancaster	91.10%	8.90%
Palmdale	84.52%	15.48%
Point Mugu	86.89%	13.11%

consumption changes (both RC and AD) in 2050 under A1F1 and A2 scenarios. Large within-county variations of RC and AD can be seen under both scenarios. In general, the RC and AD for annual total energy variation followed the same pattern as the larger increase in the south part of county and smaller increase or even decrease in the north part can be observed. This is due to the fact that current climate is warmer in the south and the current heating energy demand is low there. In other words, there is a limitation on heating energy consumption decrease, because the minimum usage of heating energy could not be less than zero, but there is no limitation on the cooling energy demand increase. As the climate

would be warmer by 2050, the little decrease of heating energy demand in the south cannot be offset by its larger cooling energy demand, leading to a larger increase in total energy demand than in the north. An increase in energy demand was founded to be more substantial under the A1F1 scenario compared to A2 scenario. The number of neighborhoods with larger than 4.5% increase in annual total energy demand was 188 under A1F1 scenario but only 33 under the A2 scenario. The similar difference can be observed when using AD as the measure metric. The number of neighborhoods with larger than 17 MJ/sqm that increased in annual total energy demand was 145 but only 45 under the A2 scenario.

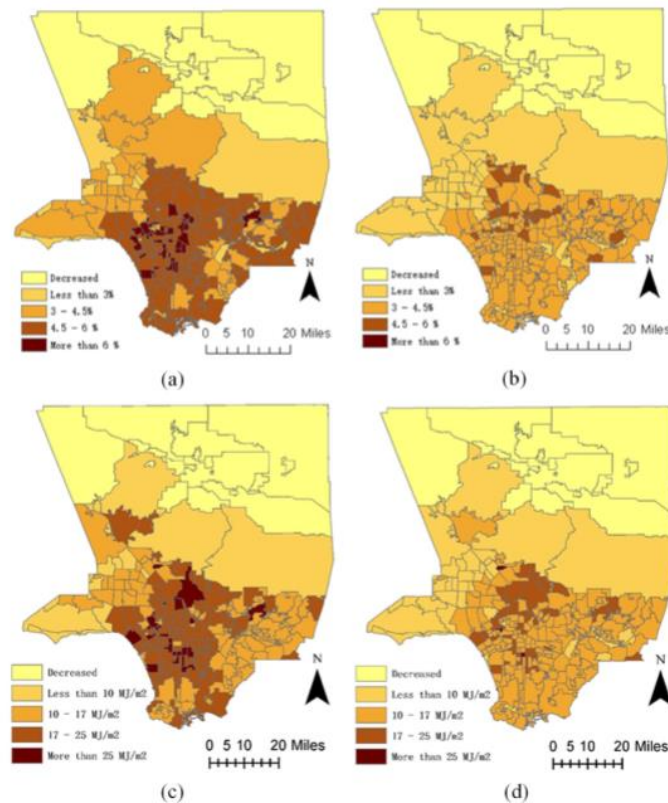


Fig. 10. The spatial variation of total energy consumption changes in 2050 due to climate change in Los Angeles: annual relative change under A1F1 scenario (a), annual relative change under A2 scenario (b), annual energy intensity absolute difference under A1F1 scenario (A1F1) (c), annual energy intensity absolute difference under A2 scenario (d). This sixth version of neighborhood boundary was defined by the Los Angeles Times in June 2010, which represents the boundary of communities and social networks within each city. Note: definition of neighborhood boundary.

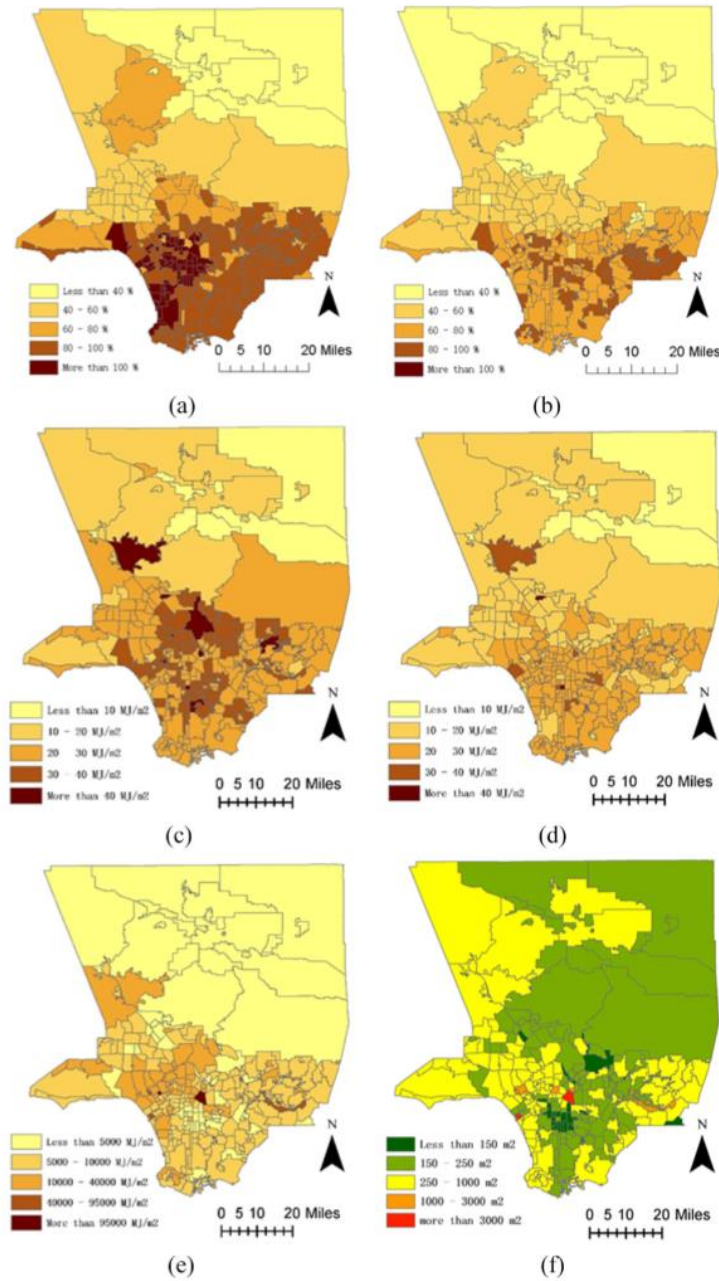


Fig. 11. The spatial variation of cooling energy consumption changes by 2050 caused by climate change in Los Angeles County at the neighborhood scale: (a) annual relative change under A1F1 scenario, (b) annual relative change under A2 scenario, (c) annual energy intensity absolute difference under A1F1 scenario, and (d) annual energy intensity absolute difference under A2 scenario; the spatial variation of the absolute difference of cooling energy consumption per building in 2050 caused by climate change in Los Angeles County at the neighborhood scale: (e) under A1F1 scenario; and (f) average floor area per building.

The increase of cooling energy demand would be more severe than that of the total energy demand (Fig. 11a through d). The RC of cooling energy demand ranged from 27% to 122% under the A1F1 scenario and 25%–95% under the A2 scenario, compared to –1.8% to 7.9% and –1.8% to 6.7% in total energy demand RC, respectively. Neighborhoods with larger than 100% RC of cooling energy demand were mostly located in the Los Angeles International Airport weather zone because it had the highest percentage of commercial buildings (Table 4). Commercial buildings were found to have a higher energy demand increase than in residential buildings, as has been discussed in the previous section. The dramatic increase in RC for commercial buildings could cause a huge challenge for cooling energy supply, while frequent power outage could happen in the future if no change would be made to the current configuration of electronic system. The AD of cooling energy demand under A1F1 scenario did not follow the same trend as the AD for total energy demand. The “hotspots” (larger than 30 MJ/sqm) in cooling energy demand increase are located in the Glendale/Burbank weather zone. The probable cause is there would be more warmer-months than other locations since it is located in the valley and basin. Moreover, building size and density played an important role in the AD of energy demand. Neighborhoods with the largest increase in energy consumption intensity were located in the major commercial zones with high density of tall buildings. As Fig. 11e and f showed, the downtown had the highest increase of per building energy demand because it has the largest average building floor areas (more than 3000 sqm) among all neighborhoods in the Los Angeles County.

4. Discussion

This section discussed the major findings, implications, and the strengths and limitations of our approach compared to the previous published works. The results of previous studies suggested that buildings in warmer climate zones would have larger annual total energy increase compared to those in colder climate zones. The findings of our study matched with those previous findings, but more importantly, discovered a large variation even within the same climate zone, which was caused by building types and ages. In examining the change of energy demand at smaller temporal scales (i.e., monthly and diurnal), it can be found that the variation of energy increase across different building types were even larger, suggesting that the simulations on high spatial and temporal resolutions were indeed necessary. The diurnal variation of building energy AD for different types of buildings followed the diurnal population flows, which indicated that the human activities can further exacerbate the impact of climate change on building energy demand. Although lighting and equipment uses were not directly affected by climate change, they can increase the internal heat gain and raise the indoor temperature, so as to cause more cooling energy consumption.

Unlike the previous studies which used representative buildings [1,19,20,22,25] or assumed that each type of buildings would have the same floor area fraction to the total building stock [3], our approach linked the building energy simulation and climate change model to the fine scale urban building inventory data. Therefore, our approach would allow analysts and policy makers to assess the sensitivity of different regions in the city to climate change with regard to building energy demand increase at different spatial and temporal scales. In addition, a complete database of each building in Los Angeles County was built and ready to be combined with other data. Policy makers can take the database as the reference to choose appropriate policies that targeted specific regions. At the county scale, our results suggested that the likely dramatic increase of cooling energy demand would be the major driving force to

cause the total energy increase at all time scales. Since electricity was the source for space cooling, the high cooling demand would exceed the current electricity generate capacity. Moreover, due to electricity is the secondary energy source, the raising cooling energy demand will also lead to the increased consumption of other energy sources, such as coal and natural gas, which widely used to generate the electricity. According to California Energy Commission, only 29% of electricity was generated through renewable energy sources, and the traditional energy sources were still the major source in 2017. As a result, more greenhouse gases were emitted. Several strategies may help to avoid the future energy consumption path to move towards the high carbon emission scenario (A1F1), including speeding up the process of transforming fossil fuel into a type of renewable energy, reducing the transmission loss of electricity, and increasing the awareness of general public to reduce unnecessary cooling energy use. This study found that the amount of energy demand increase was not distributed evenly throughout the Los Angeles County at the neighborhood scale. Regions with high density of tall commercial buildings (Downtown and major commercial zones) would foresee the largest energy demand increase. Advanced building technologies can help to save large amount of energy, as the buildings built after 2004 were proved to be more energy efficient compared to those built before 2004 at annual, monthly, and hourly time scales. However, there are 188,060 existing commercial buildings in Los Angeles County were built before 2004, which account for 97.84% of total existing commercial buildings. In contrast, only 4152 (2.16%) existing commercial buildings were built after 2004. In this case, policy makers may consider the potential of zero net energy building [28] throughout the county, and give the highest priority to regions that were most vulnerable to the climate change. In order to achieve this goal, the high-resolution database of building sustainability created in this study can be combined with the solar potential rate for each region in Los Angeles County. At the individual building scale, two types of restaurants were identified to have much higher energy demand increase than other types of buildings despite their locations and ages. Given that their peak energy demand increase was during the lunch and dinner time in summer, reduction of solar heat gain and the effectiveness of cooling should be considered simultaneously for all restaurants. Strategies, such as installing solar panels, cool roofs, green roofs, cooling system update, and window retrofit, can all help.

5. Conclusions

This study proposed an integrated approach of modeling and GIS to assess the impact of climate change on building energy consumption for different types and ages of buildings in Los Angeles County at both high spatial and temporal resolutions. The results suggested that under the same climate conditions, the different composition, technologies, size, and density of buildings can still cause large spatial variations on energy demand, even within the same city. How to control the cooling energy consumption is vital for sustainability of Los Angeles under the climate change context. Advanced building technologies, including increased level of insulation, energy efficient equipment, and materials, can all contribute significantly on the saving of cooling energy and while maintain the comfort level. Other strategies, such as transforming to renewable energy and increased levels of insulation, should also be considered.

This research designed an innovative approach to study the climate change effect on building energy consumption at fine spatial and temporal scales. By utilized the unique capability of GIS, which integrates different types of data and organizes them based on spatial locations, our approach can capture the spatial and